

Fall 2007

Microcantilever surface modification for chem- /bio-sensing

Hongwei Du
Louisiana Tech University

Follow this and additional works at: <https://digitalcommons.latech.edu/dissertations>



Part of the [Analytical Chemistry Commons](#)

Recommended Citation

Du, Hongwei, "" (2007). *Dissertation*. 498.
<https://digitalcommons.latech.edu/dissertations/498>

This Dissertation is brought to you for free and open access by the Graduate School at Louisiana Tech Digital Commons. It has been accepted for inclusion in Doctoral Dissertations by an authorized administrator of Louisiana Tech Digital Commons. For more information, please contact digitalcommons@latech.edu.

**MICROCANTILEVER SURFACE MODIFICATION
FOR CHEM-/BIO-SENSING**

by

Hongwei Du, M.S.

A Dissertation Presented in Partial Fulfillment
of the Requirements for the Degree
Doctor of Philosophy

**COLLEGE OF ENGINEERING AND SCIENCE
LOUISIANA TECH UNIVERSITY**

November 2007

UMI Number: 3283297

INFORMATION TO USERS

The quality of this reproduction is dependent upon the quality of the copy submitted. Broken or indistinct print, colored or poor quality illustrations and photographs, print bleed-through, substandard margins, and improper alignment can adversely affect reproduction.

In the unlikely event that the author did not send a complete manuscript and there are missing pages, these will be noted. Also, if unauthorized copyright material had to be removed, a note will indicate the deletion.

UMI[®]

UMI Microform 3283297

Copyright 2007 by ProQuest Information and Learning Company.

All rights reserved. This microform edition is protected against unauthorized copying under Title 17, United States Code.

ProQuest Information and Learning Company
300 North Zeeb Road
P.O. Box 1346
Ann Arbor, MI 48106-1346

LOUISIANA TECH UNIVERSITY

THE GRADUATE SCHOOL

OCTOBER 18, 2007

Date

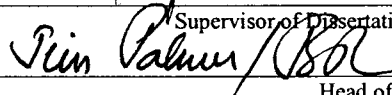
We hereby recommend that the dissertation prepared under our supervision
by Hongwei Du

entitled MICROCANTILEVER SURFACE MODIFICATION FOR CHEM-/BIO-SENSING

be accepted in partial fulfillment of the requirements for the Degree of
Ph.D. in Engineering (Micro/Nanotechnology and Micro/Nanoelectronics
Emphasis)



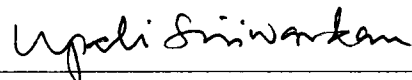
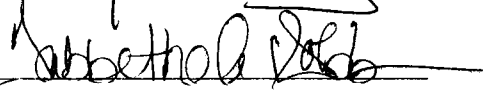
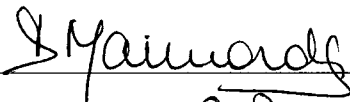
Supervisor of Dissertation Research



Head of Department

Department

Recommendation concurred in:



Advisory Committee

Approved:



Director of Graduate Studies

Approved:



Dean of the Graduate School



Dean of the College

GS Form 13a
(6/07)

ABSTRACT

One focus of the microcantilever (MCL) sensing area is to develop a novel surface modification approach to increase the microcantilever bending amplitudes and thus further improve sensitivities. In this dissertation, enzyme incorporated using the Layer-by-Layer (LbL) process, LbL deposition of micro-, nano- hydrogel particles and electrophoretic deposition (EPD) of micro-, nano- hydrogel particles were applied to prepare a multilayer or thin hydrogel films on the surface of microcantilevers. Prior to applying to the microcantilevers, LbL and electrophoretic deposition techniques were also applied to gold coated silicon wafer surfaces to investigate the feasibility and deposition behavior using these techniques. The multilayers prepared through self-assembling of poly(styrenesulfonate) (PSS), poly(ethylenimine) (PEI), and organophosphorus hydrolase (OPH), responded to organic phosphorus compounds such as paraoxon, parathion, and dimethyl phosphate at different bending amplitudes and bending rates. The bending mechanism investigation suggested that the conformational change of the OPH might be the primary contributor of the MCL bending. The micro-, nano- hydrogel particle deposition on the silicon wafer and microcantilever through LbL process was investigated and discussed based on the observation and characterization using optical microscope, SEM and AFM techniques. A pseudo-3D mechanism was promoted to explain the hydrogel particle deposition process. The research on the EPD demonstrated that the technique was a convenient and reliable approach to deposit a

uniform and continuous hydrogel thin film on the microcantilever devices. The bending responses of hydrogel coated microcantilever correlated with changes in environmental pH, demonstrating the feasibility of this hydrogel film for micro-sensor development.

APPROVAL FOR SCHOLARLY DISSEMINATION

The author grants to the Prescott Memorial Library of Louisiana Tech University the right to reproduce, by appropriate methods, upon request, any or all portions of this Thesis. It is understood that "proper request" consists of the agreement, on the part of the requesting party, that said reproduction is for his personal use and that subsequent reproduction will not occur without written approval of the author of this Thesis. Further, any portions of the Thesis used in books, papers, and other works must be appropriately referenced to this Thesis.

Finally, the author of this Thesis reserves the right to publish freely, in the literature, at any time, any or all portions of this Thesis.

Author Hongwei' Kl,

Date October 25, 2007

TABLE OF CONTENTS

ABSTRACT.....	iii
LIST OF FIGURES.....	ix
ACKNOWLEDGEMENTS	xiii
CHAPTER ONE INTRODUCTION	
1.1 Microcantilever and Microcantilever Based Chem-/Biosensors.....	1
1.1.1 Dynamic Mode.....	3
1.1.2 Static Bending Mode.....	5
1.1.3 Cantilever Surface Modifications and Chem-/Biosensors.....	7
1.2 Layer-by-Layer Assembly of Thin Films and Application in Microcantilever Surface Modification.....	11
1.2.1 Layer-by-Layer Technique.....	11
1.2.2 Layer-by-Layer Assembly of Thin Films.....	16
1.2.3 Microcantilever Surface Modification via LbL.....	19
1.3 Electrophoretic Deposition and Thin Film Formation.....	21
1.3.1 Electrophoretic Deposition and Its Advantages.....	21
1.3.2 Particle Surface Charge and Electric Double Layer.....	23
1.3.3 Parameters Effecting EPD.....	25
1.4 Objectives and Organization of the Dissertation.....	26
CHAPTER TWO INSTRUMENTATIONS	
2.1 Atomic Force Microscope.....	28
2.1.1 Basic Principle.....	28
2.1.2 Imaging Modes.....	30
2.1.3 AFM Resolution.....	31
2.1.4 AFM Characteristics.....	33
2.2 Scanning Electron Microscope.....	34
2.2.1 Brief History.....	34
2.2.2 Basic Principle.....	34
2.2.3 Energy Dispersive X-ray Spectroscopy.....	37
2.2.4 Sample Preparation.....	37
2.2.5 Resolution of the SEM.....	38

CHAPTER THREE ORGANOPHOSPHORUS HYDROLASE MULTILAYER

MODIFIED MICROCANTILEVERS AND ORGANOPHOSPHORUS DETECTION

3.1 Introduction.....	39
3.2 Experimental.....	43
3.2.1 Materials.....	43
3.2.2 Deflection Measurement.....	45
3.2.3 Microcantilever Layer-by-Layer OPH Surface Immobilization Process.....	46
3.3 Results and Discussion.....	48
3.3.1 Relationship between Deflection Amplitudes and the Concentrations of Paraoxon.....	48
3.3.2 Deflection Profiles of Microcantilevers upon Exposure to Paraoxon.....	50
3.3.3 Stability of the OPH-modified Microcantilever.....	51
3.3.4 Thermodynamic and Equilibrium Study of Multilayer Shrinking.....	52
3.3.4.1 OPH amount in OPH/PSS bilayer-modified Microcantilever.....	52
3.3.4.2 OPH Catalyzed Paraoxon Hydrolysis Reaction Velocity.....	53
3.3.4.3 pH versus Paraoxon Concentration Profile.....	54
3.3.4.4 Effect of pH on Cantilever Bending.....	56
3.3.5 Conformational Change of the OPH Enzyme.....	57
3.3.6 Response to Other OPs.....	57
3.4 Conclusions.....	59

CHAPTER FOUR MICRO/NANO HYDROGEL PARTICLE ASSEMBLY

ON THE SURFACE OF SILICON AND MICROCANTILEVER VIA LBL

4.1 Introduction.....	60
4.2 Experimental.....	62
4.2.1 Materials.....	62
4.2.2 Silicon Wafer Slides and Microcantilever Preparation.....	62
4.2.3 Synthesis of Micro-, Nano- Hydrogel Particles.....	63
4.2.4 Characterization of the Micro-, Nano- Hydrogel Particles.....	64
4.2.5 Alternate Layer Deposition on Si Wafer Slides and Microcantilevers via LbL.....	65
4.2.6 Hydrogel Film Characterization.....	65
4.3 Results and Discussion.....	66
4.3.1 Synthesis of the Micro-, Nano- Hydrogel Particles.....	66
4.3.2 Characterization of the Micro-, Nano- Hydrogel Particles.....	68
4.3.3 Micro-, Nano- Hydrogel Particle Assembly on the Silicon Wafer.....	70
4.3.4 Micro-, Nano- Hydrogel Particle Assembly on the Microcantilevers.....	74
4.3.5 Polystyrene Microparticle Assembly on the Microcantilevers.....	77
4.4 Conclusion.....	80

CHAPTER FIVE MICRO/NANO HYDROGEL PARTICLES DEPOSITION
ON SILICON WAFER AND MICROCANTILEVER VIA ELECTROPHORETIC
DEPOSITION

5.1 Introduction.....	81
5.2 Experimental.....	83
5.2.1 Synthesis of Micro-, Nano-Hydrogel Particles.....	83
5.2.2 Micro-, Nano-hydrogel Particle Electrophoretic Deposition.....	83
5.2.3 Methods for Microcantilever Test.....	84
5.2.3.1 Materials.....	84
5.2.3.2 Deflection Measurement.....	85
5.3 Results and Discussion.....	86
5.3.1 The Hydrogel Film Formation from the Suspensions of Micro-/Nano- Hydrogel Particles on Si Wafers.....	86
5.3.2 EPD Behaviour of the of Nano-Hydrogel Particles on Si Wafers.....	88
5.3.3 Explanation of the EPD Behaviour of the Nano-Hydrogel Particles on Si Wafers.....	91
5.3.4 The AFM Images of the Hydrogel Film on Si Wafers.....	94
5.3.5 The Hydrogel Films on the Surface of Microcantilevers.....	95
5.3.6 The Bending Measurement of the Hydrogel Coated Microcantilevers in Different pH Solutions.....	97
5.4 Conclusion.....	100
CHAPTER SIX FINAL CONCLUSIONS AND FUTURE WORK	
6.1 Final Conclusions.....	101
6.2 Future work.....	103
REFERENCES.....	106

LIST OF FIGURES

Figure 1.1 Different Shapes of Microcantilevers.....	1
Figure 1.2 Schematic of an optical detection system for detecting microcantilever deflection.....	2
Figure 1.3 Mechanisms of analyte-induced stresses in different surface modifications [1].....	6
Figure 1.4 Molecular structures of the commonly used polyelectrolytes in the LbL.....	14
Figure 1.5 Illustration of the different interactions between the layers and the alternative absorption.....	15
Figure 1.6 Schematic illustration of the LbL self- assembly process.....	17
Figure 1.7 General procedures for LbL assembly with immobilized enzyme on the microcantilever.....	20
Figure 1.8 Schematic showing electrophoretic deposition [57].....	22
Figure 1.9 Schematic illustrating electrical double layer structure and the electric potential near the solid surface with both Stern and Gouy layers [57].....	23
Figure 2.1 (A-C) Three common types of AFM tip. (A) normal tip (3 μm tall); (B) supertip; (C) ultralever (3 μm tall) [68].....	28
Figure 2.2 Block diagram of the atomic force microscope [69].....	29
Figure 2.3 Tip broadening arises when the radius of curvature of the tip is comparable or greater than the size of the feature trying to be imaged [70].....	32
Figure 2.4 Aspect ratio of a particular tip is crucial when imaging steep sloped features [70].....	33
Figure 2.5 Schematic diagram illustrates how a scanning electron microscope works [76].....	35
Figure 2.6 Schematic Diagram shows the electron-specimen interaction [76].....	36

Figure 3.1 Total reaction of the OP hydrolysis by the OPH.....	41
Figure 3.2 Reaction process of the OP hydrolyzed by the enzyme.....	42
Figure 3.3 Top view of MCL (Veeco Instruments, Santa Barbara, CA) used in this experiment.....	44
Figure 3.4 Schematic diagram of the apparatus used in the study.....	45
Figure 3.5 (A) Dynamics of bending amplitude for a freshly-made (PSS/OPH) ₃ modified MCL (solid line) and a (PSS/OPH) ₃ multilayer modified MCL (dashed line) after storing in a dry state in the refrigerator at 4 °C for 2 months upon exposed to 10 ⁻³ M paraoxon in 0.01 M phosphate buffer.....	49
Figure 3.5 (B) Dynamics of bending amplitude for a freshly-made (PSS/OPH) ₃ modified MCL (solid line) and a (PSS/OPH) ₃ multilayer modified MCL (dashed line) after storing in a dry state in the refrigerator at 4 °C for 2 months upon exposed to 10 ⁻⁵ M paraoxon in 0.01 M phosphate buffer.....	49
Figure 3.5 (C) Dynamics of bending amplitude for a freshly-made (PSS/OPH) ₃ modified MCL (solid line) and a (PSS/OPH) ₃ multilayer modified MCL (dashed line) after storing in a dry state in the refrigerator at 4 °C for 2 months upon exposed to 10 ⁻⁷ M paraoxon in 0.01 M phosphate buffer.....	50
Figure 3.6 Correlation between maximum bending amplitudes of a (PSS/OPH) ₃ modified MCL and paraoxon concentration in a 0.01 M phosphate buffer. Insert: Three replicates (dashed line) of bending responses as a function of time for a (OPH/PSS) ₃ multilayer modified MCL following injection of a 10 ⁻³ M paraoxon in 0.01M phosphate buffer at 4.5 mL/h flow rate.....	51
Figure 3.7 The calculated/predicted paraoxon hydrolysis rate (y-axis on the left) according to equation (2) in a (PSS/OPH) ₃ film on the modified MCL and the resultant pH (y-axis on the right) in the (OPH/PSS) ₃ multilayer film on the modified MCL as a function of paraoxon concentration.....	54
Figure 3.8 Maximum bending responses for a (OPH/PSS) ₃ modified MCL after injection of a 0.01 M phosphate buffer with different [H ⁺] (pH) at 4.5 mL/h flow rate.....	56

Figure 3.9 Bending responses as a function of time for a (OPH/PSS) ₃ modified MCL upon exposure to 10 ⁻³ M paraoxon, parathion, and DFP at 40 mL/h flow rate.....	58
Figure 4.1 Idealized schematic for the alternate layer deposition scheme followed in this study.....	66
Figure 4.2 SEM view of the as-synthesized micro-, nano- hydrogel particles by precipitation polymerization.....	68
Figure 4.3 The SEM image of the hydrogel nanoparticles deposited on the silicon wafer. The wafer was firstly coated with three bilayers of (PEI/PSS) plus one PEI layer at the outmost surface and then exposed to the nanoparticle suspension in water for 1 hour.....	69
Figure 4.4 The AFM image of the hydrogel nanoparticles deposited on the silicon wafer. The wafer was firstly coated with three bilayers of (PEI/PSS) plus one PEI layer at the outmost surface and then exposed to the nanoparticle suspension in water for 1 hour.....	70
Figure 4.5 (A-D) SEM pictures taken of (A) 1, (B) 5, (C) 10 and (D) 15 hydrogel particle alternate layer films. From the pictures it can be seen that as the number of the hydrogel particle alternate layer increases the hydrogel particle density increases indicating a multilayer buildup mechanism.....	72
Figure 4.6 (A, B) AFM images of (A) 10 and (B) 15 hydrogel particle alternate layer films.....	73
Figure 4.7 (A-F) Optical images of the microcantilevers deposited with one operation of micro-, nano-, hydrogel particles on the Au surface (A) and Si surface (B), 5 operations on the Au surface (C) and Si surface (D), 8 and 12 operations on the Au surface (E and F). Multilayer buildup is obvious after 8 and 12 alternate operations (750×).....	75
Figure 4.8 (A, B) Optical images of the Si side of the microcantilever bodies used in this research after 1 (A) and 5 (B) alternate operations of micro-, nano-hydrogel particle deposition. It is obvious that the hydrogel particles absorbed on the Si surface (750×).....	77
Figure 4.9 (A-F) Optical images of the microcantilevers deposited with (A) 2; (B) 4; (C) 6; (D) 8; (E) 10 and (F) 12 alternate assembly operations of polystyrene microparticles on the Au surfaces of the microcantilevers. Multilayer buildup occurred after 8 alternate operations. (750×).....	78

Figure 4.10 (A, B) Optical images of the Si side of the microcantilevers used in this research after (A) 2 and (B) 12 assembly operations of PS microparticle deposition. It is obvious that the PS particles absorbed to the Si surface. (750×).....	79
Figure 5.1 SEM picture of of the deposited film on Si wafer via the EPD from the suspension of the micro-/nano- hydrogel particles at 10V for 30 min.....	87
Figure 5.2 Optical microscopy image of the deposited film on Si wafer via the EPD from the suspension of the micro-/nano- hydrogel particles at 10V for 30 min. The magnification is 750×.....	87
Figure 5.3 (A-E) Optical microscopy images of the hydrogelfilms on the surface of silicon wafers via EPD from the suspension of nano- hydrogel particles at 2V for (A) 2 min, (B) 8 min, (C) 15 min, (D) 25 min, and (E) 35 min. The magnifications are 750×.....	89
Figure 5.4 (A-E) Optical microscope images of the hydrogel films on the surface of silicon wafers via EPD from the suspension of the micro-/nano- hydrogel spheres under 5V for (A) 2 min, (B) 10 min, (C) 15 min, (D) 25 min, and (E) 35 min. The magnifications are 750×.....	91
Figure 5.5 (A,B) AFM images of a film of 100-nm gel particles deposited on a Si plate through EPD at 2 V for 35 min. (A) 3-D image of the hydrogel film; (B) Tape mode image of the hydrogel film.....	94
Figure 5.6 The roughness measurement (between a lowest and a highest points) of the hydrogel film of 100-nm gel particles deposited on a Si plate through EPD at 2 V for 35 min. The average thickness of the gel film was approximately 100 nm.....	95
Figure 5.7 (A-D) The optical images of the hydrogel film coated microcantilevers (B,D) and the hydrogel film coated bodies of the corresponding microcantilevers (A, C). The hydrogel films were produced by EPD of the suspension of hydrogel nanoparticles under 0.8 V for 20 min. The magnifications are 750×.....	96
Figure 5.8 The Response of Hydrogel Coated Microcantilever to the Different pH Phosphate Buffer Solutions.....	98

ACKNOWLEDGEMENTS

I would like to acknowledge many people for helping me during my graduate studies at LA Tech. I would especially like to thank my research advisor, Dr. Haifeng Ji, for his advice, direction and encouragement thorough out the period. This dissertation would not have been possible without his expertise guidance and generous support.

I gratefully acknowledge all the members of my committee: Dr. Yuri Lvov, Dr. Dale Snow, Dr. Upali Siriwardane, Dr. Daniela Mainardi and Dr. Tabbetha Dobbins. They have not only given their generous time to read this manuscript, they have also offered valuable advice and direction during my graduate program.

My research in this dissertation was made feasible and also much more extensive with help from instrumentation and other resources. Thus, I gladly express my gratitude to Dr. Xiaoke Xu for her assistance in the SEM and AFM characterization work that was used thorough out this dissertation. I am also grateful to Mr. Danny Eddy for his helpful and enthusiastic support for my research. I am also grateful to Dr. Sven Eklund and Dr. Marilyn Cox for their encouragement and support.

I am also indebted to the officers and staff of the Graduate School, the College of Engineering & Science Graduate Studies, Louisiana Tech University, for their advice on guide lines and encouragement during my graduate program. I am much thankful to numerous librarians for their assistance, especially the reference librarians and inter-library loan officers at the Prescott Memorial Library. I also greatly appreciate all the

help and guidance from the International Student Office for my family and myself. My graduate studies would not have been the same without their love.

Last, but certainly not least, I would like to thank my wife, Lanxiu Lu, for everything she has sacrificed for me to make progress in my career. Over the past years, while I pursued my career, she has shown me extreme patience as well as offered me unconditional love and support to my every endeavor I have pursued.

CHAPTER ONE

INTRODUCTION

1.1 Microcantilever and Microcantilever Based Chem-/Biosensors

Microcantilevers are simple micromachined devices with typical dimensions about 0.2-1 μm thick, 20-100 μm wide, and 100-500 μm long. Microcantilevers are commonly fabricated from silicon and silicon nitride using well-established batch processes that involve photolithographic patterning and a combination of surface and bulk micromachining [1]. They can be V-shaped or bar-shaped with one end connected to an appropriate support for convenient handling. Figure 1.1 shows some of the different shapes for microcantilevers.

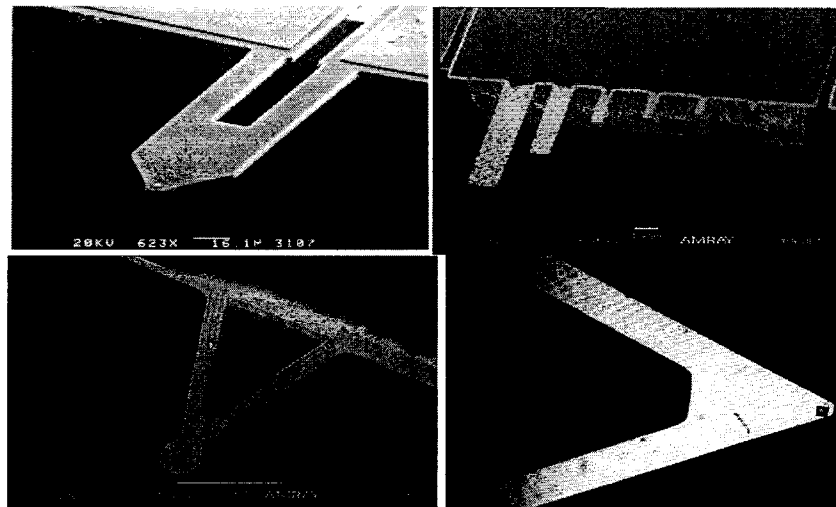


Figure 1.1 Different Shapes of Microcantilevers

Initially, the microcantilevers that are used as probes in atomic force microscopy (AFM) to translate small forces into topographic images were converted into a platform for a new class of sensors in 1994 [1]. While being among the simplest of structures, a cantilevered beam can be a highly effective sensing element, offering numerous transduction applications. Once the new possibilities of the microcantilevers was realized, numerous chemical and biological sensing applications based on the microcantilevers mechanically have been set up to detect an analyte. For the measurement, microcantilevers adopt the same optical lever read-out scheme from the AFM as illustrated in the Figure 1.2. The reflected laser light from the deflected microcantilever projects at a different position on the position sensitive photodetector (PSPD). Depending on the distance between the two positions of the laser beam on the PSPD, the deflection of the microcantilever is determined.

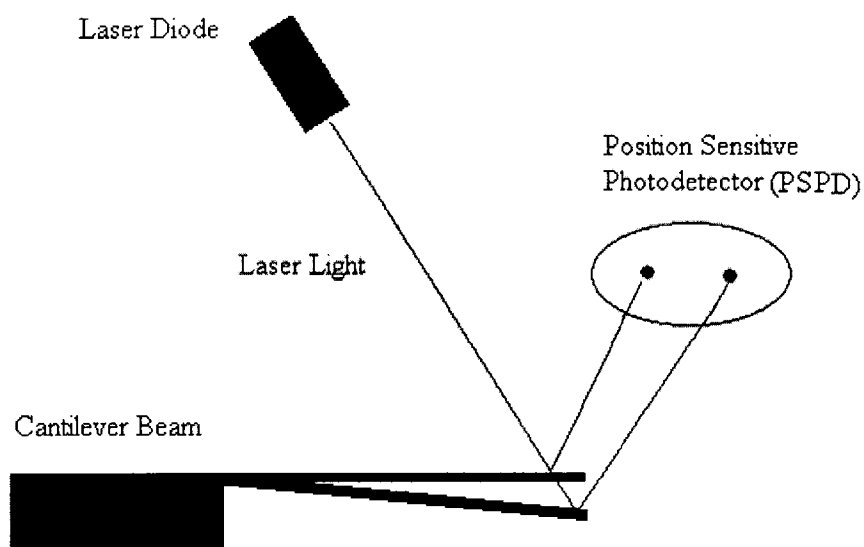


Figure 1.2 Schematic of an optical detection system for detecting microcantilever deflection.

In this scheme, a laser beam reflected from near the end of a cantilever is displaced as the cantilever bends. This displacement is converted into an electronic signal by projecting the reflected laser beam onto a position-sensitive photodetector (PSPD).

As previously mentioned, analogous to the two basic working modes of the AFM, contact mode and tapping mode, cantilever-based sensors can also make measurements based on cantilever deflections or shifts in resonance frequencies. However, the MCL mechanisms that translate interactions of various components of a physical, chemical, or biological environments into these parameters are generally different from that operate in an AFM. Usually, there are two operation modes for the cantilever-based sensors: a) dynamic mode and b) static bending mode.

1.1.1 Dynamic Mode

When operated in dynamic model, microcantilevers are essentially mechanic oscillators that can be described using traditional models [2-5]. In many sensing applications, the frequency of the cantilever oscillators is not significantly damped by the environment in which the microcantilever is placed or by any surface modifications applied. Under these conditions, if there is an additional mass increase resulting from the analyte binding or absorbing on the cantilever surface, a shift directly related to this mass change is monitored in the cantilever resonance frequency by the system. The relationship between these parameters is presented in the Equation (1) [2].

$$\frac{1}{f_1^2} - \frac{1}{f_0^2} = \frac{\Delta m}{4\pi^2 K} \quad (1)$$

where Δm is the net mass increase, f_0, f_1 are the cantilever resonance frequencies before and after the mass change respectively, K is the cantilever spring constant, which is an intrinsic property of the cantilever and directly related to the structure and materials employed in the fabrication of the microcantilevers.

From the above equation, it can be concluded that, in order to achieve appreciable mass sensitivity, only higher amplitudes of fundamental frequencies are required for the microcantilevers. Though most cantilevers only have lower resonance frequencies at a range of 20-200 kHz compared to traditional quartz crystal microbalances (QCM) have much higher oscillating frequencies in the range of 5-500 MHz. However, MCLs have superior mass sensitivity compared to QCM. This sensitivity is a consequence of the relatively low stiffness and micro-size of the beam of a cantilever structure. With an effort of further enhancing the sensitivity, researchers have developed nanoscale cantilevers with higher fundamental frequencies of 10^5 - 10^6 . It can be predicated that mass sensitivity of these nanoscale cantilevers can reach the single-molecule level (10^{-21} g) [1].

In dynamic mode, there are three mechanisms to explain the sensor based resonating cantilevers. The first is the adsorbate-induced loading to MCL as we discussed above. The second is the damping caused by the viscosity of the media, if the damping effect of the media is rather strong. And finally, interactions between the environment (for example differences in pH media) and the cantilevers may affect the mechanic properties of the cantilevers, such as stiffness, and induce elasticity changes in microcantilever materials.

1.1.2 Static Bending Mode

In the static bending mode, the deflection of the cantilever is directly related to the asymmetric, out-of-plane mechanical stress generated in the cantilever. For metal coated (such as gold) cantilevers, due to the different coefficients of thermal expansion between the base materials (such as silicon) and the metal coating, thermally induced stress is typical. Thus, a temperature change in the environment where the cantilever is located can result in the deflection of the cantilever due to the unequal thermal expansion of the layers in a biomaterial cantilever. There is practical application, if the analyte species can produce heat when they combine through adsorption on the cantilever, or chemical reactions are associated with the adsorption on the cantilever, then the analyte species can be detected by the cantilever [6].

There are three distinctive surface modification models to explain the behavior of the cantilever as a function of MCLs chemical or biosensing in static bending mode (Figure 1.3). In the first model, the cantilever produces bending due to an adsorbate-induced surface stress change due to chemical binding. For example, Figure 1.3a shows chemisorption of straight-chain thiol molecules on a gold-coated cantilever. The surfaces usually tend to expand as a result of adsorptive processes. Adsorbate-induced deflections can be accurately described by the Stoney equation [7]. The changes in the film's or the cantilever's radius of curvature, R , and deflection, z_{\max} , can be related to the differential surface stress, $\Delta\sigma$, by

$$\frac{1}{R} = \frac{6(1-\nu)\Delta\sigma}{Et^2}; \quad z_{\max} = \frac{3l^2(1-\nu)\Delta\sigma}{Et^2} \quad (2)$$

where ν is Poisson's ratio, E is Young's modulus for the substrate, t is the thickness of the cantilever, and l is the cantilever length. The analysis according to Equation 2 gives accurate predictions when adsorbate-induced stresses are generated on ideally smooth surfaces or within coatings that are very thin compared with the cantilever.

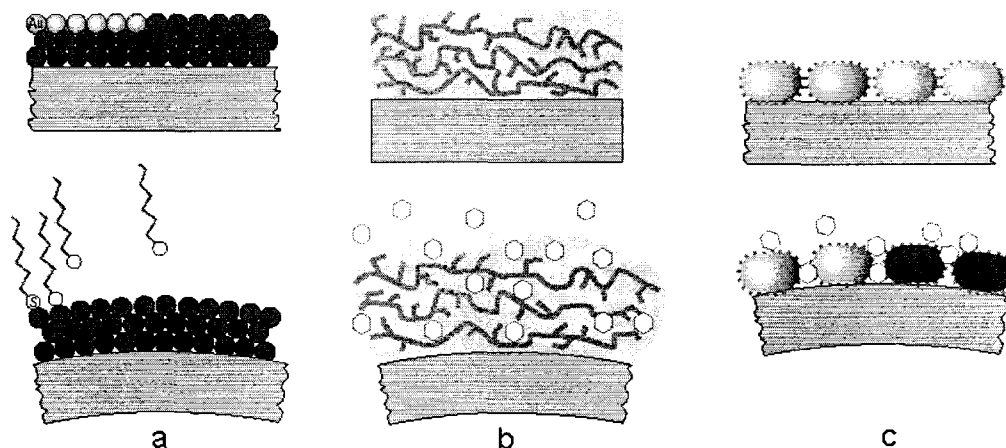


Figure 1.3 Mechanisms of analyte-induced stresses for different surface modifications [1]. (a) Compressive stresses are demonstrated for chemical binding of thiol compound modified gold-coated surface; (b) Swelling of a thin film on a surface due to analyte absorption; (c) Interstitial forces are generated when analytes bind to a nanostructured surface.

In the second mode, the cantilever is modified with an analyte-permeable coating, such as polymer, hydrogel, etc, and the cantilever will undergo deflection due to the swelling of the coating when the analyte penetrates into the coating. This cantilever deflection is described as analyte-induced swelling of the coating. Figure 1.3b demonstrates this model. In this third model, instead of a smooth, gold surface, the cantilever surface can be fabricated into nanostructured morphology (Figure 1.3c). When receptor molecules are immobilized on a nanostructured surface, the cantilever

response can be enhanced up to 2 orders of magnitude. In all the models, analyte induced deflections of cantilevers with these phases involve mechanisms of bulk, surface, and intersurface interactions [1].

1.1.3 Cantilever Surface Modifications and Chem-/Biosensors

A cantilever based chemical or biological sensor is normally modified using different approaches to make one side of the cantilever is relatively passive and the other side is active. This active side exhibits higher affinity to the target analyte. Consequently, changes in the surface stress are determined by the surface inactions, adsorption or absorption, between the cantilever and the target analytes on the active side of the cantilever. For chemical or biological sensors that the proper surface modification is very important to detect analytes, therefore, most of the research work has been done or is being carried is on this subject. Today, the techniques that are employed in the cantilever surface modification include deposition of self-assembled monolayer (SAM) [8-10], polymer [11-13], sol-gel [14], hydrogel [15-18], etc.

The technique of self-assembled monolayer by spontaneous adsorption of molecules on microcantilever surface has attracted a huge interest due to their high sensitivity and selectivity of analyte detection. Diverse selections of SAMs made up of various bio-molecules on the substrate surface forming biological probes have made the micro-cantilever an excellent device for modeling interactions between artificial surfaces and biological systems. In Fritz and coworkers' [8] pioneering research, synthetically thiol-modified oligonucleotides with different base sequences were covalently immobilized on the gold-covered active side of the cantilevers in an

array. One cantilever array was functionalized with a 12-mer oligonucleotide and the other with a 16-mer oligonucleotide in parallel under identical conditions. The cantilevers in each array were found to provide differential deflection, a true molecular recognition signal of characteristic of an oligonucleotide despite large nonspecific responses of individual cantilevers. Hybridization of complementary oligonucleotides in the cantilever array showed that even a single base mismatch between two 12-mer oligonucleotides could be clearly detectable. Similar experiments were conducted on protein A-immunoglobulin interactions demonstrated that the wide-ranging applicability of nanomechanical transduction to recognize biomolecules through interactions that could reach via surface stress changes through the cantilever modification. Haifeng Ji' group [9] prepared a Cu^{2+} /L-cysteine bilayer on a gold-coated microcantilever by immersing the cantilever into a 10^{-3} M solution of L-cysteine in tris buffer solution and then microcantilever was immersed in a 10^{-3} M CuSO_4 tris buffer solution to form a self-assembled bilayer of Cu^{2+} /L-cysteine on the gold surface of the cantilever. This Cu^{2+} /L-cysteine bilayer-coated microcantilever has demonstrated a high sensitivity and selectivity toward organophosphorus compounds in aqueous solutions. Due to the complexation of the phosphonyl group of the dimethyl methyl phosphonate (DMMP), a Sarin nerve gas stimulant, and the Cu^{2+} /L-cysteine bilayer on the microcantilever surface, the microcantilever undergoes bending upon exposure to the DMMP even at concentrations as low as 10^{-15} M.

The cantilever can also be the modified with an analyte-permeable polymer coating that is much thicker than a monolayer. In this case, interactions of the analyte

molecules with the polymer result in the deflection of the cantilever and the mechanism of the cantilever deflection is caused by analyte-induced swelling of the polymer coating. The operating principle of MCL relies on transduction of chemical or physical processes into a mechanical response. Battison and coworkers [11] prepared and investigated a chemical sensor based on an array of silicon cantilevers that were functionalized by polymer coatings. After exposure to analyte vapors, such as water, primary alcohols, alkanes and perfumes, analyte molecules diffuse into the cantilever coating and resulted in the swelling of the polymer coating. In addition to the mass increase, a change of interfacial stress between coating and cantilever took place to produce a bending of the cantilevers. Cantilevers coated with both high and low crosslinked plasma-polymerized allylamine (PPAA) films were investigated by Iqarashi [19] in N_2 atmospheres at various humidity conditions. The results demonstrated that a dense plasma-polymerized allylamine film of high cross-linked and could transduce more efficient swelling of the film to the cantilever bending than a low density film of low cross-linked under identical environmental conditions.

In cantilever surface modification, Sol-gel technique also found useful in modifying cantilever modified application as a sensing transducer. Fagan et al. [14] prepared a chemical sensor by modifying a micro-cantilever surface with a thin film of sol-gel deposition using a spin coating procedure. These sensors showed different responses to variations in chemical composition and concentrations of various vapor phase analyte. Ethanol, a highly polar molecule, exhibits a stronger affinity for the polar sol-gel coating and resulted in a larger response; pentane, a non-polar

hydrocarbon, showed very little response. The sol-gel coating has also been shown to function as a matrix for the immobilization of chemically selective phases on the cantilever surface. Another extensive sol-gel research area to coat the cantilever surface is to deposit a sol-gel derived lead zirconium titanate thin film to fabricate piezoelectric cantilevers [15-17].

Stimuli-response of hydrogels also affect volume in response to small changes in ionic strength, solvent, stress, light intensity, electric field, and magnetic fields. Such hydrogel behavior has led to efforts to develop chemical and biological sensors for species such as CrO_4^{2-} [18], Pb^{2+} [19], pH [20, 21], etc. In Dr. Ji's group [18], hydrogels containing various amounts of tetraalkylammonium salts were used to modify microcantilever surface for measuring concentration of CrO_4^{2-} in aqueous solutions. These microcantilevers exhibited bending deflection upon exposure to solutions containing various CrO_4^{2-} concentrations, as a result of swelling or shrinking of the hydrogels. The microcantilever deflection as a function of the concentration of CrO_4^{2-} ions, was nearly linear for most concentration ranges and the lowest detection limitation could be as low as 10^{-11} M. A ultrahigh sensitive pH sensor was reported [21] based on a microcantilever structure with a lithographically-defined cross-linked copolymeric hydrogel consisting of poly(methacrylic acid) (PMAA) and poly(ethylene glycol) (PEG) dimethacrylate. The components were patterned and polymerized through free-radical UV polymerization. As the pH around the cantilever was increased above the pK_a of PMAA, the polymer network expanded and resulted in a reversible

change in surface stress causing the microcantilever to bend with a maximum deflection sensitivity of $1 \text{ nm}/5 \times 10^{-5} \Delta \text{pH}$.

With various surface modification approaches, the cantilevers based on chemical or biosensing offer a great attraction to various fields of industries, such as healthcare and environment monitoring. The high sensitivity, compactness, low cost, low power-consumption and versatility of microcantilever sensors will continue to drive the development and application of the surface modification technique.

1.2 Layer-by-Layer Assembly of Thin Films and Application in Microcantilever Surface Modification

1.2.1 Layer-by-Layer Technique

Improvements in fabrication or patterning thin films on surfaces of the various substrates or devices has been arousing great research interests on a variety of applications such as sensors [22], drug delivery [23], anticorrosive surfaces [24] and photonic materials [25]. Usually, these films are composed of multiple components arranged in a designed order and controlled thickness. Currently, the techniques for thin film fabrication or patterning include spin coating [26], Langmuir-Blodgett technique [27], electrophoretic deposition [28], Layer-by-Layer (LbL) [29, 30]. The spin coating technique is frequently used for the coating of photoresists onto a SiO_2 surface prior to photolithography. By taking advantage of a standard spin coater, this technique allows for the adsorption of polyelectrolytes onto surfaces in a multilayer fashion with controlled thickness within a relatively short time, usually several minutes. The limitations of the spin coating technique result from following aspects. First, spin

coating can only be carried out on the flat and symmetrical surfaces. It could not be applied to spin coat other various geometric surface shapes or asymmetric substrates. This speciality greatly limits its practical applications. Second, the thickness of the deposited films usually is in the order of micros. It is difficult for the spin coating method to form a thin film at nano-scale thickness. Third, special equipment is needed for this operation. Another classic technique for fabricating thin films with some control over layer ordering or orientation is the Langmuir-Blodgett technique. This technique allows for the transfer of a self-assembled, specifically orientated monolayer of molecules from an air-water interface to the surface of a planar substrate. The deposited molecules consist of two sections. One is the relatively short and hydrophilic head, which could attach with water. The other section is the long and hydrophobic tail, which points straightforward into the air. The operation is processed by slowly dipping the substrate into and out of the solution containing the self-assembled molecules. While this technique has the benefit of depositing molecularly thin layers in a highly precise manner, it also has the drawbacks of requiring special equipment, difficulty in depositing on large surfaces and is limited to planar surfaces as is the spin coating. This technique has another drawback of not being able to deposit layers containing multiple components with various compositions, i.e. nanoparticle modified surfaces. Electrophoretic deposition is mainly employed to form single or multiple thin layers on different surfaces with various shapes with the aid of an electric field. It seems to be a desirable technique to meet the goals we mentioned previously but, because the deposition components are typically micro- or nanoparticles instead of molecules, we

will specifically discuss this in the latter section. Because of these film requirements, there are few technologies available to achieve such goals, and the technology that is available is typically complicated and difficult to scale to the coating of large substrate surfaces made of a variety of materials and dimensions.

Starting in the early 1990s, Drs. Decher, Lvov and coworkers [29, 30] began work on a realistic method for the electrostatic self-assembly of multilayers over charged substrates. Their extensive initial work gave birth to Layer-by-Layer assembly (LbL) and resulting in a breakthrough in thin film deposition technology. In their initial study, the authors constructed multilayer thin films by exposing a charged substrate to an aqueous solution containing different polyelectrolytes, molecules that were end-functionalized with charged moieties. These molecules were shown to adsorb to the surface in a self-assembly manner due to the electrostatic forces. Under the effect of electrostatic forces, molecules adsorb to the substrate until the charge on the surface of the substrate is reversed and this charge reversion blocks further molecule adsorption to the substrate by electrostatic repulsion. After rinsing and drying, the substrate is then sequentially immersed in each solution until the desired film thickness or composition is reached. The frequently used polyelectrolytes for the assembly include the polycations, poly(dimethyldiallylammonium chloride) (PDDA), poly(ethylenimine) (PEI), poly(allylamine chloride) (PAH) and the polyanions, poly(styrenesulfonate) (PSS), poly(vinylsulfate) (PVS), poly(acrylic acid) (PAA). Figure 1.4 presents the molecular structures of the commonly used polyelectrolytes in the LbL process.

Currently, this technique of alternately adsorbing polyelectrolytes onto surfaces is one of the most common and versatile techniques for fabricating polymeric thin films with various compositions [31-33]. In LbL, in addition to fabricating films stabilized by electrostatics, thin films have also been constructed using hydrogen bonding [34] and ligand-receptor interactions (through coordinate covalent or covalent bonding, biological recognition) [35]. In order to attract the molecules in the aqueous solution, the substrate surface is modified to present functional groups that have attractive interactions with the adsorbate molecules. Thus, it is possible to use a variety of interactions to assemble films. In general, as long as these attractive interactions are present, regardless of the nature of the interactions, molecules will attach to the substrate surface. Another requirement to achieve stable multilayer thin films is that the layers must have multiple attractive interactions with the substrate and the other components of the film. Figure 1.5 illustrates the different interactions between the layers and the alternative absorption.

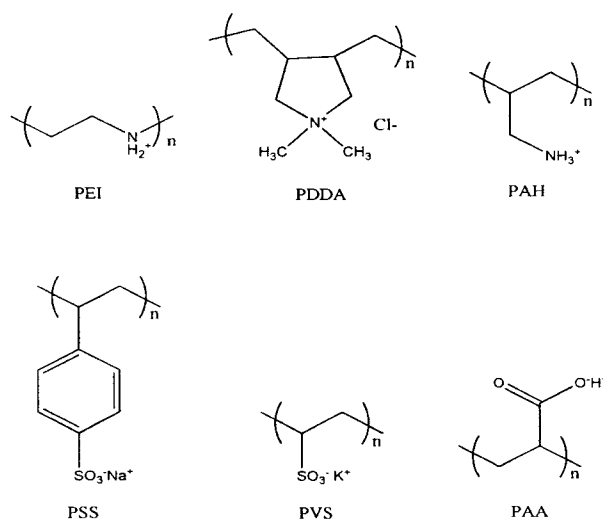


Figure 1.4 Molecular structures of the commonly used polyelectrolytes in LbL.

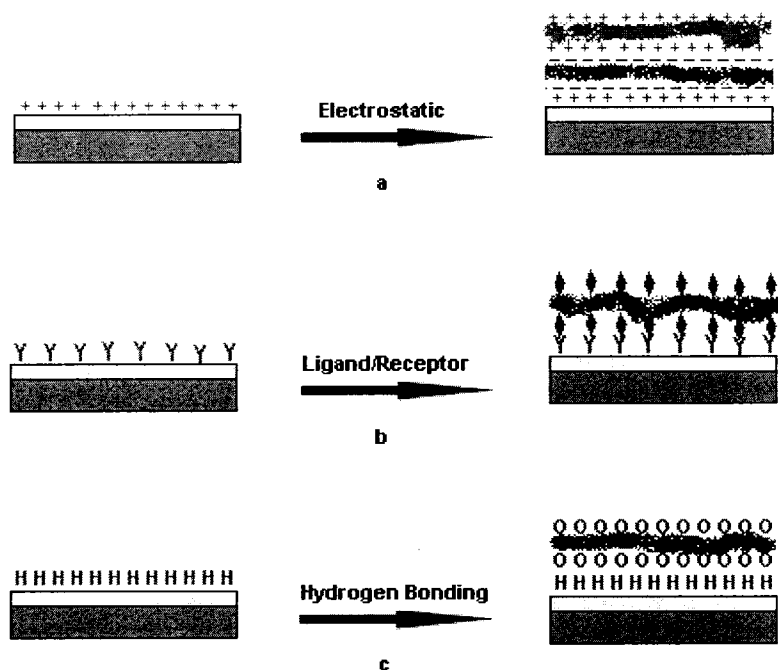


Figure 1.5 Illustration of the different interactions between the layers and the alternative absorption. (a) electrostatic forces; (b) ligand-receptor interactions;(c) hydrogen bonding.

The LbL technique has many advantages over other thin film fabrication methods. First, it is not only applicable to scaling down to coat micro- or nano-sized surfaces such as microcantilevers, cotton fibers and nanowires, it is also has the ability to scale up the deposition to the coating of large substrates. Second, because this is a solution based technique, there are no substrate limitations. Actually, in practice, any shape, morphology or composition can be coated as long as multiple attractive interactions are present in the film. Third, this technique also has the ability to control the layer orientation or the layer sequence (in one dimension) and composition of the individual layers in the films, which is difficult to achieve using other methods.

1.2.2 Layer-by-Layer Assembly of Thin Films

Typically, the LbL processes mainly involve the passive adsorption of macromolecules on surfaces [30]. As mentioned previously, the surface can be actually any size, shape, morphology, or composition, although in research, the most common case is planar glass substrates. A general prerequisite for the adsorption of a macromolecule on a surface is that the macromolecule must have multiple attractive interactions with the substrate surface. As mentioned above, there are a variety of possible interactions that can be exploited for the deposition of layers but this section will be limited to the discussion of polyelectrolyte adsorption to surfaces.

To begin the LbL process, the substrate surface must be properly treated to render it charged. This can be accomplished in a variety of ways depending on the surface composition of the substrate being used. For example, if a glass substrate is being used for deposition it can be rendered negatively charged by exposure to a strong oxidizing solution such as piranha solution, or positively charged by covalently attaching positively charged silanes to the surface. If the surface is gold, thiol compounds are usually used for the interactions between the gold atoms and the sulfur atoms, though the nature of these interactions is not well understood [36-39]. Regardless of the initial charge on the substrate, polyelectrolyte deposition is performed in the same manner. In a standard process, a charged substrate is exposed to an aqueous polyelectrolyte solution at the desired pH, ionic strength and concentration (typically on the order of milligrams/mL), and the polyelectrolyte is allowed to adsorb onto the substrate surface for ~20 minutes. The 20 minute adsorption time is standard

for the adsorption of relatively low molecular weight polyelectrolytes ($\sim 70,000$) but can be increased for the deposition of large molecular weight polyelectrolytes and colloidal species [21]. This substrate is then rinsed with DI water, dried with N_2 gas, and exposed to an aqueous solution of oppositely charged polyelectrolyte. After 20 minutes this substrate is again rinsed with DI water and dried with N_2 gas and exposed to the original polyelectrolyte solution. This process can be repeated numerous times to achieve a film with the desired properties. A schematic depiction of the deposition process is shown in Figure 1.6.

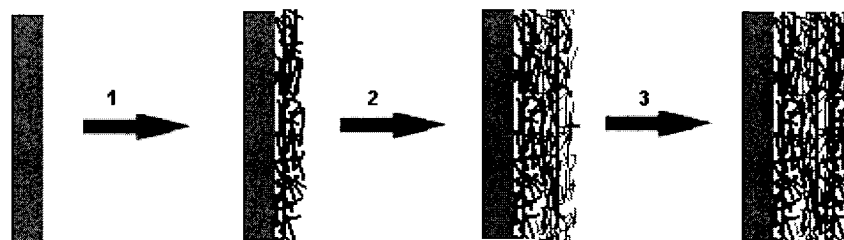


Figure 1.6 Schematic illustration of the LbL self-assembly process. Step 1 shows a positively charged substrate that adsorbed polyanion (blue) to its surface followed by rinsing the surface copiously with DI water and drying. Step 2 shows the polyanion modified surface adsorbing polycation (red) to its surface followed by rinsing with DI water and drying. Step 3 shows subsequent addition of polyanion to the polycation modified surface. This process can be repeated numerous times to achieve the desired number of layers.

The LbL process developed by Decher and coworkers has increased in popularity since its introduction. This is a result of the method's simplicity and the fact that polyelectrolytes as well as charged nanomaterials can be deposited in a controlled manner. This technique has been exploited to deposit polyelectrolyte layers on

colloidal micro/nanoparticles using passive adsorption of polyelectrolytes [40]. This technique is performed using the same steps as illustrated in figure 1.6: exposure of the surface to the polyelectrolyte solution, washing the surface free of any unbound polyelectrolyte and exposure of the surface to a polyelectrolyte of opposite charge. This process can also be repeated until the desired film properties are achieved. The only modification to the basic LbL scheme is the need to wash the colloids using several centrifugation/resuspension or filtration cycles to separate the unbound polyelectrolyte from the coated colloids. Also, there are some additional factors that must be considered when coating colloidal particles, such as aggregation of the particles instead of layer growth. To prevent aggregation, the particles are always added to a polyelectrolyte solution containing a large excess of polyelectrolyte. This technique has also been used to construct polymeric capsules by dissolving out the colloidal core template using chemical degradation. This technique has been used to produce a variety of capsules containing multiple functional groups for applications mainly in the field of encapsulation and drug delivery [40].

Another important extension of this technique is to fabricate films for in vivo repair of blood vessels [41], preparation of polymeric nanotubes [42], nanoscale reactors [43] micropatterning [44], membrane synthesis [45], drug delivery [46], photonics [43] and bio-composite film assembly [47]. In addition to the fabrication of the above materials, there is a significant amount of research being conducted on fabricating colloid functionalized substrates using LbL assembly. Using this technique a variety of nanoparticles such as: polystyrene [48], Au [49], Fe₃O₄ [50], CdS [51], etc.

have been incorporated into thin films. This idea of nanoparticle incorporation into thin films via the LbL process is especially important to the work that will be described in this dissertation.

1.2.3 Microcantilever Surface Modification via LbL

The LbL technique is able to provide a multiple thin layer on surface of any subject with different components and controllable thickness at the nanoscale. In microcantilever based chemical or biological sensors, surface modification is a key process to functionalize the microcantilever to various analyte species. Taking advantage of the LbL technique, Dr. Ji's group successfully developed a general method to modify the microcantilever surface for biological sensors [52, 53]. The basic idea behind this modification is to immobilize or embed a specific or highly specialized enzyme, which only catalyzes a series of specific bio-/chem- reactions, into the thin film through the LbL process on the cantilever surface. When the target species is present in the environment surrounding the modified microcantilever, the embedded enzyme will trigger the corresponding bio-/chem- reactions and the conformation of the enzyme will be changed during the reactions. The enzyme is a kind of protein and possesses its own specific structure. This structure changes when the enzyme functionalizes and contributes to the conformation change. This conformation change will generate a surface stress in the thin film and hence result in the cantilever deflection. This deflection or surface stress or the extent of conformation changing will reflect the concentration of the analyte species.

The general procedures for modification of a microcantilever surface through LbL are as follows. First, the gold surface of the microcantilever is treated with thiol compounds to introduce surface charges on the surface of the cantilever. Then, three or more multilayers, such as PEI/PSS, are paved through the LbL to provide a base for further processing based on the charge nature of the surface. Lastly, three or more multilayer containing enzyme molecules is subsequently deposited. For PEI/PSS, each bilayer is about 1-2 nm [53] and about 8 nm for PEI/GO_x [52]. The total thickness of the assembly is about several tens of nanometers. All of the whole procedures are illustrated in Figure 1.7.

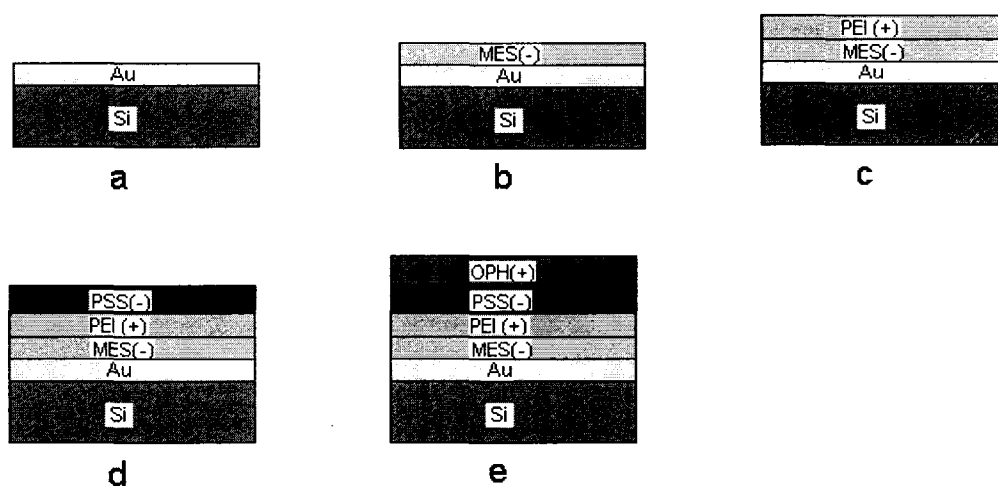


Figure 1.7 General procedures for LbL assembly with immobilized enzyme on the microcantilever. (a) gold coated microcantilever; (b), (c) a bilayer of mercaptoethane sulfonate (MES) and PEI subsequently self-assembles onto the gold surface. This process can be repeated several times as desired; (c), (d) a bilayer of PEI and PSS is further subsequently deposited. The process can be repeated several times as needed.

In practice, the modified LbL procedure specific for microcantilever surface modification used in glucose measurement is as follows [53]: (A) A monolayer of

MES was self-assembled on the gold surface of a microcantilever by immersing the microcantilever in a 5 mM MES solution for 12 hours and then rinsing with EtOH three times followed with deionized (DI) water three times. (B) The MCL was immersed in a PEI solution for 10 min and then rinsed with flowing water at a flow rate faster than 100 mL/min for 1 min. The microcantilever was then immersed in the opposite polyelectrolyte for 10 min, followed with another rinse with flowing water. C) This cycle was repeated several times until a desired number of multilayers was reached. The research results showed that the multilayer approach was a superior approach for microcantilever surface modifications for enzyme-based biosensor development. The bending mechanism investigation suggested that the conformational change of the GOx enzyme and the protonation to polymers on the microcantilever were the main reasons for the bending response of the GOx multilayer modified microcantilever.

1.3 Electrophoretic Deposition and Thin Film Formation

1.3.1 Electrophoretic Deposition and Its Advantages

Electrophoretic deposition (EPD) is a process in which the charged particles suspended in a liquid medium, such as a colloidal system or a sol solution, migrate under the drive of an electric field and deposit on an electrode to form a film on the surface of the electrode. This technique was discovered in 1809 [54] and initially was mainly applied in the deposition of ceramic particles (such as TiO₂, Al₂O₃, etc.) to provide a coating on the surface of various substrates. Recently, this technique has

been developed in film deposition from the latex of polymers, nanoparticles, etc [55, 56]. Figure 1.8 schematically illustrates this process [57].

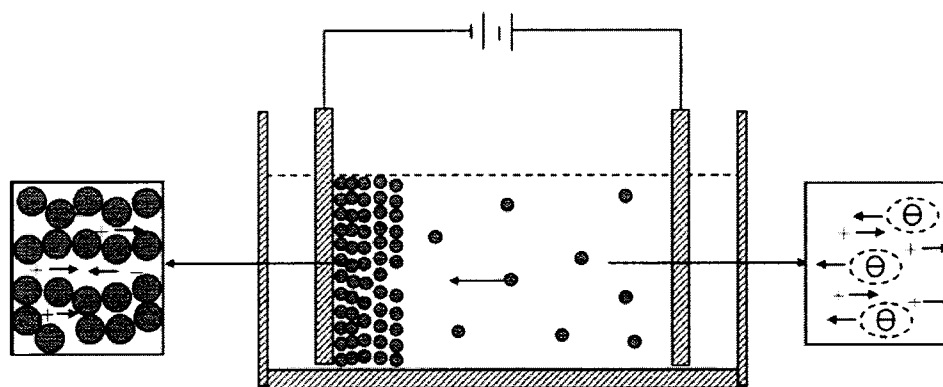


Figure 1.8 Schematic showing electrophoretic deposition [57].

Upon application of an external electric field to a colloidal system or a sol solution, the constituent charged nanoparticles or nanoclusters are set in motion in response to the electric field, whereas the counterions diffuse in the opposite direction. For a given suspension system, through the adjusting the strength of the applied electric field, film thickness and deposition rate can be controlled effectively in the process of electrophoretic deposition. If an electric field set up between the electrode and the substrate is uniform, for example, between two parallel electrodes, the film can be formed uniformly. Because of these characteristics, the EPD offers rigid control of film thickness, uniformity, and deposition rate and is especially attractive owing to its low cost equipment and starting materials. Due to the use of an electric field, electrophoretic deposition is particularly suited for the formation of uniform films on substrates of complicated shape, impregnation of porous substrates, and deposition on selected areas of the substrates.

1.3.2 Particle Surface Charge and Electric Double Layer

In general, suspensions can be dispersed by electrostatic, steric, or electrosteric stabilization mechanisms. The particles must be electrically charged to permit forming by electrophoretic deposition. The charge on a colloidal particle could originate from one or more of the following mechanisms: (1) preferential dissolution or (2) deposition of charges or charged species, (3) preferential reduction or (4) oxidation, and (5) adsorption of charged species such as polymers [57]. Development of a net charge at the particle surface affects the distribution of ions in the surrounding interfacial region, resulting in an increased concentration of counter ions close to the surface. Counter ions are those of opposite charge to that of the particle. Thus, an electrical double layer exists round each particle. Figure 1.9 schematically illustrates the electric double layer structure [57].

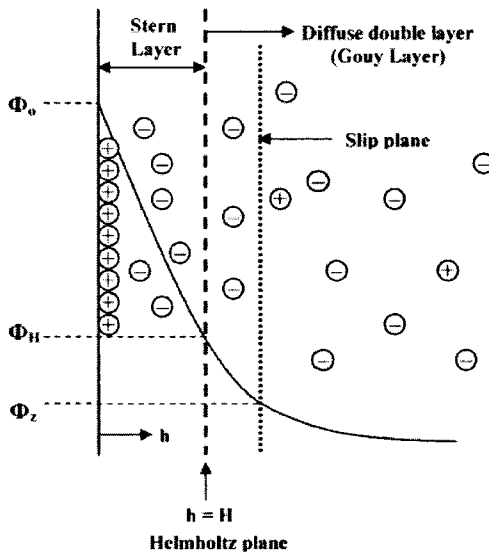


Figure 1.9 Schematic illustrating electrical double layer structure and the electric potential near the solid surface with both Stern and Gouy layers [57].

In the Figure 1.9, the surface charge of the particle is assumed to be positive. The liquid layer surrounding the particle consists of two parts: an inner region, called Stern layer and an outer region, called diffuse layer. Within this diffuse layer is an imaginary boundary known as the slipping plane, within which the particle acts as a single entity. In the Stern layer the ions are strongly bound and the electric potential near to the particle surface decreases linearly. In the diffusion layer the ions are less firmly associated and the electric potential decreases exponentially [57]. The surface charge density of particles is a function of the pH in the aqueous medium. Anna [58] and Chorom [59] investigated the effect of changing pH on the surface charge density of manganese oxides and clay particles in aqueous solutions with various electrolyte concentrations. The results showed that the particle surface charge decreased from positive charge at pH 3 to negative charge at pH 10 as pH increased and the electrolyte alleviated this changing trend to some extent [58]. It is believed that the electrical charge at the interface of metal oxide/electrolyte solution is formed as a result of the reactions of acid-base hydroxyl groups and due to complexation reactions of surface hydroxyl group with the background electrolyte ions [58]. Thus, when pH increases more protons are neutralized around the particle surface and more negative charge produces, resulting in the surface charge decrease. On the other hand, protons are given off if the particle adsorbs the electrolyte ions from the solution. Thus, the increase of the electrolyte concentration results in the increase of the charge density.

1.3.3 Parameters Effecting EPD

A suspension for EPD is a complex system since each component has a substantial effect on deposition efficiency. There are two principal types of solvents used in the EPD: water and organic solvents (such as alcohol, etc) [54]. Organic solvents are frequently used as a suspension medium in the EPD since the use of water-based suspensions can result in gas formation on the surface of both electrodes. The gases originate from the water electro-hydrolysis when the applied voltage is greater than the decomposing potential of water. The produced gases repel the deposition of the particles on the surface and no film could form.

The deposition rate not only depends on applied electric field as mentioned above, suspension concentration, zeta potential around the particles and electrophoretic mobility of particles also have effect on the deposit rate [54, 60-62]. The zeta potential is determined by several factors, such as the particle surface charge density, the concentration of counterions in the medium, solvent polarity and temperature. The zeta potential ξ can be described as [63]

$$\xi = \frac{Q}{4\pi\epsilon_r a(1+ka)} \quad (3)$$

with

$$k = \left(\frac{e^2 \sum n_i z_i^2}{\epsilon_r \epsilon_0 kT} \right)^{1/2} \quad (4)$$

where Q is the charge on the particle, a is the radius of the particle out to the shear plane, ε_r is the relative dielectric constant of the medium, and n_i and z_i are the bulk concentration and valence of the i th ion in the system, respectively.

The mobility of a particle, μ , in a colloidal dispersion or a sol solution is dependent on the dielectric constant of the liquid medium, ε_r , the zeta potential of the particle, ξ , and the viscosity of the fluid, η . The relationship between these parameters can be expressed in the next equation [63]

$$\mu = \frac{2\varepsilon_r\varepsilon_0\xi}{3\pi\eta} \quad (5)$$

Another element that may be considered with respect to the deposition rate is the ion strength of additives. In order to supply sufficient voltage between the electrodes and obtain high deposition rates, some amount of electrolyte or phosphate ester can be added into the system to achieve a certain potential distribution [64]. It was shown that uniformity and adhesion of the deposits can be improved by the use of electrolytes [65, 66].

1.4 Objectives and Organization of the Dissertation

The primary objective of this dissertation is to develop a simple and feasible approach to prepare a thin film on the surface of the microcantilever to set up a platform for the microcantilever as chemical and biological sensors through microcantilever surface modification.

Chapter one is an introduction to all the basic concepts, processes and techniques that are used through this dissertation. At the same time, a collection of

documents are viewed concerning these basic concepts, processes and techniques. Chapter two is a brief introduction to the techniques of scanning electronic microscope (SEM) and atomic force microscope (AFM) used in this dissertation. Chapter three describes the microcantilever surface modification through LbL process. The preparation of the multilayer thin film containing organophosphorus hydrolase and its application, as well as the effect factors in the measurement of organic phosphorus compounds, are reported and discussed in this chapter. Chapter four deals with the investigation on the possibility to form hydrogel films on the surface of the microcantilever through micro-, nano- hydrogel particles alternate deposition based on the LbL process. In this chapter, the synthesis of the micro-, nano-, hydrogel particles and their assembly on the silicon wafers is also discussed. Chapter five details the process and application of the hydrogel film preparation on the surface of the silicon wafers and microcantilevers through the electrophoretic deposition from the suspension of the micro-, nano- hydrogel particles. Chapter six is the final conclusions of the dissertation. Some suggestions regarding the research described in this dissertation are presented for future work.

CHAPTER TWO

INSTRUMENTATIONS

2.1 Atomic Force Microscope

2.1.1 Basic Principle

The atomic force microscope (AFM) was invented in 1986 by Binnig, Quate and Gerber [67] and is a new member of the family of scanning probe microscope, which forms images of surfaces using a physical probe that scans the specimen. Like all other scanning probe microscopes, the AFM employs a sharp probe and the surface image is obtained by mechanically moving the probe over the surface of a sample in a raster scan and recording the probe-surface interaction as a function of position. In the case of the AFM, the probe is a tip with a tip radius of curvature on the order of nanometers. The tip is microfabricated from silicon or silicon nitride on the end of a microcantilever. Figure 2.1 shows different shapes of the AFM tip that are commonly used.

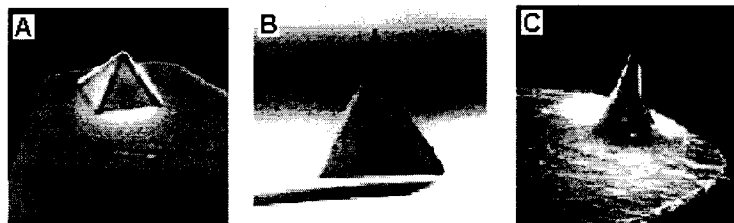


Figure 2.1(A-C) Three common types of AFM tip. (A) normal tip (3 μm tall); (B) supertip; (C) ultralever (3 μm tall) [68]

The microcantilever bends in response to the force between the tip and the sample and the cantilever bending can be sensitively detected by an optical lever technique. The diagram in Figure 2.2 illustrates how the optical lever technique works. In the diagram, an optical beam, usually a laser, is cast on the back side of the cantilever and the position of the reflected laser beam is monitored by a position-sensitive photodetector (PSPD). When the AFM tip scans the surface of a sample, the position change of the tip in the z-direction due to the different interactions between the tip and the sample produces a bending of the microcantilever, resulting in the position change of the reflected beam from the mirrored surface on the back side of the cantilever onto the PSPD. In this arrangement, a small deflection of the cantilever will tilt the reflected beam and change the position of beam on the photodetector. By measuring the difference signal from the PSPD, changes in the bending of the cantilever can be measured.

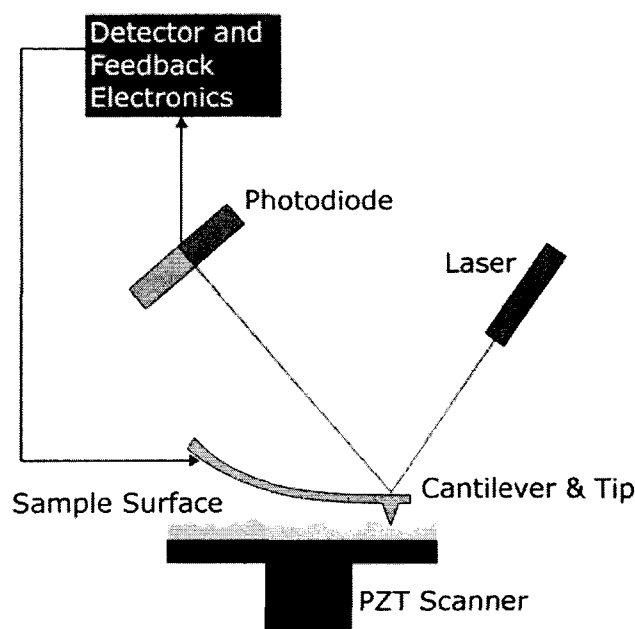


Figure 2.2 Block diagram of the atomic force microscope [69].

Since the bending of the microcantilever observes Hook's Law, the interaction force between the tip and the sample can be found. Depending on the situation, forces that are measured in the AFM include mechanical contact force, Van der Waals forces, capillary forces, chemical bonding, electrostatic forces, and magnetic forces etc. [69]. The movement of the tip or sample is carried out by a tube scanner made from piezo-electric ceramics that can precisely control the position (also see PZT scanner in Figure 2.2). The scanner is capable of sub-angstrom resolution in x-, y- and z-directions. The z-axis is conventionally perpendicular to the sample [70]. If the tip were scanned at a constant height, there would be a risk that the tip would collide with the surface, causing damage. Hence, in most cases a feedback mechanism is employed to adjust the tip-to-sample distance to maintain a constant force between the tip and the sample (also see Figure 2.2) [69].

2.1.2 Imaging Modes

The AFM can image several interactions simultaneously depending on the application. The manner of using these interactions to obtain an image is generally called a mode [71]. Generally, the AFM imaging modes fall into two categories: static modes or contact modes and a variety of dynamic modes.

Contact mode is the most common method of operation of the AFM. In this mode of operation, the static tip and sample remain in close contact, as the scanning proceeds, and tip deflection is used as a feedback signal. Because the measurement of a static signal is easily affected by noise and thermal drift that results from the friction between the tip and the sample surface when the scanning rate is relatively slow, low stiffness cantilevers are used to improve the deflection signal [69]. One of the other drawbacks of remaining in

contact with the sample is that there exist large lateral forces on the sample as the tip is "dragged" over the specimen [70]. On the other hand, the attractive forces between the tip and the sample surface can be very strong when the tip is brought into proximity of a sample surface, resulting in damaging the tip. Thus, static mode AFM is only employed in contact when the overall force between the tip and the sample surface is repulsive. In contact mode, the force between the tip and the surface is kept constant during scanning by maintaining a constant deflection [69].

In the dynamic mode, tapping mode is the next most common mode used in AFM. When operated in air or other gases, the cantilever is externally oscillated at or close to its resonant frequency (often hundreds of kilohertz) and positioned above the surface so that it only taps the surface for a very small fraction of its oscillation period [70]. The advantage of tapping the surface is improved lateral resolution on soft samples. Lateral forces such as drag, common in contact mode, dramatically reduced as the tip scans over the surface due to the very short contact time over the sample. When imaging poorly adsorbed samples on a substrate or soft samples, tapping mode may be a far better choice than contact mode for imaging [70].

2.1.3 AFM Resolution

Since AFM imaging is a three dimensional imaging technique, the concept of resolution in AFM is different from radiation or light based microscopy. Usually, lateral resolution is used in AFM. The lateral resolution is the ability to distinguish two separate points on an image. Usually the width of a DNA molecule is loosely used as a measure of resolution, because it has a known diameter of 2.0 nm in the B form [72]. One of the most important factors influencing the resolution in AFM is the apical probe or scanning

tip geometry [70]. There are four aspects from which the scanning tip has its influence on the image: a) broadening, b) compression, c) interaction forces and d) aspect ratio [73].

When the radius of curvature of the tip is comparable or greater than the size of the feature to be imaged, tip broadening occurs. Figure 2.3 illustrates this phenomenon. It can be seen from Figure 2.3, as the tip scans over the specimen, the sides of the tip make contact before the apex, and the microscope begins to respond to the feature. Thus, it is the radius of curvature that significantly influences the resolving ability of the AFM. Images of DNA made by the sharper tip have shown dramatic improvements in resolution widths [73].

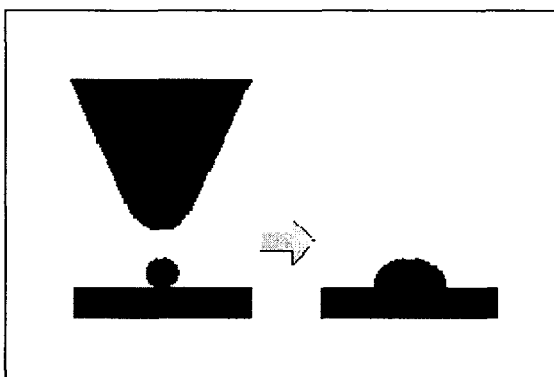


Figure 2.3 Tip broadening arises when the radius of curvature of the tip is comparable or greater than the size of the feature trying to be imaged [70].

When the tip is over the feature to be imaged, a compression or pressure exists between the tip and the sample. Although the force between the tip and the sample may only be nN, the pressure may be MPa. The studies on some soft biological polymers, such as DNA, have shown the apparent DNA width to be a function of imaging force [70]. The image contrast in AFM is produced by the difference of the interaction forces between the tip and sample. However, some changes may be resulted from a change in

force interaction and these changes may be perceived as being topographical. Forces due to the chemical nature of the tip are probably most important here, and selection of a particular tip for its material can be important. The aspect ratio of a particular tip is crucial when imaging steep sloped features. Electron beam deposited tips have been used to image steep-walled features far more faithfully than can be achieved with the common pyramidal tips. This effect has been shown very clearly in experiments on the degradation of starch granules by enzymes in the AFM [70]. Figure 2.4 illustrates this problem.

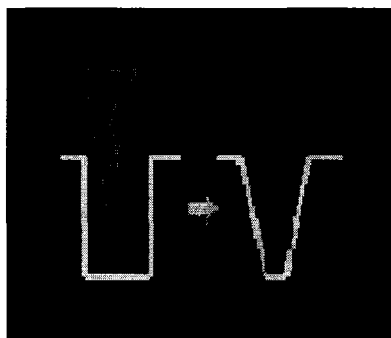


Figure 2.4 Aspect ratio of a particular tip is crucial when imaging steep sloped features [70].

2.1.4 AFM Characteristics

As a microscopic technique for imaging and measuring surface morphology, AFM has following characteristics [69].

- 1) AFM provides a true three-dimensional surface profile of a sample.
- 2) Most AFM modes can work in ambient air, liquid and vacuum.
- 3) Samples viewed by AFM do not require any special treatments.
- 4) AFM resolution in x-, y- direction is 2-10nm and in z-direction is 0.05nm.
- 5) The maximum AFM image size is $150 \times 150 \times 1 \mu\text{m}^3$.

2.2 Scanning Electron Microscope

2.2.1 Brief History

The scanning electron microscope (SEM) is a microscope that uses electrons, instead of light, to illuminate and create a three-dimensional image of a specimen with very high resolution. In 1935, M. Knoll along with other pioneers working in Germany in the field of electron optics firstly described the concept of the SEM. In 1942, the first SEM used to examine the surface of a solid specimen was described by Zworykin and colleagues, working in the RCA Laboratories in the United States. In 1948, Dennis McMullan and C. W. Oatley in Cambridge University further developed the instrument and built their first SEM [74]. The SEM now has become one of the most widely utilized instruments for materials characterization.

2.2.2 Basic Principle

In the SEM, the image is formed and presented by a very fine electron beam consisting of large amount of electrons. The electrons are emitted from a tungsten or lanthanum hexaboride (LaB_6) cathode [75], or electron gun, at high temperatures where thermal vibrational energy overcomes the electrostatic forces that hold electrons to the surface. The electrons are then accelerated towards an anode. The electron beam, which typically has an energy ranging from a few hundred eV to 100 k eV is focused by one or two electromagnetic condenser lenses into a beam with a very fine focal spot diameter of 0.4 nm to 5 nm [75]. The beam passes through pairs of scanning coils or pairs of deflector plates in the electron optical column, typically in the objective lens, which deflect the beam horizontally and vertically so that it scans in a raster fashion over a

rectangular area of the sample surface [75]. Figure 2.5 is a schematic diagram that shows the main SEM components and illustrates how a SEM works.

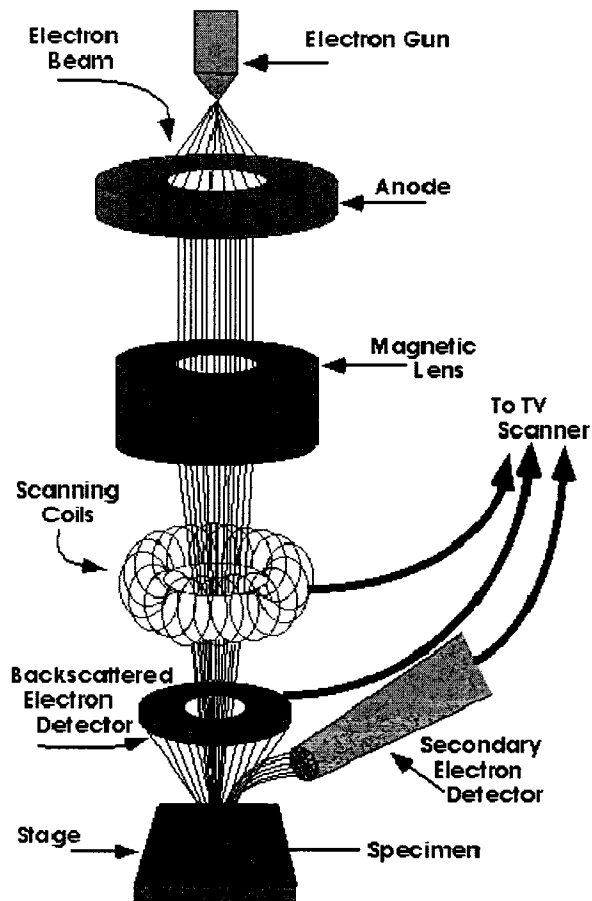


Figure 2.5 Schematic diagram illustrates how a scanning electron microscope works [76].

When the electron beam hits the sample within a very small area, the primary electrons from the electron beam collide with the electrons in the sample. Several things may happen to these primary electrons at any given moment. They may be elastically reflected from the specimen, with no loss of energy. They may be absorbed by the specimen and give rise to secondary electrons of very low energy, together with X-rays.

They may be absorbed and give rise to the emission of visible light. And they may give rise to electric currents within the specimen. All these effects can be used to produce an image [77]. Figure 2.6 schematically illustrates the electron-specimen interaction.

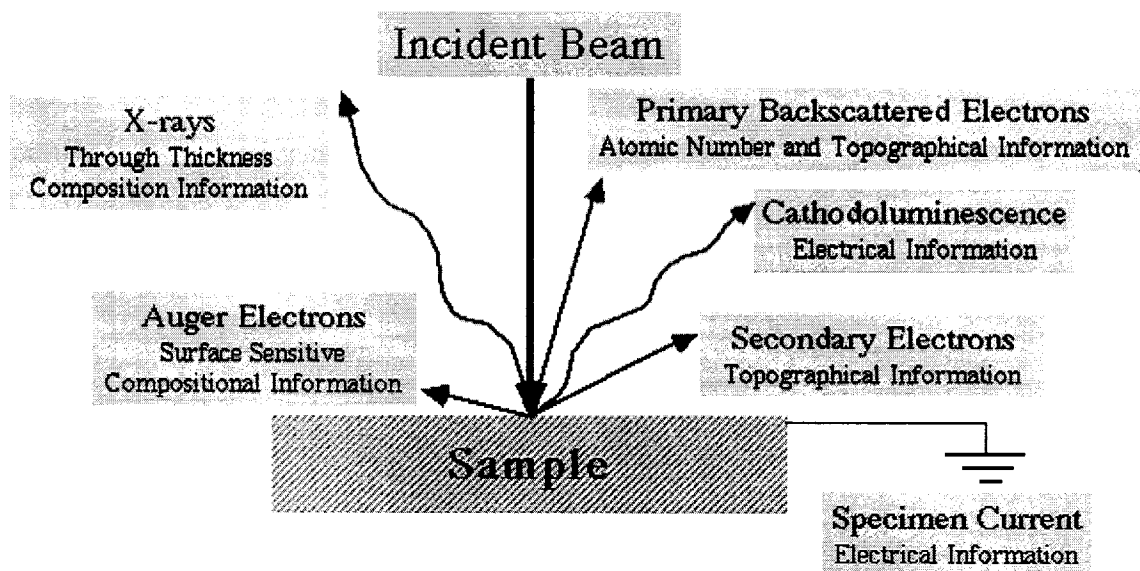


Figure 2.6 Schematic Diagram shows the electron-specimen interaction [76].

The most common imaging mode monitors low energy (<50 eV) secondary electrons. Due to their low energy, these electrons originate within a few nanometers from the surface. The electrons are detected by a secondary electron detector (also see Figure 2.5), which is a type of a scintillator-photomultiplier device, and the resulting signal is rendered into a two-dimensional intensity distribution that can be viewed and saved as a digital image. The brightness of the signal depends on the number of secondary electrons reaching the detector [75].

2.2.3 Energy Dispersive X-ray Spectroscopy

Energy dispersive X-ray spectroscopy (EDS) analysis is an additional function of modern SEM when it is fitted X-ray analysis equipment. As the electron beam of the SEM is scanned across the sample surface, it causes X-rays of characteristic wavelengths and energies to be emitted from the spot where the beam strikes the specimen. The energy of each X-ray photon is characteristic of the element which produced it. The EDS microanalysis system collects the X-rays, sorts and plots them by energy, and automatically identifies and labels the elements responsible for the peaks in this energy distribution [78]. The EDS data are typically compared with either known or computer-generated standards to produce a full quantitative analysis showing the sample composition. EDS identifies the elemental composition of materials imaged in the SEM for all elements with an atomic number greater than boron. Most elements are detected at concentrations of order 0.1% [78].

2.2.4 Sample Preparation

As the SEM image information is produced by the interaction of the primary electron beam and the specimen, a charge will tend to accumulate on the surface of the sample trying to be imaged at high voltages, if the sample is nonconductive or semiconductive. The accumulated electrons on the sample surface will greatly increase the intensity of the secondary electrons and result in the bright appearance of the specimen without any structural details. Thus, it is important to let these excessive electrons flow over the sample. This is typically achieved by coating sample surface with a few nanometers-thick layer of gold using a sputter coater [75]. The gold-coated sample is conductive and the excessive electrons can discharge without accumulation on the sample surface. There are

two concerns on the gold coating treatment. On one hand, since the secondary electrons originate within a few nanometers from the sample surface due to their low energy, gold coating on the sample surface will result in the loss of some information from the sample. On the other hand, it is difficult to remove the gold coating without damaging the sample. Thus, the gold coating is considered a semi-destructive process, though some special chemical process reported recently could remove the gold coating [75].

2.2.5 Resolution of the SEM

The resolution of the SEM can be defined as the ability to distinguish between two objects. So, it is also called spatial resolution. The spatial resolution of the SEM depends on the size of the electron spot, which in turn depends on the magnetic electron-optical system which produces the scanning beam [75]. The resolution is also limited by the size of the interaction volume, or the extent to which the material interacts with the electron beam. The spot size and the interaction volume both might be large compared to the distances between atoms, so the resolution of the SEM is not high enough to image individual atoms, as is possible in the transmission electron microscope (TEM). Depending on the instrument, the resolution can fall somewhere between less than 1 nm and 20 nm [75].

CHAPTER THREE

ORGANOPHOSPHORUS HYDROLASE

MULTILAYER MODIFIED MICRO-

CANTILEVERS AND ORGANO-

PHOSPHOUS DETECTION*

3.1 Introduction

All nerve agents belong to the family of organophosphorus (OP) compounds, which are among the most toxic of known substances. The toxicity of these compounds arises from their irreversible binding to acetylcholinesterase that is essential to nerve impulse responses [79]. Besides nerve gases, many pesticides also belong to the organophosphorus compound group. In an effort to feed the growing world population, the agriculture industry has increasingly taken the assistance of pesticides to increase the crop yield by fending off pest infestation. Their widespread use in agriculture may contaminate drinking water.

The threats posed by nerve gases and other OPs have made them important targets for detection. Analytical methods employed have included gas and liquid chromatographic methods with a variety of detection systems, e.g., mass spectrometry [80], and atomic emission spectroscopy [81]. However, most of these methods require

*The discussion in this Chapter was reproduced from *Biosensors and Bioelectronics* 22 (2007) 2636-2642, coauthored by Chandana Karnati, Hongwei Du, etc., with authorization from Dr. Haifeng Ji.

instrumentation that is not only practically non-portable but also quite expensive and very complex, which is not well suited to the field analysis of multiple samples. There are numerous optical and electrochemical methods [82-85] used for detecting and identifying OP agents. More novel methods include ion mobility spectrometry [86], immunoassays [87], fiber optic microsphere array [88], and surface acoustic wave (SAW) technology [89, 90], etc. Many of these are excellent methods for the purpose of real-time in-field analysis. However, the cost of most of these systems makes them impractical for placement in multiple sites. Recent advances in the field of micro-electro-mechanical systems (MEMS) and their uses offer unique opportunities for the design of cost-effective analytical methods. In 1994, it was realized that microcantilevers (MCLs) could be made extremely sensitive to chemical and physical changes [91-93]. MCLs can be mass produced through a typical lithography process, and can be readily integrated into a micro-electro-mechanical system (MEMS). To date, extremely sensitive chemical vapor sensors based on MCLs have been demonstrated using selective coatings on the cantilever. Examples include molecular beam [85], alcohol [94], mercury [95, 96], mercaptans [97], relative humidity [95, 96], Cs^+ [98], DNA [99], antigen-antibody interactions [100], etc. Requirements such as sensitivity, small size, low cost, and simultaneous detection of multiple species make the MCL sensor approach very attractive.

The unique characteristic of MCLs is their ability to deflect due to molecular adsorption- or binding-induced change in surface tension. These binding processes cause changes in surface stress on the MCL, which produces the upward or downward bending of the MCL. By recording the deflection magnitude or thermodynamics of the MCL, the

concentration of target biological or chemical species can be measured. This characteristic of MCLs qualifies them for detecting species both in air and solution. From molecular point of view, the binding or adsorption result in electrostatic repulsion [97] or attraction [101], steric effects [102], and intermolecular interactions [103] between molecules on the cantilever surfaces that alter the surface stresses on the cantilever. This is achieved by confining the adsorption to one side of the MCL. The key to MCL sensor development is to choose appropriate coatings for identification of specific chemical species.

Cu^{2+} complexes and acetylcholinesterase (AChE) [104] have been used for selective and sensitive recognition of OPs. These recognition agents are generally used to develop one-time-use, disposable sensors for environmental characterization. These sensors cannot be readily regenerated due to their strong complexation with the phosphonyl group. Organophosphorus hydrolase (OPH), on the other hand, can be used for continuous monitoring of OPs in the environment. Biosensors based on OPH have been reported recently for the detection of pesticides and nerve agents [83, 84, 105-107]. The foundation of these devices is the hydrolysis of OPs, producing two protons, catalyzed in a highly specific manner by OPH. The total reaction can be expressed in the Figure 3.1.

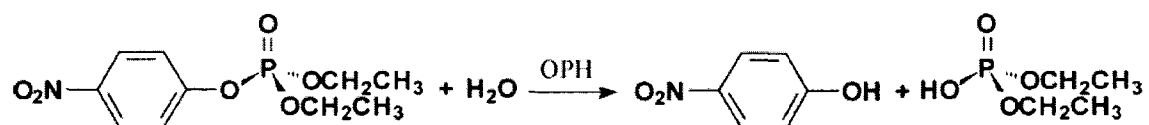
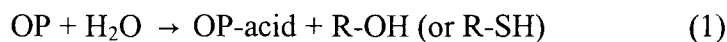


Figure 3.1 Total reaction of the OP hydrolysis by the OPH.

The reaction can be simply written as:



For example, methyl paraoxon can be hydrolyzed by OPH to diethyl phosphate (DEP) and *p*-nitrophenol (PNP) while releasing two protons. The reaction process can be expressed as shown in Figure 3.2 [106]. The resulting decrease in pH has been monitored and correlated to OPs concentration for constructing a potentiometric enzyme electrode. Other biosensors based for the detection of *p*-nitrophenol by amperometry and fiber optics have also been reported.

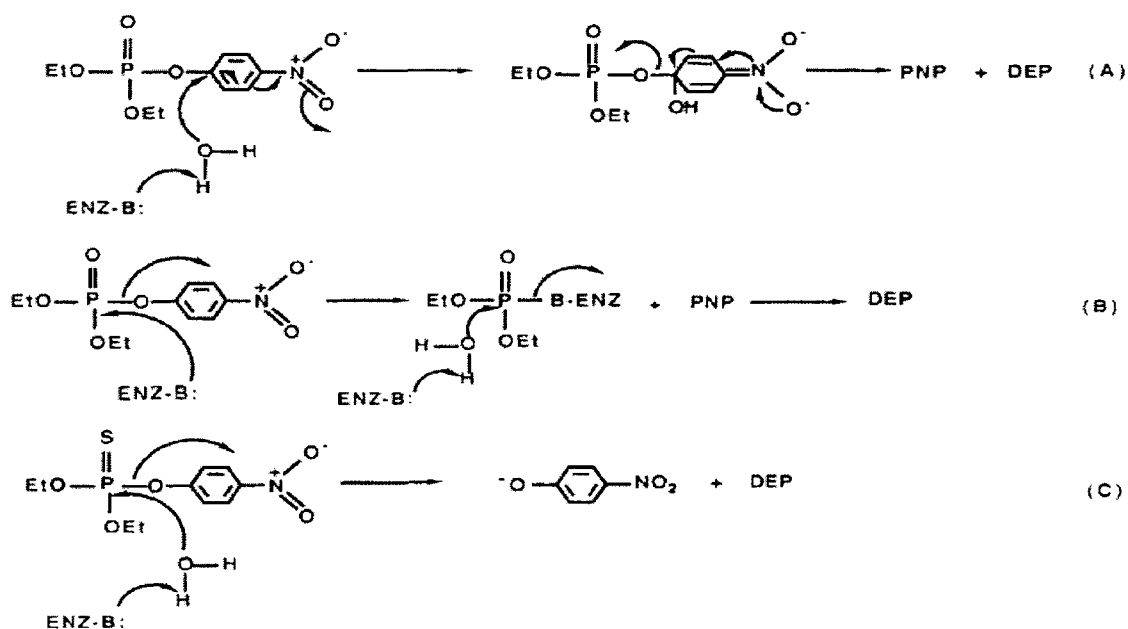


Figure 3.2 Reaction process of the OP hydrolyzed by the enzyme.

Molecular recognition agents can be assembled or covalently linked to one side of the microcantilevers. Modification of the MCLs has been realized by self-assembled monolayers (SAMs) [97, 98], polymers [94, 108, 109], sol-gels [110], and hydrogels [111-113], etc. Recently, we introduced the nanoassembled Layer-by-Layer (LBL) approach for MCL modification [114]. The Layer-by-Layer technique, which was developed in 1993 [115], allows the formation of ultrathin, organized films on any surface through the alternate adsorption of oppositely charged components, such as linear polyions and enzymes, primarily via electrostatic attraction [116-119]. It is a simple modification process with nanoscale control of the film thickness. The required component could be positioned at a desired location in the film with nanometer precision. In this chapter, we described an OPH multilayer modified MCL for the detection of OPs. The principle of detection is based on the deflection of the MCL due to the change in the film network mesh size upon the hydrolysis of OPs by the immobilized OPH. Unlike the earlier MCL-based sensors for OPs that were single use the OPH-based MCL are reusable.

3.2 Experimental

3.2.1 Materials

In this experiment, commercially available silicon microcantilevers (Veeco Instruments, Santa Barbara, CA) were utilized. The dimensions of the V-shaped silicon MCLs were 180 μm in length, 25 μm in leg width, and 1 μm in thickness. One side of these cantilevers was covered with a thin film of chromium (3 nm) followed by a 20-nm layer of gold, both deposited by e-beam evaporation. Since the gold film does not stick

well to SiO_2 , the thin chromium layer was used to improve adhesion. On the uncoated side of the commercial microcantilever is silicon with a 12–19 Å thick naturally grown SiO_2 layer, which is called “native oxide”. The shape of the MCL used in this work is shown in Figure 3.3.

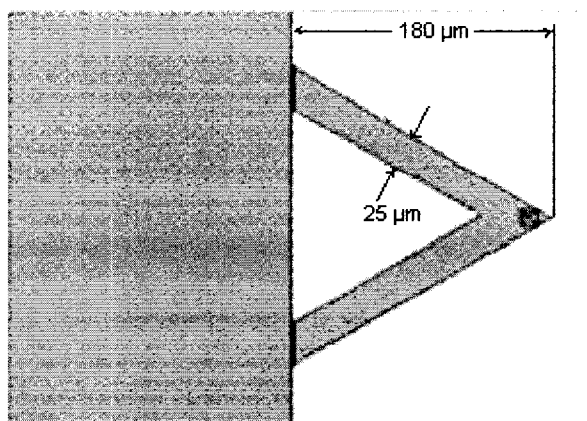


Figure 3.3 Top view of MCL (Veeco Instruments, Santa Barbara, CA) used in this experiment.

Wild type OPH was expressed and provided by University of California, Riverside. The detailed method for OPH expressing was described in the related literatures [83, 84]. Sodium salt of 2-mercaptoethane sulfonic acid (MES), PSS (Mw = 70,000, powder), paraoxon, parathion, and diisopropyl fluorophosphates (DFP) were used as received from Sigma–Aldrich. Polyethyleneimine (PEI, 14%, Mw = 25,000, $\rho = 1.043$) was a donation from Max Planck Institute, Germany. A 1×10^{-2} M MES solution was prepared in ethanol. All other solutions were prepared in a 0.01M and pH=7 phosphate buffer (an additional 0.05×10^{-3} M CoCl_2 in OPH solution).

3.2.2 Deflection Measurement

The deflection experiments were performed in a flow-through glass cell (Digital Instruments, Santa Barbara, CA) similar to those used in atomic force microscopy (AFM). The MCL was immersed in the 0.01M phosphate buffer (pH=7.0) solution. For continuous flow-through experiments, the buffer solution was initially circulated through the cell using a syringe pump. A schematic diagram of the apparatus used in this study is presented in Figure 3.4 [120].

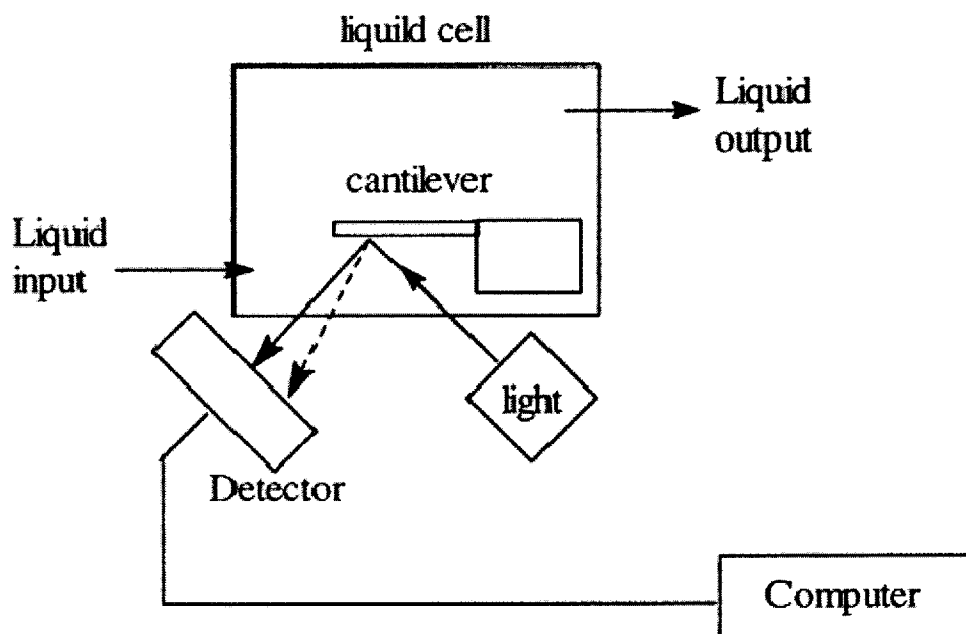


Figure 3.4 Schematic diagram of the apparatus used in the study [120].

A constant flow rate was maintained during each experiment. Experimental solutions containing different concentrations of paraoxon were injected directly into the flowing fluid stream via a low-pressure injection port sample loop arrangement with a loop volume of 2.0 ml. This arrangement allows for continuous exposure of the cantilever

to the desired solution without disturbing the flow cell or changing the flow rate. Since the volume of the glass cell, including the tubing, was only 0.3 ml, a relatively fast replacement of the liquid in contact with the cantilever was achieved. Microcantilever deflection measurements were determined using the optical beam deflection method. The bending of the cantilever was measured by monitoring the position of a laser beam reflected from the gold-coated side of the cantilever onto a four-quadrant AFM photodiode. We define bending toward the gold side as “bending up” and towards silicon side as “bending down”. In case adsorption occurs on the gold surface, the downward bending is usually caused by repulsion or expansion of molecules on the gold surface, which is called compressive stress; conversely, the upward bending is caused by attraction or contraction of molecules on the gold surface, which is called tensile surface stress. The cantilever was immersed in the buffer solution until a baseline was obtained and the voltage of the position-sensitive detector was set as background corresponding to 0 nm. Cantilever based detection systems are prone to drift problems. We observed similar drifting problems in these experiments. The drifting problem, however, was alleviated after equilibrating the prepared cantilevers in the buffer solutions for one hour. Typically, a good baseline (<4 nm noise) was obtained in one to two hours after equilibrating the cantilevers in the buffer solutions. In these experiments, we injected the sample after a good baseline was obtained.

3.2.3 Microcantilever Layer-by-Layer OPH Surface Immobilization Process

The electric charge of a polyelectrolyte in a solution depends on the isoelectric point (pI) of the polyelectrolyte and the solvent. At pH 7.0, the OPH is a positively

charged polyelectrolyte (the pI of OPH is 8.0) [106].

Since microcantilever bending is generated from adsorption induced surface stress from one side of the microcantilever, the key to surface modification technology is to control the formation of multilayers on only one surface of the microcantilever by choosing appropriate surface materials. In a typical multilayer formation procedure, the substrate is alternately dipped into a polycation and polyanion solution, and the process is repeated several times for multilayer formation. When this procedure was applied, multilayer nanoassembly film formation was found on both sides of the cantilever. Recently, we reported a modified multilayer growing process [121] taking advantage of hydrophobic/lipophobic properties of the perfluorocarbon materials. In this method, (tridecafluoro-1,1,2,2-tetrahydrooctyl)triethoxysilane (TTS) was used to develop a thin perfluorocarbon monolayer on a silicon surface using a typical silicon surface modification procedure, and the polymeric multilayers were found only on the gold surface of the MCL.

The modified LbL procedure specific for MCL surface modification used in this experiment is as follows: (A) A microcantilever was immersed in Piranha solution, 4:1 H₂SO₄: H₂O₂, for about two min to remove any organics from the microcantilever surface (Caution: Piranha solutions react violently in the presence of many organic compounds and should be handled with extreme caution). Next, the microcantilever was rinsed copiously with H₂O then copiously with 95% ethanol. (B) A monolayer of MES was self-assembled on the gold surface of the MCL by immersing it in a 5 mM MES aqueous solution for 12 hours, and then rinsing with deionized (DI) water three times. (C) The MCL was immersed in a 1.5 mg/mL of PEI solution for 10 min and then rinsed with

flowing water at a flow rate equal or faster than 1 mL/s for 1 min. The MCL was then immersed in the 3.0 mg/mL oppositely charged polyelectrolyte (PSS in these experiments) for 10 min, followed with another rinsing with flowing water. (D) This cycle was repeated several times until a desired number of multilayers were reached.

This modified multilayer formation was applied to all the MCLs used in these experiments. In the case of enzymemodified MCL, the cantilever was first coated with three bilayers of PEI/PSS to provide a solid base followed by three bilayers of OPH/PSS. The enzyme monolayer was formed by immersing the MCL in an OPH enzyme solution (4 mg/mL of OPH) for 10 min followed by rinsing in flowing DI water. The process was continued until three bilayers of OPH/PSS were formed on top of the PEI/PSS base. Each PEI/PSS bilayer was about 1–2 nm in thickness [98]. Although the OPH/PSS bilayer thickness was not determined, based on the dimension of the OPH it is expected that the thickness was approximately 8 nm. Thus, we assume the thickness of the (OPH/PSS)₃ layer was approximately 25 nm.

3.3 Results and Discussion

3.3.1 Relationship between Deflection Amplitudes and the Concentrations of Paraoxon

Figure 3.5 (A-C) shows the bending response of an OPH multilayer modified MCL to various concentrations of paraoxon. The MCL deflection was fully reversible and increased as the concentrations of paraoxon increased. The detection limit was approximately 10^{-7} M. This is an order of magnitude better than the OPH-based potentiometric and optical biosensors that also measured the pH modulation [122].

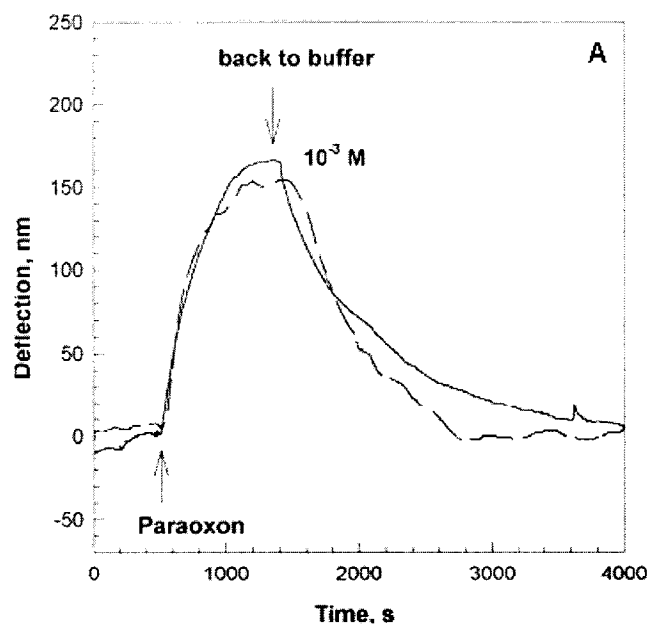


Figure 3.5(A) Dynamics of bending amplitude for a freshly-made (PSS/OPH)₃ modified MCL (solid line) and a (PSS/OPH)₃ multilayer modified MCL (dashed line) after storing in a dry state in the refrigerator at 4°C for 2 months upon exposed to 10⁻³ M paraoxon in 0.01 M phosphate buffer (the injection point is indicated with arrows).

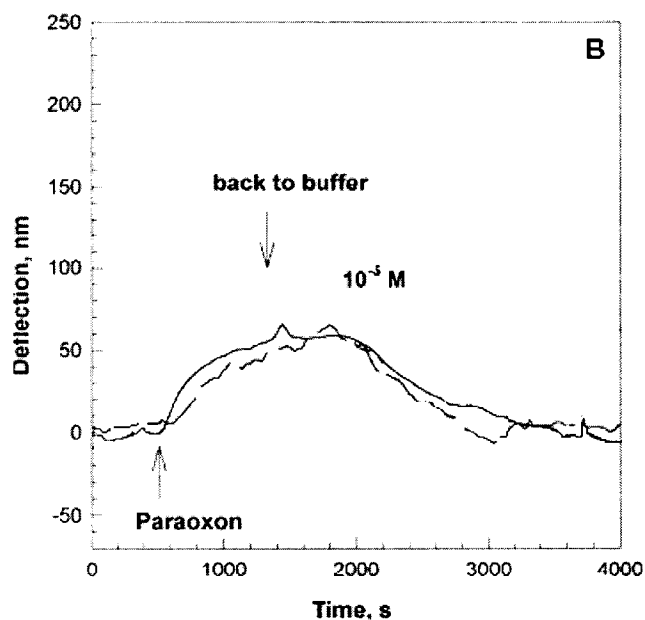


Figure 3.5(B) Dynamics of bending amplitude for a freshly-made (PSS/OPH)₃ modified MCL (solid line) and a (PSS/OPH)₃ multilayer modified MCL (dashed line) after storing in a dry state in the refrigerator at 4°C for 2 months upon exposed to 10⁻⁵ M paraoxon in 0.01 M phosphate buffer (the injection point is indicated with arrows).

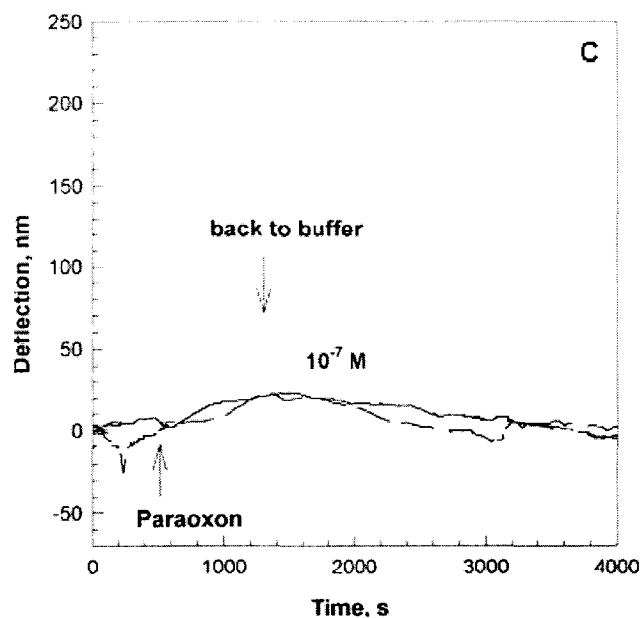


Figure 3.5(C) Dynamics of bending amplitude for a freshly-made (PSS/OPH)₃ modified MCL (solid line) and a (PSS/OPH)₃ multilayer modified MCL (dashed line) after storing in a dry state in the refrigerator at 4°C for 2 months upon exposed to 10⁻⁷ M paraoxon in 0.01 M phosphate buffer (the injection point is indicated with arrows).

3.3.2 Deflection Profiles of Microcantilevers upon exposure to paraoxon

Figure 3.6 shows the maximum deflection was a function of the paraoxon concentration and had a wide dynamic range. As shown in the insert of Figure 2.6, repeat exposure of a MCL to a 10⁻³ M solution of paraoxon caused similar deflection amplitudes. The standard error for the three measurements was within 5%, thus demonstrating good sample-to-sample reproducibility. Exposure of a 10⁻³ M solution of paraoxon to five different MCLs prepared under the same conditions also caused similar deflection amplitudes and the standard error was within 15% indicating an acceptable MCL-to-MCL reproducibility. The MCLs bent up showing the multilayer film shrunk upon exposure to paraoxon. Control experiments were performed by exposing a

(PSS/PEI)₆ modified MCL to a 10⁻³ M solution of paraoxon. No deflection of the cantilever was observed (also shown in Figure 3.6 insert).

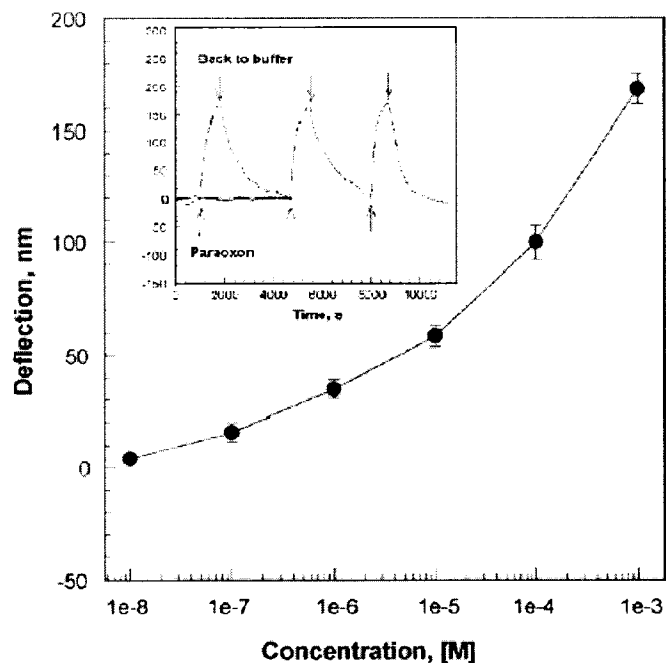


Figure 3.6 Correlation between maximum bending amplitudes of a (PSS/OPH)₃ modified MCL and paraoxon concentration in a 0.01 M phosphate buffer. Insert: Three replicates (dashed line) of bending responses as a function of time for a (OPH/PSS)₃ multilayer modified MCL following injection of a 10⁻³ M paraoxon in 0.01M phosphate buffer (the injection point is indicated with arrows) at 4.5 mL/h flow rate. Control experiments were performed by exposing a (PSS/PEI)₆ modified MCL to a 10⁻³ M solution of paraoxon (solid line).

3.3.3 Stability of the OPH-modified Microcantilever

The OPH-multilayer modified MCLs demonstrated excellent stability for more than 2 months when stored in a dry state at 4 °C as evidenced by similar profiles and bending amplitude (Figure 3.5). However, the OPH activity was lost in less than 2 weeks when the multilayer film modified MCL was stored in the buffer solution at room temperature.

3.3.4 Thermodynamic and Equilibrium Study of Multilayer Shrinking

Recently, Thundat and coworkers [123] and our group [114] have concluded that the enthalpy change of the enzymatic reaction does not contribute to the deflection of the MCLs. The possible contributions to the MCL bending include pH change and the conformational change of the enzymes. In order to interpret the mechanism of the enzymatic reaction induced stress on the MCLs at the molecular level, we studied the thermodynamics and kinetics of the MCL response to paraoxon catalyzed paraoxon hydrolysis and correlated it with changes in the bending response of the MCL. The following provides the details of this investigation.

3.3.4.1 OPH amount in OPH/PSS bilayer- modified microcantilever

The MCLs used in these experiments were V-shaped SiO₂ microcantilevers that have dimensions of 180 μm × 38 μm × 1 μm and a layer of 20 nm gold on one surface. The MCL surface area was 1.12 × 10⁻² mm². Assuming the thickness of the (OPH/PSS)₃ multilayer film was approximately 25 nm, the volume of the (OPH/PSS)₃ film was approximately 2.8 × 10⁻¹³ L. Based on the molecular weight of 68.8 kDa for OPH dimer and the reported density of 267 ng/0.586 cm³ or 0.456 μg/cm³ corresponding to 6.63 × 10⁻¹² mol/cm³ or 7.43 × 10⁻¹⁶ mol on the MCL surface for the OPH/PSS layers [89], the concentration of the OPH in the multilayer film was calculated to be 2.65 × 10⁻³ M.

3.3.4.2 OPH Catalyzed Paraoxon Hydrolysis Reaction Velocity

Consider the OPH-catalyzed reaction to follow Michaelis–Menten model represented by the following equation [89]:

$$\text{velocity (ms}^{-1}\text{)} = \frac{V_{\max} [\text{OP}]}{[\text{OP}] + K_m^{\text{OP}}} = \frac{k_{\text{cat}} [\text{enzyme}] [\text{OP}]}{[\text{OP}] + K_m^{\text{OP}}} \quad (2)$$

where V_{\max} is the maximum reaction rate (i.e. at saturation) and K_m^{OP} is the substrate concentration at which half the maximum velocity rate occurs. V_{\max} can be expressed as a function of the total enzyme concentration and the irreversible forward rate of reaction (k_{cat}). Additionally, we assume that at equilibrium the paraoxon concentration inside the multilayer film was constant and was equal to the concentration of paraoxon injected; this assumption was reasonable because of the very small film thickness (~25 nm), the high diffusion constant of paraoxon, and the fast liquid flow rate (0.4 mm/s) over the MCL surface. Further, based on the report by Lee et al. [117] that the kinetic parameters of OPH in multilayers were close to those in solutions, we used the values of kinetic parameters for OPH in solution, $k_{\text{cat}} = 1.5 \times 10^4 \text{ s}^{-1}$ and $K_m = 0.12 \text{ mM}$ reported by diSioudi et al. [124]. Solving Equation (2) with the above assumptions the theoretical/predicted OPH catalyzed paraoxon hydrolysis velocity in the OPH/PSS bilayer of the MCL as a function of paraoxon concentration was determined (Figure 3.7).

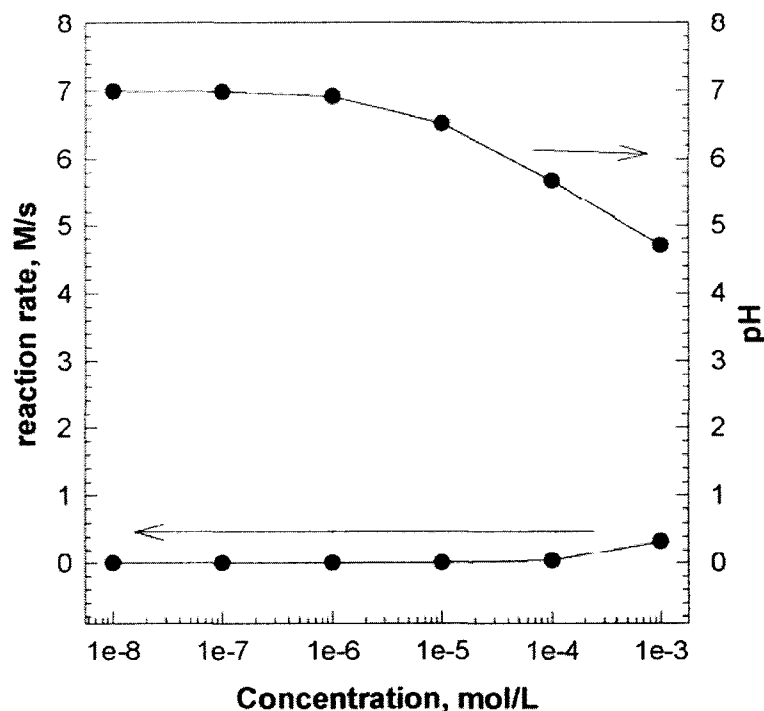


Figure 3.7 The calculated/predicted paraoxon hydrolysis rate (y-axis on the left) according to equation (2) in a (PSS/OPH)₃ film on the modified MCL and the resultant pH (y-axis on the right) in the (OPH/PSS)₃ multilayer film on the modified MCL as a function of paraoxon concentration.

3.3.4.3 pH versus Paraoxon Concentration Profile

The OPH catalyzed hydrolysis of paraoxon produces *p*-nitrophenol (PNP) and *O,O*-diethyl phosphoric acid (DEP), that are responsible in lowering the pH inside the multilayer film and changing the structure of the multilayer film. The formation rate of *O,O*-diethyl phosphoric acid or *p*-nitrophenol on the MCL surface can be expressed as

$$\frac{\partial P}{\partial t} = V - D_p \frac{\partial^2 P}{\partial t^2} \quad (3)$$

where P is the concentration of products, D_p the diffusion constant of phosphoric acid or p -nitrophenol in the (OPH/PSS)₃ multilayer film, and V is the reaction rate described above. At steady state, $\partial P/\partial t = 0$, therefore

$$D_p \frac{\partial^2 P}{\partial t^2} = V \quad (4)$$

The diffusivity of organic compounds through the multilayers (10^{-8} cm²/s) is generally two orders of magnitude smaller than in water [125, 126]. For instance, the diffusion constants for ascorbic acid (D_A) in a multilayer film is 4.7×10^{-8} cm²/s compared to 5.8×10^{-6} cm²/s in water [108]. No diffusion constant of *O,O*-diethyl phosphoric acid and p -nitrophenol in the OPH/PSS multilayer film has been reported, however, these constants can be estimated using the Stokes–Einstein equation [127]:

$$\frac{D_1}{D_2} = \left(\frac{M_2}{M_1} \right)^{1/3} \quad (5)$$

According to this equation, similar molecular weight compounds, such as ascorbic acid ($M_A = 176$ g/mol), *O,O*-diethyl phosphoric acid ($M_P = 154$ g/mol), and nitrophenol ($M_N = 139$ g/mol), will have a similar diffusion constant. Using equation (5), the diffusion constant of *O,O*-diethyl phosphoric acid (D_P) and 4-nitrophenol (D_N) were calculated to be 5.14×10^{-8} and 5.05×10^{-8} cm²/s, respectively. Solving equation (4) gave the concentration of diethyl phosphoric acid and 4-nitrophenol in the multilayer film on

the MCL surface at equilibrium as a function of the paraoxon concentration injected. The pK_a of diethyl phosphoric acid and 4-nitrophenol are 2.0 and 7.0, respectively. The concentration of protons (in the form of pH) versus the concentration of paraoxon injected was then calculated and is shown in Figure 3.7.

3.3.4.4 Effect of pH on Cantilever Bending

In order to determine the effect of pH on MCL bending, (OPH/PSS)₃ multilayer modified MCLs were exposed to different pH 0.01 M phosphate buffer. As shown in Figure 3.8, changing the MCL environment pH from 7 to 4 produced ~30 nm deflection only. This deflection is much less than the amplitude of the MCL bending upon exposure to paraoxon (Figure 3.6), suggesting that pH change was not the only contribution to MCL bending.

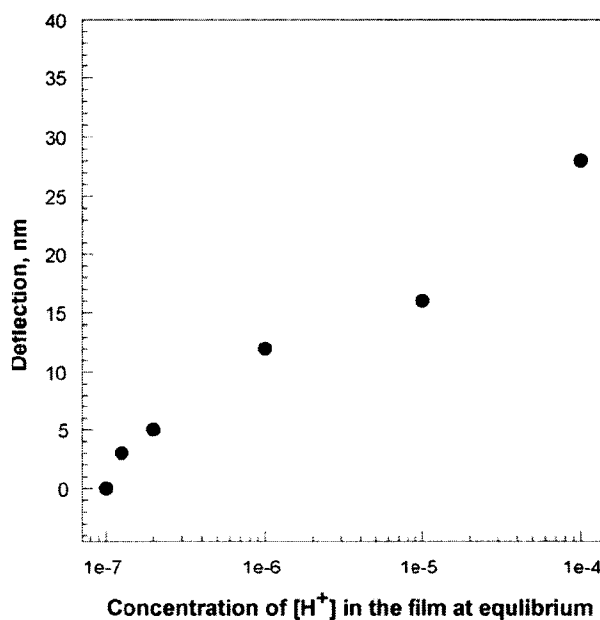


Figure 3.8 Maximum bending responses for a (OPH/PSS)₃ modified MCL after injection of a 0.01 M phosphate buffer with different $[H^+]$ (pH) at 4.5 mL/h flow rate. The MCL was pre-equilibrated in a 0.01M buffer solution with pH 7.0.

3.3.5 Conformational Change of the OPH Enzyme

OPH is a dimeric bacterial protein with a molecular weight of approximately 70 kDa. The corresponding dimensions of the dimer are $90\text{\AA}\times 56\text{\AA}\times 40\text{\AA}$ [110]. Since the OPs in these experiments were electrically neutral, the possible bending mechanism based on the absorption induced electrostatic repulsion or attraction between OPs and OPs with OPH or PSS can be ruled out. Steric effects and intermolecular interactions between OPs were too weak to contribute to the surface induced stress changes on the cantilevers because of the long-distance between two OPH-bound OPs. Recently, the conformational changes of OPH in multilayer film upon exposure to paraoxon have been investigated by Leblanc and coworkers [106, 129-133]. Using circular dichromism (CD) measurements, it was determined that in the presence of paraoxon the β -strand of OPH increased from 3.37% to 17.33%. This was attributed to the binding of paraoxon with OPH. Based on the above results, it is more likely that the conformational change of OPH upon binding of paraoxon and the subsequent interactions between OPHs and OPH with PSS plays a major role in the multilayer film volume change and the consequent bending response of the MCLs.

3.3.6 Response to Other OPs

It is known that wild-type OPH has higher selectivity towards paraoxon than other OPs, such as parathion and DFP. For instance, the $k_{\text{cat}}/K_{\text{M}}$ value of OPH for DFP is four-orders of magnitude lower than that for paraoxon [124]. MCLs' responses to parathion and DFP were measured and the results showed the expected smaller amplitude

and slower bending rate response of the OPH-multilayer modified MCLs (Figure 3.9) than that of paraoxon.

It was also noticed that after the parathion or DFP were fluxed out from the fluid cell, the MCL kept bending up for the next 400 s before bending back. One possible explanation of this phenomenon is a relatively slower post-binding conformational change of the OPH, supporting the proposed OPH conformational change of induced mechanism for MCL bending. It is possible to obtain the binding constants of these OPs with OPH using MCL bending dynamics. These phenomena merit further investigation in the future.

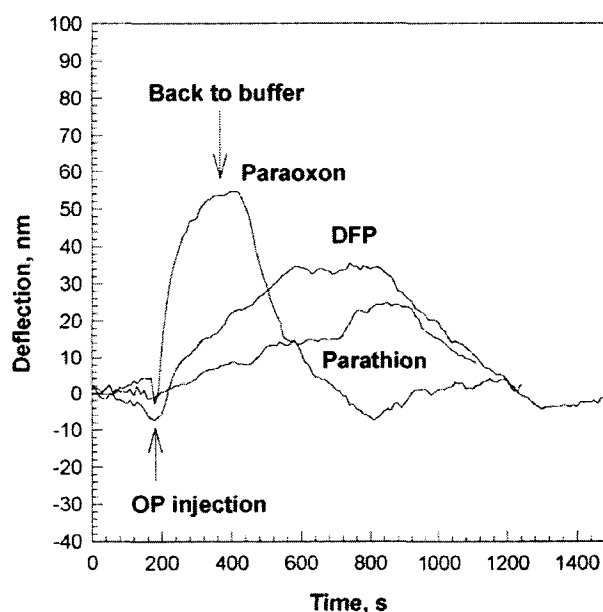


Figure 3.9 Bending responses as a function of time for a (OPH/PSS)₃ modified MCL upon exposure to 10^{-3} M paraoxon, parathion, and DFP at 40 mL/h flow rate. At this flow rate, the OPs flux through the fluid cell in 3 min. The MCL may not reach its maximum bending in this time scale.

3.4 Conclusions

OPH was immobilized on the MCL surface using Layer-by-Layer nano-assembly technology for OPs detection. The detection limit for paraoxon was approximately 10^{-7} M. This is an order of magnitude better than the OPH-based potentiometric and optical biosensors that measured the pH modulation. The multilayer modified MCLs responded to paraoxon, parathion, and DFP at different bending amplitude and bending rate. The bending mechanism investigation suggests that the conformational change of the OPH may be the primary contributor of the MCL bending. The results also suggest that research in molecular biology to increase the first binding constant of the OP to OPH could be a new strategy to improve the sensitivity of enzyme based biosensors. This strategy would make it possible to develop a sensor with both high sensitivity and continuous monitoring of target molecules.

CHAPTER FOUR

MICRO/NANO HYDROGEL PARTICLE

ASSEMBLY ON THE SURFACE OF

SILICON AND MICRO-

CANTILEVER VIA LbL

4.1 Introduction

Microcantilevers have proven to be an outstanding platform for chemical and biological sensors [134]. One unique characteristic of microcantilevers is their ability to undergo bending due to a molecular or binding-induced change in the surface tension. This is achieved by confining the adsorption or binding to one side of the cantilever surface [135]. The key to microcantilever sensor development is to choose appropriate coatings for the identification of chemically or biologically specific species. A good coating candidate is stimuli-response hydrogels, which change their volume in response to small changes in the environment. However, as we know from the Chapter one, the direct synthesis of hydrogel film on the surface of the microcantilever through radical polymerization is troublesome and not practical. Another method is to immerse the cantilever in the mixture of the monomers and directly coat the hydrogel film on the microcantilever when the polymerization takes place. This method lacks reproducibility since the microcantilever has to be carefully assembled to create a gap within a

micrometer. On the other hand, as we know, the Layer-by-Layer assembly (LbL) developed by G. Decher is one of the most prospective new methods of thin film deposition. In this process, oppositely charged polymers or polyelectrolytes are often used to form a thin layer through alternative adsorption of the oppositely charged polyelectrolytes via electrostatic forces between them [136-138]. Recently, this technique has also been successfully applied to thin film assembly consisting of nanoparticles and various other inorganic materials [139-144]. The LbL assembly of nanoparticles can be described as the sequential adsorption of nanoparticles on oppositely charged layers of polyelectrolytes. The facile formation and stability of the nanoparticle LbL films could be attributed to the combination of both electrostatic and van der Waals attractive forces [145,146]. This process is not only simple and universal but also could produce high quality coatings with uniform distribution of nanoparticles in a film thickness and composition controllable manner. Another important advantage is that the LbL prevents phase segregation between the nanoparticles and the polymer matrix, which often occurs for other methods [147-149] and is detrimental for many applications.

Based on the above understanding, the research in this chapter is aimed at developing intelligent hydrogel micro-, nano-particle coated microcantilevers that are expected to be used as chemical and biological sensors. First, surface charged micro-, nano- hydrogel particles are synthesized through precipitation polymerization. Then, selectively modify the surface of the microcantilever and form a thin layer of hydrogel film on the surface of the microcantilever via LbL assembly of the micro-, nano-hydrogel particles.

4.2 Experimental

4.2.1 Materials

All the reagents were purchased from Sigma-Aldrich unless otherwise specified. The stabilizers in the acrylamide (AAm) and methacrylic acid (MAc) were removed by passing them through a glass column filled with inhibitor remover. Methylene bisacrylamide (MBAAm), azobisisobutyronitrile (AIBN) and anhydrous alcohol were used as received. Aminopropyltrimethoxysilane (APTMS) was stored and dispensed in a dry box. 11-Mercaptoundecanoic acid (MUA), 2-Mercaptoethanesulfonic acid (MES) were used as received. Polyethylenimine (PEI, $M_w = 25,000$) and polystyrenesulfonate (PSS, $M_w = 70,000$) were donated by Max Planck Institute, Germany. A 1wt% APTMS was prepared in anhydrous toluene. 1×10^{-5} M MUA and MES were prepared in alcohol. 1.5 mg/ml PEI and 3.0 mg/ml PSS were prepared in 18 M Ω deionized water. The suspensions of hydrogen micro-, nano- particles and polystyrene microparticles (537 nm, 0.05% NaAzide, Seradyn Particle Technology) used for the LbL were aqueous. Sulfuric acid and 30% hydrogen peroxide were used to make Piranha cleaning solutions. The silicon wafer slides used in this research were cut from new wafers with a dimension of about 10 \times 20 mm². The microcantilevers used in this research were fabricated from our laboratory, and all the microcantilevers were coated with 5 nm Cr and 100 nm gold using sputter depositoin.

4.2.2 Silicon Wafer Slides and Microcantilever Preparation

APTMS (aminopropyltrimethoxysilane) functionalized silicon wafer slides were used as positively charged substrates for alternate layer deposition. Prior to functionalization, the wafer substrates were first wiped clean of any dust using a soft

paper wipe. Following this step the substrates were immersed in Piranha solution (4:1 98% H₂SO₄: 30% H₂O₂) for 2 hours to remove any organics from the substrate surface (Caution: Piranha solutions react violently in the presence of many organic compounds and should be handled with extreme caution). Next, the substrates were rinsed copiously with H₂O and then rinsed copiously with 95% ethanol. Following this rinsing procedure the substrates were immersed in the 1% APTMS absolute ethanol solution for 2 hours. After 2 hours the substrates were removed from the APTMS solution and again rinsed copiously with 95% ethanol. These substrates were stored in 95% ethanol for no longer than 5 days prior to use. Prior to alternate layer deposition, these substrates were rinsed with H₂O and dried under a stream of nitrogen gas.

Microcantilevers were functionalized with MUA (11-Mercaptoundecanoic acid) or MES (2-Mercaptoethanesulfonic acid) to provide the gold surface with a monolayer of negatively charged molecules. Microcantilevers were immersed in the Piranha solution for just 2 minutes and then were rinsed copiously with H₂O followed by copious 95% ethanol. Following this rinsing procedure the microcantilevers were then immersed in 1×10^{-5} M MUA or MES alcohol solution overnight. These cantilevers were stored in 95% ethanol for no longer than 5 days prior to use. Prior to alternate layer deposition, these microcantilevers were rinsed with H₂O and dried under a stream of nitrogen gas.

4.2.3 Synthesis of Micro-, Nano-Hydrogel Particles

The micro-, nano- hydrogel particles employed in this research, poly(acrylamide-methacrylic acid-methylene bisacrylamide), P(AAm-Mac-MBAAm) micro-particles, were synthesized by precipitation polymerization from acrylamide (AAm), methacrylic acid (MAc) and methylene bisacrylamide (MBAAm) in ethanol according to reference

[176]. Specifically, 3.20 g AAm, 0.484g MAc, and 0.6784g MBAAm were dissolved in 60.0 mL ethanol in a 100 mL dry round-bottom flask. The solution was degassed with N₂, and then heated to 60 °C for 1 hour. Under stirring, a degassed solution of 0.026 g azobisisobutyronitrile (AIBN) in 5.0 mL alcohol was added into the mixture. The solution was stirred at 60 °C for 22 hours. The resultant was a milky suspension. The mixture suspension was dialyzed against alcohol over one week with the alcohol changed twice every day. The suspension was then refined by centrifugation and stored at 4 °C in the refrigerator in the medium of 95% alcohol. The sample was diluted with deionized water and additionally treated by ultrasonic for 30 minutes. The sample was then used as the source of the micro-, nano- hydrogel particles in the LbL assembly. The nano- hydrogel particles were prepared from the sample via ultrasonic treatment as follows. After ultrasonic, the sample was stored over night and the decanted supernatant was used as the source of nano- hydrogel particles.

4.2.4 Characterization of the Micro-, Nano- Hydrogel Particles

An optical microscope equipped with a digital camera (Nikon, Japan), an atomic force microscope (AFM) and scanning electronic microscope (SEM) were employed to characterize the size and morphology of the as-synthesized micro-, nano- hydrogel particles. The sample was naturally deposited on the surface of the silicon wafer slides and dried with a nitrogen stream.

4.2.5 Alternate Layer Deposition on Si Wafer Slides and Microcantilevers via LbL

For the assembly of micro-, nano- hydrogel particles on the silicon wafer slides and microcantilevers, poly(AAm-MAc-MBAAm), micro-, nano- gels were used as the polyanion. Polystyrene microparticles were also used as the polyanion in the assembly on the microcantilevers. Since each hydrogel particle has a high number of negative charges, surface charge reversal should be possible, although the mechanism of the charge reversal will be different from the traditional linear polyelectrolyte systems. PEI was used as the polycation and has a well-known deposition behavior. Alternate layer deposition was performed on APTMS functionalized silicon wafer slides and MUA or MES functionalized microcantilevers following the standard protocol introduced by Decher and co-workers, as discussed in section two, Chapter one. Before the deposition, three bilayers of (PSS/PEI)₂ or (PEI/PSS)₂ were set up to provide the wafer slides or microcantilevers with a precursor layer for further deposition. For microcantilevers, after three bilayers were completed an additional PEI layer was added to change the surface charge positively for micro-, nano- hydrogel particle deposition. The time interval was 20 minutes and the substrates were dried with a nitrogen stream for the next assembly. The whole deposition process on the wafer slides is schematically illustrated in the Figure 4.1.

4.2.6 Hydrogel Film Characterization

An optical microscope equipped with a digital camera (Nikon, Japan) was used to check the surface of the substrates and record the morphology of the deposited films during the whole micro-, nano- hydrogel particle LbL assembly. The AFM and SEM were employed to characterize the morphology and thickness of the hydrogel films.

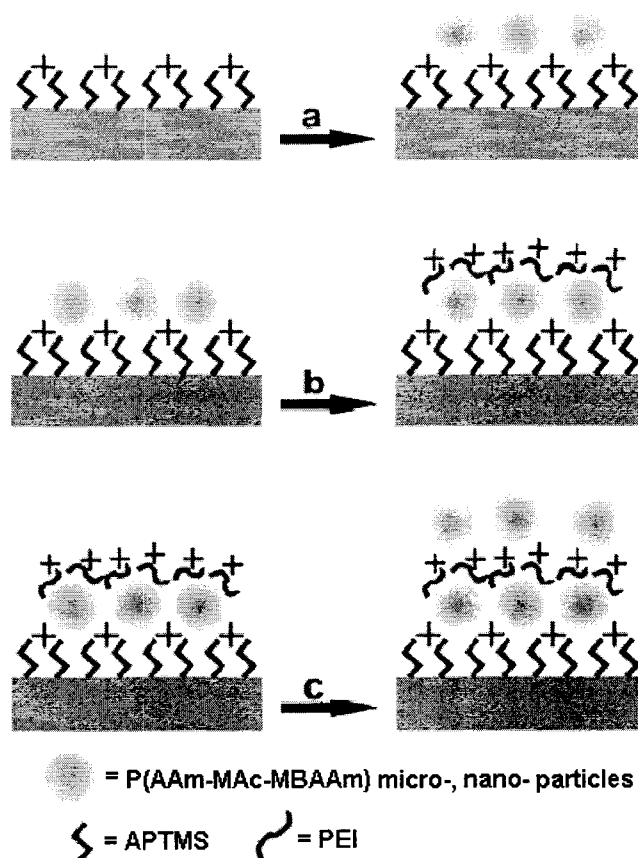


Figure 4.1 Idealized schematic for the alternate layer deposition scheme followed in this study. (a) micro-, nano- hydrogel particle attachment to an APTMS functionalized wafer substrate; (b) addition of PEI; (c) subsequent addition of microgel results in their attachment to the PEI layer. The three precursor bilayers are not shown in this scheme.

4.3 Results and Discussion

4.3.1 Synthesis of the Micro-, Nano-Hydrogel Particles

Microgels can be prepared by precipitation or emulsion polymerization under suitable conditions. In this synthesis, acrylamide (AAm) is the monomer. The methylene bisacrylamide (MBAAm) is the cross-linker and azobisisobutyronitrile (AIBN) is the initiator. The hydrogel microspheres were prepared by precipitation polymerization from acrylamide (AAm) and methylene bisacrylamide (MBAAm) in alcohol by adding a proper amount of methacrylic acid (MAc) without using any stabilizer. Upon addition of

the initiator AIBN, polymerization of the monomers in the solution occurs by solution polymerization. The polymer phase separates from the continuous phase by the precipitation of the insoluble polymer particles (primary particles). The poly(methacrylic acid) in the primary particles acts as a stabilizer due to its amphiphilic property. The hydrophilic part containing the carboxylic groups orients towards the ethanol and the hydrophobic part orients towards the poly(acryamide) chains in the particles. Electrostatic repulsive forces contribute to the stabilization of the particles. Polymerization within the primary particles occurs due to the absorption of ethanol, monomer, and oligo-radicals from the solution. Scavenging of the oligo-radicals prevents the formation of the primary particles in the later stages. If a few radicals escape and result in primary particles, they coalesce with the highly swollen and soft poly(AAm-Mac-MBAAm) copolymer particles in a monodispersed suspension [150, 151]. The resultant is a copolymer, poly(AAm-Mac-MBAAm). In this polymerization process, poly(methacrylic acid) (PMAc) plays the role of a stabilizer for particle dispersion since it is soluble in alcohol. On the other hand, PMAc can dissociate and give out protons producing highly dense carboxylic groups on the surface and within the hydrogel particles. This surface charge could provide electrostatic force between the hydrogel particles and prevent them from setting down and forming an aggregate. Poly(AAm-Mac-MBAAm) is a pH sensitive hydrogel. Its volume can swell or shrink in different pH medium. The volume change of the hydrogel particles are directly related to the dissociation and association of the PMAc. Thus, the monomer methacrylic acid plays an important role for the pH sensitive hydrogel particles. The particle size could be controlled to some extent by adjusting the molar ratio between the monomers and

solvent, monomer concentration in polymerization, and the amount of the initiator.

4.3.2 Characterization of the Micro-, Nano- Hydrogel Particles

Figure 4.2 shows the SEM view of the as-synthesized micro-, nano- hydrogel particles by precipitation polymerization. It can be seen the hydrogel particles are an almost perfect spherical shape and have a narrow size distribution, although some irregular particles can be found, which may be due to mechanical damage or undesirable nucleation of the hydrogel particles. The particles were aggregated as seen in the SEM picture view and this phenomenon should have occurred after the solvent evaporated. The majority of the particles had a diameter of about 0.5 μm or 500 nm and a few particles with much smaller diameter around 200 nm could be found. It can be concluded that synthesis of the micro-, nano- hydrogel particles through the precipitation polymerization was successful.

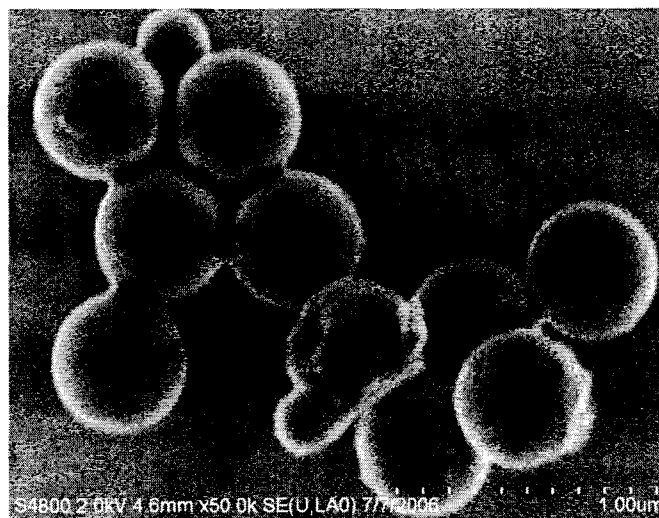


Figure 4.2 SEM view of the as-synthesized micro-, nano- hydrogel particles by precipitation polymerization.

Figure 4.3 shows an SEM image of the hydrogel particles that were derived from the as-synthesized micro-, nanoparticles through a further 30 minute ultrasonic treatment. The average size of the as-treated hydrogel particles separated from the supernatant liquid was about 100 nm. It can be seen that the morphology of most of the particles still remained spherical after ultrasonic treatment. This may be due to the small size of the nanoparticles and the soft character of the hydrogel. They try to lower the surface energy to maintain equilibrium by reducing the surface area. The smallest particles are less than 50 nm. This proved that the ultrasonic treatment was an effective and simple approach in preparing the soft nanoparticles.

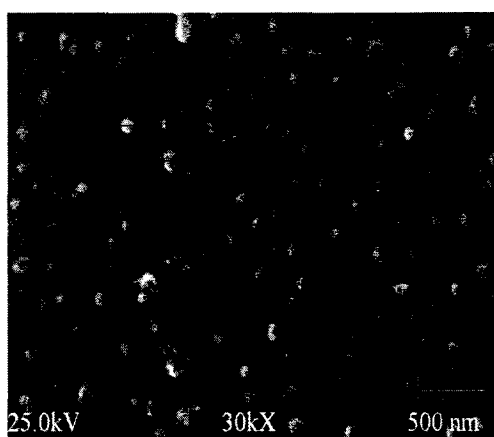


Figure 4.3 The SEM image of the hydrogel nanoparticles deposited on the silicon wafer. The wafer was first coated with three bilayers of (PEI/PSS) plus one PEI layer as the outermost surface and then exposed to the nanoparticle suspension in water for 1 hour. The average size of the hydrogel particles is approximately 100 nm.

On the other hand, from the SEM image aggregation can be observed and this phenomenon results in the irregularity and large size of the particles. The aggregation most likely formed during the process of natural deposition and drying instead of in the suspension. It is the particle surface charge, which results from the dissociating of the

carboxylic groups, that keeps the particles separated from each other. The larger size particles will upset the balance between the electrostatic forces and particle gravity and lead to the particles to settling down to the bottom of the suspension and falling into the category of micro- hydrogel particles.

Figure 4.4 is the AFM image of the prepared hydrogel nanoparticles deposited on the silicon wafer. Most of the particle sizes were within or around 100 nm. The aggregation was also found in the AFM image where hillock (particle size) formation is bigger or consists of a group of humps. The AFM results are in good agreement with the SEM results for the hydrogel particle size measurement.



Figure 4.4 AFM image of the hydrogel nanoparticles deposited on the silicon wafer. The wafer was first coated with three bilayers of (PEI/PSS) plus one PEI layer as the outermost surface and then exposed to the nanoparticle suspension in water for 1 hour.

4.3.3 Micro-, Nano- Hydrogel Particle Assembly on the Silicon Wafer

Shown in Figure 4.5 (A-D) are a set of SEM images of the films after alternate layer deposition at room temperature. From Figure 4.5 (A) it can be seen that the first layer deposition displays a sparse distribution of the micro-, nano- hydrogel particles. Some aggregation can also be observed and may have resulted from the original coalescence in

the suspension instead of the process of deposition. This deposition behavior has been previously observed in other particle based alternate layer deposition schemes [152-154] and is related to Coulombic repulsion between particles. This is similar to the self-assembly mechanism observed for traditional polyelectrolyte layer deposition, as discussed in Chapter one. Despite the sparse hydrogel distribution for the first layer, the addition of more layers appears to produce homogenous films. After 5 alternate layer of hydrogel particle deposition, Figure 4.5 (B) shows an increase in particle density with respect to the first layer. It can be seen that there is a moderate improvement in the homogeneity of the film in Figure 4.5 (B). The increase in particle density for the 5 layer film is interesting because it shows the micro-, nano- hydrogel particles adsorbing to the surface rather than building up a true multilayer structure in the z-direction. This result may come from the possibility that PEI could neutralize and reverse the charge on the hydrogel the particles bound to the surface and therefore remove the repulsive interaction between particles bound to the surface and the particles in solution. This will allow hydrogel particles to access the surface and therefore bind to the free charged amine sites [152]. This process will proceed until the surface becomes saturated with hydrogel particles. Once the surface is saturated with hydrogel particles, buildup in the z-direction can occur. Hydrogel particle layer number 10 (Figure 4.5 (C)) shows a dramatic increase in particle density and film homogeneity, though some pinholes can be identified. This film also begins to show signs of multilayer buildup. Figure 4.5 (D) shows that an obvious multilayer buildup occurred when the number of deposition layers reached 15. This multilayer buildup most likely is a result of surface charge saturation by the hydrogel particles and, therefore, allowing for multilayer buildup in the z-direction.

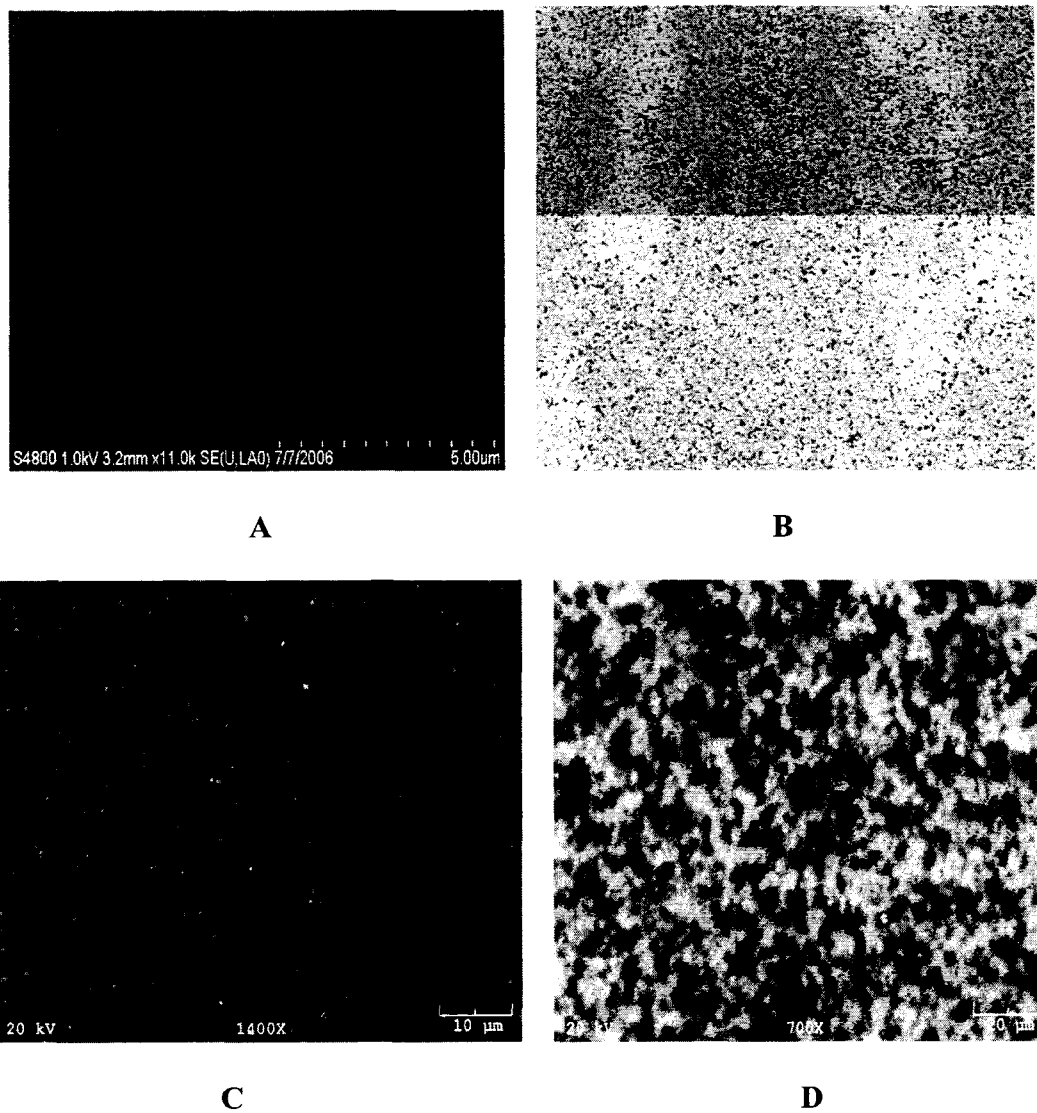


Figure 4.5 (A-D) SEM images taken of (A) 1, (B) 5, (C) 10 and (D) 15 hydrogel particle alternate layer films. From the images it can be seen that, as the number of the hydrogel particle alternate layer increases, the hydrogel particle density increases indicating a multilayer buildup mechanism.

Figure 4.6 (A) and (B) shows the AFM images of the 10 and 15 hydrogel particle alternate layer films. Since there are some pinholes distributed in the films, the probe of the AFM machine can reach and detect these pinholes and record the lowest position in the z-direction as 0 nm. The scale in the z-direction is marked with the color changing from darkest to brightest in the AFM image. Thus, it is possible to estimate the average thickness of the hydrogel films from their AFM image color scale.

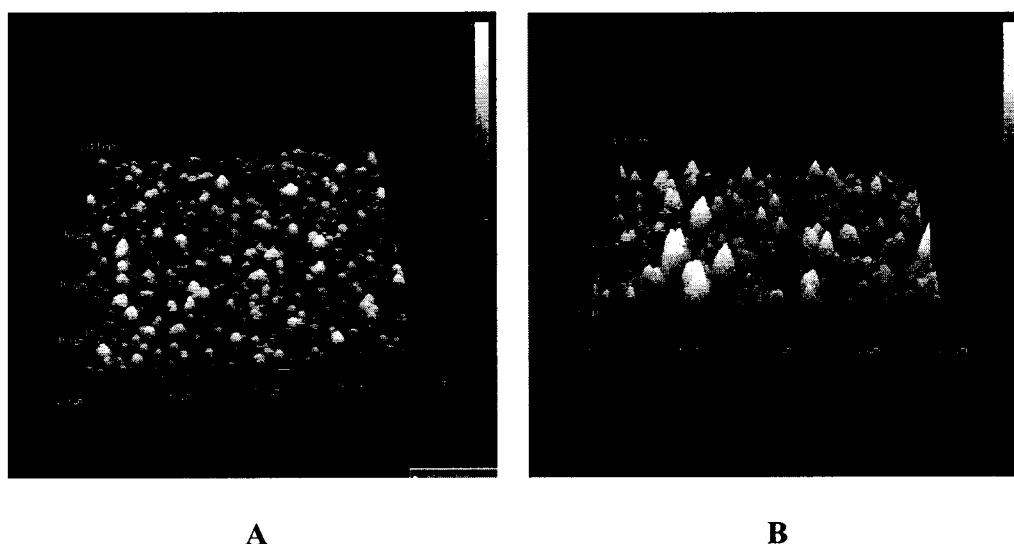


Figure 4.6 (A, B) AFM images of (A) 10 and (B) 15 hydrogel particle alternate layer films.

It can be seen from Figure 4.6 (A) that the average thickness of the hydrogel film is about 120 nm and the highest point in the z-direction is about 300 nm for the 10-alternate-layer hydrogel particle deposition. These figures are reasonable. Since after the 10 alternate layer deposition, the surface of the wafer is saturated with a layer of film consisting of the micro-, nano- hydrogel particles with average size about 100 nm. Due to some extension of aggregation and multilayer buildup in some areas (bright spots), the average thickness could reach 120 nm and the thickest point could reach 300 nm. It is

easier to see the heavy multilayer buildup in Figure 4.6 (B) for the 15-alternate-layer deposition. The average thickness of this film is about 220 nm and the highest point in the z-direction is about 430 nm.

4.3.4 Micro-, Nano- Hydrogel Particle Assembly on the Microcantilevers

11-Mercaptoundecanoic acid (MUA) and 2-Mercaptoethanesulfonic acid (MES) both have thiol groups on one end and a carboxylic or sulfonic group on the other side. They are the common thiol compounds that usually are used for gold surface modification to provide a self-assembly monolayer (SAM) on top of the gold surface [137]. The interaction between the gold surface and the thiol compounds is the strong chemical adsorption between the sulfur atoms and the gold atoms. When the microcantilever is immersed in the diluted solution of MUA or MES, MUA or MES forms a SAM through molecular self assembly with the head (thiol group) pointing toward the gold surface and the tail (carboxylic or sulfonic group) pointing away from the surface. The carboxylic or sulfonic group can dissociate in aqueous solution and result in the gold surface becoming negatively charged. This surface modification allows for the alternate layer deposition of the electrolytes and micro-, nano- hydrogel particles through the LbL process.

Figure 4.7 (A-F) presents the series optical images of the micro-, nano- hydrogel particle deposition with a different number of LbL operations on the gold and silicon surfaces of the microcantilevers. It can be seen that for the gold surface the hydrogel particle deposition behavior is the same as that on the silicon wafer (Figure 4.7 (A) and (C)). After 8 alternate layers of deposition, the multilayer buildup occurs (Figure 4.7 (E)) and this situation became serious when there are 12 alternate layers (Figure 4.7 (F)).

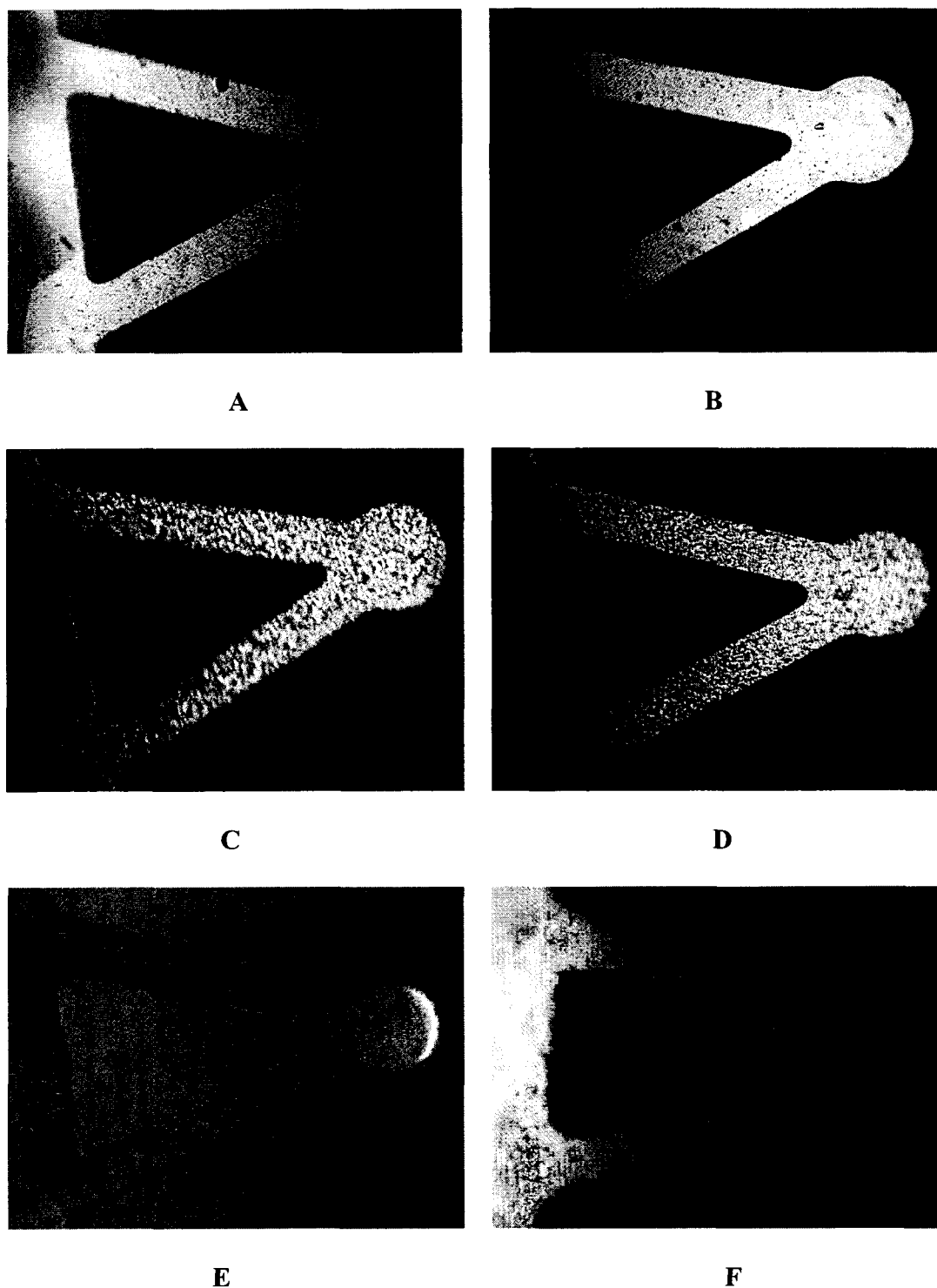


Figure 4.7 (A-F) Optical images of the microcantilevers deposited with one operation of micro-, nano-, hydrogel particles on the Au surface (A) and Si surface (B), 5 operations on the Au surface (C) and Si surface (D), 8 and 12 operations on the Au surface (E and F). Multilayer buildup is obvious after 8 and 12 alternate operations. (750 \times)

Since the multilayer buildup prevents the further deposition of the hydrogel particles on the gold surface of the microcantilevers, a continuous and uniform hydrogel film could not form using this approach. The major reason that prevents the hydrogel particle deposition through LbL may come from the small size of the microcantilever and the gold surface condition. For example, due to the small size, the surface electrostatic distribution is uneven with more charge accumulation on the edge. This uneven charge distribution might prevent the deposition process through electrostatic repulsion and lead to the loose layer formation on the top as the deposition continues. On the other hand, the gold surface contamination will also make the situation become more complex since for a fresh gold surface it is very easy to adsorb some organic vapors from the air. This contamination will result in the failure of the MES or MUA modification at the very beginning.

Another problem in the process of the hydrogel deposition on the microcantilever surface is that the deposition also occurred on the silicon back side of the microcantilevers, as can be seen in Figure 4.7 (B) and (C). Figure 4.8 (A, B) also provides the evidence of the hydrogel deposition on the Si side of the microcantilevers. This reverse deposition is detrimental to this approach since it is expected that only one side, the gold surface, will be coated with a layer of hydrogel to set up a platform for the chemical or biological sensors. Thus, further investigation onto this approach may have to consider the two aspects mentioned above.

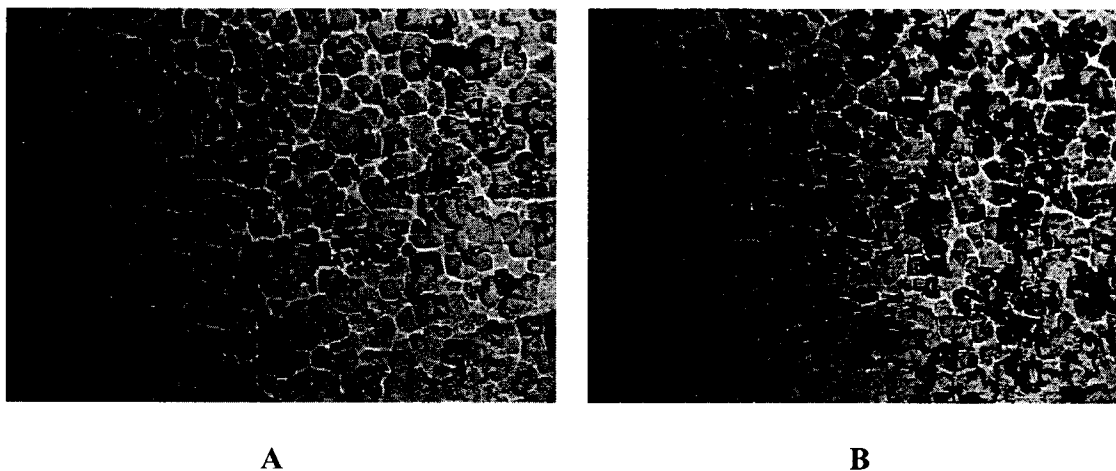


Figure 4.8 (A, B) Optical images of the Si side of the microcantilever bodies used in this research after 1 (A) and 5 (B) assembly operations of micro-, nano- hydrogel particle deposition. It is obvious that the hydrogel particles absorbed to the Si surface. (750 \times)

4.3.5 Polystyrene Microparticle Assembly on the Microcantilevers

We repeated the LbL assembly process on the microcantilever surface using polystyrene (PS) microparticles to compare the deposition results with the results obtained from hydrogel particle assembly on the microcantilever surface. The PS microparticle could be considered “hard” sphere due to the thick and rigid aromatic rings in its chemical structure. PS microparticles used in this research are uniform in size with a diameter of 0.537 μm or 537 nm. The microparticles were previously treated with 0.05% NaAzide and the particle surface is negatively charged. Thus, the same assembly procedure was strictly followed as that used in the hydrogel particle assembly on the microcantilever surface. Figure 4.9 (A-F) shows the series optical images of the PS microparticle deposition with a different number of the LbL assembly operations on the gold surfaces of the microcantilevers.

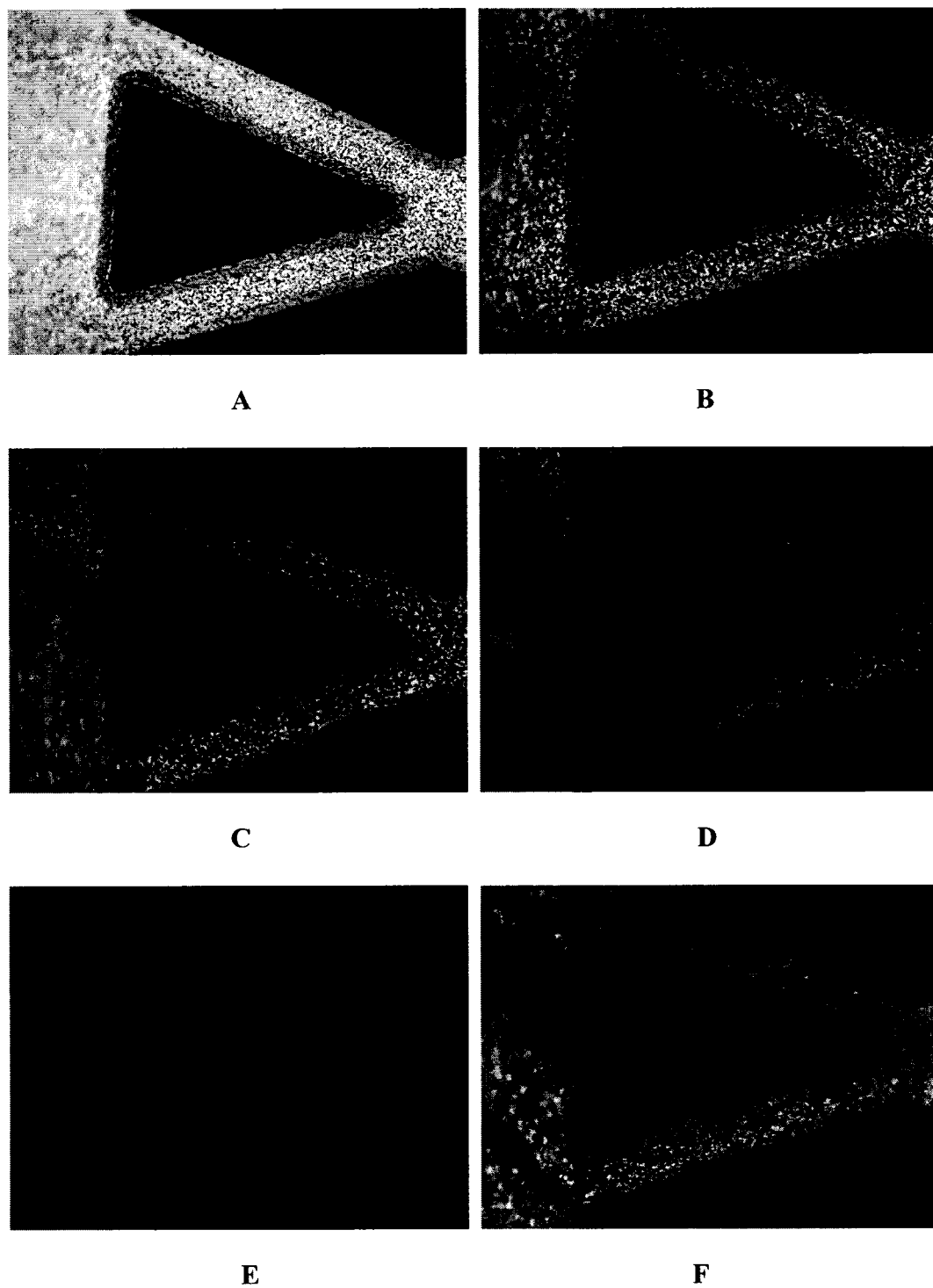


Figure 4.9 (A-F) Optical images of the microcantilevers deposited with (A) 2; (B) 4; (C) 6; (D) 8; (E) 10 and (F) 12 alternate assembly operations of polystyrene microparticles on the Au surfaces of the microcantilevers. Multilayer buildup occurred after 8 alternate operations. (750 \times)

It can be seen from Figure 4.9 (A-F) that PS particles almost evenly distributed on the Au surface before 6 alternate assembly operations. The multilayer build-up occurred after 8 alternate assembly operations and there is no uniform and continuous film observed after 12 alternate assembly operations. On the other hand, the PS particles also absorbed on the back of microcantilevers as shown in Figure 4.10 (A-B). Thus, the PS microparticle assembly behavior on the microcantilever surfaces is almost the same as that we observed in Figure 4.7 (A-F) and Figure 4.8 (A-B).

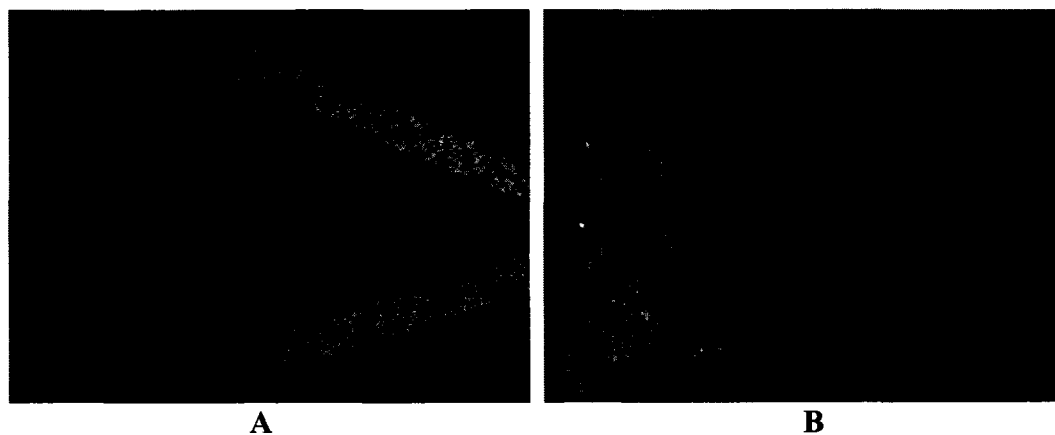


Figure 4.10 (A, B) Optical images of the Si side of the microcantilevers used in this research after (A) 2 and (B) 12 assembly operations of PS microparticle deposition. It is obvious that the PS particles absorbed to the Si surface. (750 \times)

4.4 Conclusion

The pH sensitive micro-, nano- hydrogel particles were successfully synthesized through precipitation polymerization and further ultrasonic treatment. The micro-, nano-hydrogel particle deposition behavior on the silicon wafer and microcantilever through the LbL process was described and discussed based on the observation and characterization using optical microscope, SEM and AFM techniques. It was believed that the electrostatic interactions between anionic hydrogel particles and polycationic PEI made the hydrogel particle deposition possible through the LbL process. The results showed that the particle deposition could be considered a pseudo-3D mechanism, where the first few particle depositions contribute to the saturation of the substrate. Further depositions then proceed to build up the film in the z-direction. The small size of the microcantilever and surface contamination of the microcantilever may be the main reasons preventing formation of a good quality hydrogel film on the gold surface using the LbL process.

CHAPTER FIVE

**MICRO/NANO HYDROGEL PARTICLES
DEPOSITION ON SILICON WAFER AND
MICROCANTILEVER VIA ELECTRO-
PHORETIC DEPOSITION**

5.1 Introduction

Microcantilevers have been proven to be a cost-effective and ultrasensitive sensing device for chemicals and biological species in air and solutions [156]. Microcantilevers undergo bending due to molecular adsorption or absorption by confining the adsorption and absorption to one side of the cantilever. One focus of the microcantilever sensing area is to develop a novel surface modification approach to increase the microcantilever bending amplitudes and thus further improve sensitivities. Self assembled monolayer (SAM) [157], self assembled multilayer [158], surface conjugation chemistry [159], and spin polymer coatings [160], etc. have been widely used for microcantilever surface modifications. Recently, microcantilevers modified by stimuli-responsive hydrogels have shown significant bending amplitudes compared to other technologies [161,162].

Hydrogels have received a great deal of attention because of their wide range of chemical and biological applications attributing to their good biocompatibility and volume change property in response to physical or chemical stimuli in the environment,

such as temperature [163], pH, ionic strength [164], and other chemical and biological species [165]. Hydrogels have thus found wide applications in cell cultures, cell immobilization, tissue engineering [166], biological and chemical sensing [167], drug delivery [168], intelligent coatings [169], etc.

For microcantilever sensing applications, the challenge is to develop adequate surface coating techniques to achieve gel immobilization on the sensor platform with high stability and reproducibility. Furthermore, an ultrathin film is required for fast response since the gel swelling time is proportional to the gel thickness [170]. Although hydrogel modified microcantilevers have shown much enhanced microcantilever bending amplitudes and sensitivity, the direct surface modification process, i.e. polymerization of the hydrogel on the microcantilever surfaces, is tedious and problematic [161,162].

One indirect approach would be to develop hydrogel microspheres or nanoparticles, and assemble these particles on the microcantilever surface in an organized manner by electrostatic attraction and other intermolecular interactions, which is commonly called the Layer-by-Layer (LbL) self-assembly technique [171,172]. However, due to the microsize of the microcantilever, our initial investigation, as described in Chapter three, showed that the LbL technique did not produce a continuous, reproducible ultrathin film on a microdevice, such as a microcantilever, although it was possible to prepare a continuous and relatively dense hydrogel film on the bulk silicon wafer.

In this research work, based on the investigation of the electrophoretic deposition (EPD) of the micro-/nano- hydrogel particles on bulk silicon wafers, the technique of electrophoretic deposition was introduced to develop a process to prepare a uniform,

compact, ultrathin hydrogel film on a microcantilever sensor device from the deposition of the micro-/nano- hydrogel suspension.

As we know from the Chapter one, EPD has been extensively used for fabricating thin films from suspensions of nano- or micro-sized particles. The EPD technique offers precise control of film thickness, uniformity, and deposition rate. However, the EPD had only been used on hard particles, including ceramic particles [173], colloidal gold particles [174], and polystyrene particles [175] etc. In this research, we expand the application of EPD on soft particles, such as hydrogel microspheres and nanoparticles.

5.2 Experimental

5.2.1 Synthesis of Micro-, Nano-Hydrogel Particles

The micro-, nano- hydrogel particles employed in this research, poly(acrylamide-methacrylic acid-methylene bisacrylamide), P(AAm-MAc-MBAAm), micro-particles, were synthesized by precipitation polymerization from acrylamide (AAm), methacrylic acid (MAc) and methylene bisacrylamide (MBAAm) in ethanol according to reference [176]. The synthesis details and discussion were specifically described in Chapter three.

5.2.2 Micro-, Nano-Hydrogel Particle Electrophoretic Deposition

A pair of parallel plate electrodes [50-nm-thick Au on 5-nm Cr on Si (100)] with lateral dimension about 15mm×5mm served as the electrodes in the EPD. As for the deposition on the surface of the microcantilevers, the microcantilever served as the anode and a 2×2 mm² platinum thin plate served as the cathode. Before the deposition, all the electrodes, gold coated silicon wafer slides, microcantilevers and platinum slides, were immersed in Piranha solution, 4:1 H₂SO₄: H₂O₂, for about two min. to remove any organics

from the electrode surface (Caution: Piranha solutions react violently in the presence of many organic compounds and should be handled with extreme caution). Next, the electrodes were rinsed copiously with H₂O then copiously with 95% ethanol. As for the anode, in order to increase the adhesion between the hydrogel particles and the surface of the anode, the gold surface of the anodic electrodes was further treated with 5.0×10^{-5} M 6-mercapto-1-hexanol for 24 hours and then coated with three alternative layers of poly(ethylenimine) (PEI)/poly(styrenesulfonate) (PSS) through the Layer-by-Layer technique [171]. For silicon wafer slide deposition, the electrodes were placed vertically with a spacing 5mm between them and immersed into 20ml of a diluted suspension of micro-/nanoparticles of hydrogel. For microcantilever deposition, the distance between the microcantilever and platinum electrode was about 2 mm. The solvent for the suspension is 95% ethanol and the concentration is ~0.5wt% for nanoparticles and ~2wt% for microspheres. The deposition process was performed using a constant voltage mode at room temperature. After EPD, the samples were removed and rinsed gently with distilled water three times, and then dried under nitrogen gas before measurements were performed.

5.2.3 Methods for Microcantilever Test

5.2.3.1 Materials

In these experiments, we used microcantilevers fabricated in our laboratory [159]. The dimensions of the V-shaped SiO₂ microcantilevers were 200 μm in length, 25 μm in leg width, and 2 μm in thickness. One side of the SiO₂ cantilevers was covered with 3-nm of chromium followed by 20-nm of gold.

11-mercapto-1-undecanoic acid, PEI ($M_w = 25,000$), and PSS ($M_w = 70,000$) were used as received from Sigma-Aldrich. The phosphate buffer solutions were 0.001 M and pH = 7.0. A series of solutions with different pH values were prepared as follows: (A) prepared 100 mL 0.001 M K_3PO_4 , K_2HPO_4 , KH_2PO_4 and H_3PO_4 aqueous solutions individually and measured their pH values respectively via a pH meter; (B) took 50 mL KH_2PO_4 solution and adjusted the pH value to be 4.00 ± 0.02 by addition of K_2HPO_4 or H_3PO_4 solution drop by drop while the mixture was monitored with the pH meter; (C) followed the same procedure to prepare the solutions with other different pH values. The solutions were stored in plastic bottles at room temperature and the pH values were measured again before using.

5.2.3.2 Deflection Measurement

The deflection experiments were performed in a flow-through glass cell (Digital Instruments, Santa Barbara, CA) similar to those used in atomic force microscopy (AFM). The microcantilever was immersed in the 0.001 M phosphate buffer (pH 7.0) solution. For continuous flow-through experiments, initially the buffer solution was circulated through the cell using a syringe pump. A schematic diagram of the apparatus used in this study was the same as previously used in Chapter three [178]. A constant flow rate was maintained during each experiment. Experimental solutions containing standard buffer solutions with different pH values were injected directly into the flowing fluid stream via a low-pressure injection port sample loop arrangement with a loop volume of 2.0 mL. This arrangement allows for continuous exposure of the cantilever to the desired solution without disturbing the flow cell or changing the flow rate. Since the volume of the glass cell, including the tubing, was only 0.3 mL, a relatively fast

replacement of the liquid in contact with the cantilever was achieved. Microcantilever deflection measurements were determined using the optical beam deflection method. The bending of the cantilever was measured by monitoring the position of a laser beam reflected from the gold-coated side of the cantilever onto a four-quadrant AFM photodiode.

5.3 Results and Discussion

5.3.1 The Hydrogel Film Formation from the Suspensions of Micro-/Nano-Hydrogel Particles on Si Wafers

At first, the electrophoretic depositions were carried out in aqueous suspensions. The results showed that in the aqueous medium bubbles were observed to evolve from both of the electrodes when the applied voltages were equal to or greater than 2.0 V and there were no hydrogel particles deposited on the surface of the electrodes. The same results were obtained even when the applied voltage was less than 2 V and there were no obvious bubbles observed. Therefore, the solvent of the suspension was changed to 95% alcohol afterwards.

Figure 5.1 and Figure 5.2 show that the hydrogel films obtained through the EPD with micro-/ nano- hydrogel particles at the applied potential of 10 V for 30 min. The hydrogel particles with a maximum average size of 3 μ m were densely deposited on the Au surface of the anode, forming a continuous film. These films are uniform with the particles distributed evenly and the pinholes are difficult to observe even using the SEM at a magnification of 1400 \times .

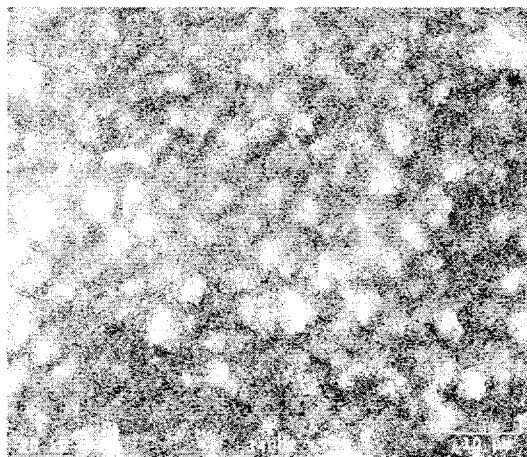


Figure 5.1 SEM picture of the deposited film on Si wafer via the EPD from the suspension of the micro-/nano- hydrogel particles at 10V for 30 min.



Figure 5.2 Optical microscopy image of the deposited film on Si wafer via the EPD from the suspension of the micro-/nano- hydrogel particles at 10V for 30 min. The magnification is 750 \times .

The average thickness of the film is around 800 nm measured by surface profiler. This value is significantly less than the average diameter of the hydrogel particles measured by the SEM. This dimensional difference suggests that the shape of the hydrogel particles were changed into that of a plate after they were deposited on the surface of the anode. According the general theory of the EPD [176], the negatively

charged hydrogel particles were driven toward the anode by a pressure resulting from the electric field. When the hydrogel particles reach the anode they redistributed themselves on the surface to assemble into a uniform film. Since the hydrogel particle is a kind of soft material, it will relax under the pressure of the electric field that is vertical to the surface of the anode. This relaxation most likely results in two conditions. One is the change in shape of the particles, and the other is edge to edge fusion between neighbouring hydrogel particles. Hence, both of these factors contribute to the formation of a thin and continuous film. The same experiments were repeated at a potential of 5 and 8 V, but the films did not form or were not continuous. On the other hand, when the voltage was above 12 V, the multilayer began to form, especially on the periphery of the anodic surface and the film became coarser. This result not only showed that the proper strength of the applied electric field was essential to the formation of uniform and continuous thin films of hydrogel, but also supports the proposed explanation for the formation of the hydrogel film.

5.3.2 EPD Behaviour of the of Nano-Hydrogel Particles on Si Wafers

In order to investigate the deposition behavior of the hydrogel particles in the EPD, we used nano-particles with an average size of around 100 nm and observed the growth of the hydrogel films under the optical microscope over a series of electrophoretic deposition times. There are two different growth patterns observed when the applied voltage was 2V and 5V respectively. The series of optical micrographs in Figure 5.3 (A-E) show the growth pattern of the deposited films from hydrogel nanoparticles at different electrophoretic deposition times when the potential was kept at 2 V.

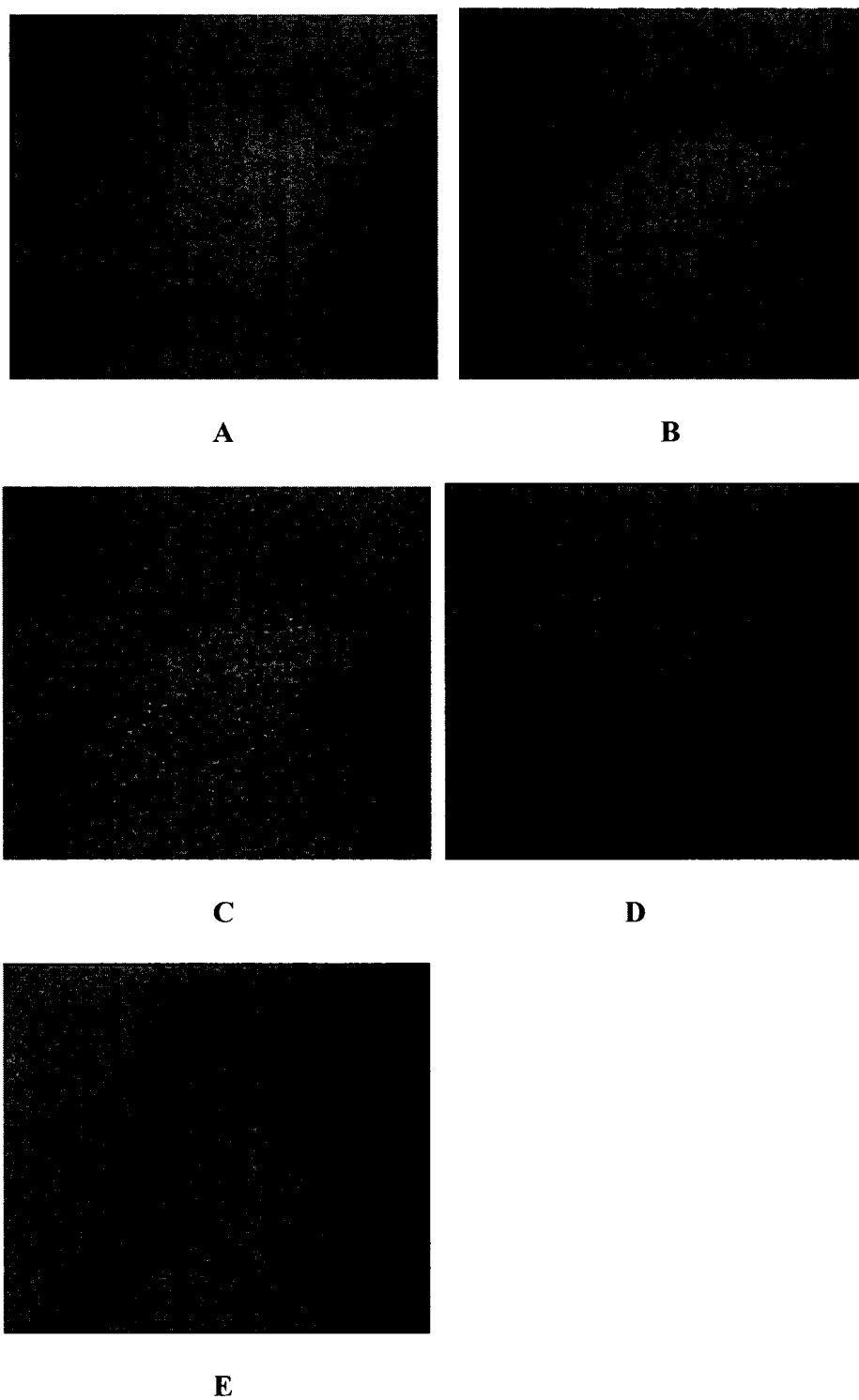


Figure 5.3(A-E). Optical microscopy images of the hydrogelfilms on the surface of silicon wafers via EPD from the suspension of nano- hydrogel particles at 2V for (A) 2 min, (B) 8 min, (C) 15 min, (D) 25 min, and (E) 35 min. The magnifications are 750 \times .

It can be seen that after 2 min, the hydrogel particles evenly distributed on the anode and some of them began to merge together, though most were spread out as isolated particles. After 8 min, the hydrogel particles clearly merged together and began to assemble into a two-dimensional network. The distance between the deposited particles increased and some small randomly distributed isolated particles could be observed. After 15 min, the two-dimensional network had clearly formed and the coverage of the deposited film increased. At this stage, the small isolated particles still could be identified. As the EPD proceeded, the void areas in the network gradually reduced and after 25 min the coverage of the deposited film increased greatly. As the 2-D network was filled with more particles, a uniform film began to form. Many pinholes could be easily seen at this stage. About 10 min later, the pinholes disappeared and a continuous uniform hydrogel film completely formed. It is worthwhile to mention that the obtained 2-D network or the film remained the same with reversal of potential.

We repeated the experiment with the applied voltage increasing to 5 V and held the other conditions constant. A different deposition pattern was observed as shown in Figure 5.4 (A-E). As we can see, as the potential increased, the particles deposited densely at the beginning and no clear 2-D network was observed during the whole process. The film almost became continuous after 10 min. This observation exhibits no big differences when compared with the micro-particles deposition at high voltage that was mentioned previously. What is interesting is the observation that the surface of the deposited hydrogel film began to grow smoothly after 15 min. As it is shown, the smoothing process was nearly finished after 25 min and was fully completed after 35 min, leaving a continuous and smooth film on the anode.

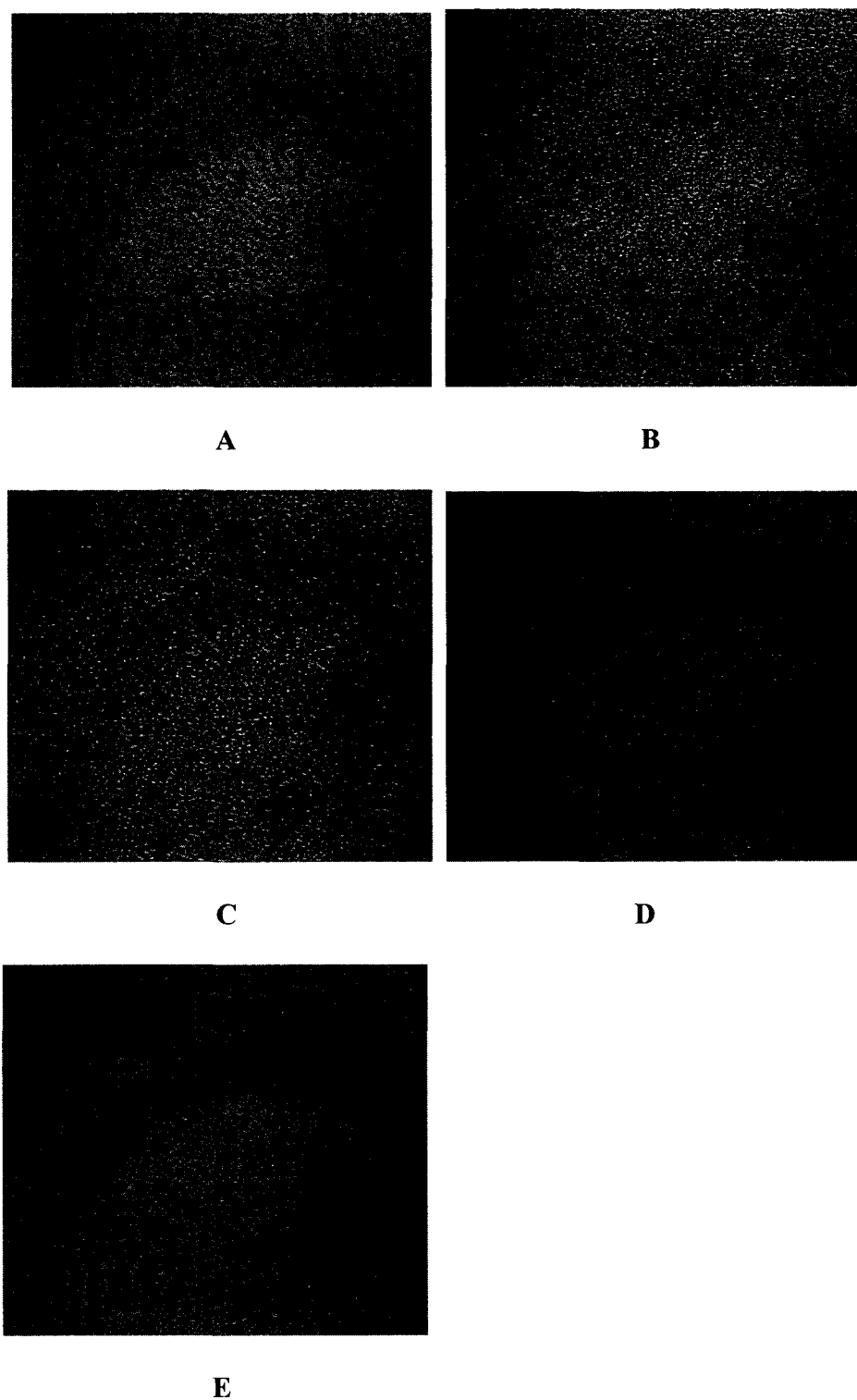


Figure 5.4 (A-E). Optical microscope images of the hydrogel films on the surface of the silicon wafers via EPD from the suspension of the micro-/nano- hydrogel spheres under 5V for (A) 2 min, (B) 10 min, (C) 15 min, (D) 25 min, and (E) 35 min. The magnifications are 750 \times .

The thickness of the film is about 70 nm as measured by the AFM. This value is less than the average diameter of 100 nm for the hydrogel particles. We contribute this phenomenon to the relaxation of the soft hydrogel particles under the pressure of the electric field as mentioned previously. We could also infer that the deposited film is a monolayer.

The above two deposition patterns at different applied voltages can be briefly described as follows. When the applied voltage was 2V, a 2-dimensional network consisting of nanoparticles gradually formed on the substrate and became obvious when the electrophoretic time was 15 min. As the EPD continued, the blank area in the 2-D network was gradually reduced as more particles filled in the system. A uniform and continuous thin hydrogel film formed after 35 min. When the voltage was increased to 5V, the particles were deposited directly on the substrate and no obvious 2-D network was observed. The film almost became continuous after 10 min. This observation is the same as that for micro-particle deposition at high voltage as previously mentioned. What made this process different is the interesting phenomenon that the surface of the deposited hydrogel film began getting smoother after 15 min and this smoothing process completed after 35 min, leaving a uniform and continuous hydrogel film on the substrate.

5.3.3 Explanation of the EPD Behaviour of the Nano- Hydrogel Particles on Si Wafers

The observation in Figure 4.3 is partly coincident with Böhmer's research [179, 180] on the EPD of micro-sized polystyrene (PS) latex particles, where "cluster-cluster aggregation" of the PS particles was observed. Miyake and coworkers [179] also found a 2-D network pattern when Pt nanoparticles were used. What is different is that neither the PS

particles nor the Pt nanoparticles could merge or fuse together. And another remarkable difference is that the “cluster-cluster aggregation” broke up upon reversal of the potential. We contribute these differences to the different nature of the starting materials. As we know, a PS particle is “hard” since the PS contains a large volume of rigid aromatic rings and the Pt particle is also hard. It is very difficult, if not impossible, for these “hard spherical particles” to fuse together without additional treatment. On the other hand, the hydrogel Poly(AAm-MAc-MBAAm) is soft for it mainly consists of network of flexible alkyl chains.

According to Anderson and Böhmer [179, 180], the motion of particles deposited on an electrode by electrophoresis is governed by electrokinetics, electrohydrodynamics, and Brownian diffusion. During the EPD, once the hydrogel particles reach the surface of the anode, two particles attract each other through electroosmotic flow and began to fuse at the edges of the particles. They will be fixed on the surface if one of them is already attached to the surface or has fused with other attached particles through the same process. If the applied potential is low (such as 2 V in our experiment), the electric field is not strong and hence just a limited number of particles are driven to randomly adhere to the anode under the applied potential. The 2-D network pattern will form while most particles are moving around as Brownian diffusion and finally fuse with the attached particles. It is easy to understand that the more particles that reach the surface, less void area remains and the coverage increases and a deposited film is obtained. On the other hand, if the applied potential is high (such as 5 V in our experiment), the force is strong enough to drive most of the hydrogel particles to adhere to the anode directly. Therefore, the number of the particles that move around as Brownian diffusion decreases greatly. So, no clear 2-D

network occurs in this case. However, the particle attraction resulting from the electroosmotic flow is still present and it is this attraction that drives the deposited particles to form a continuous and smooth film.

5.3.4 The AFM Images of the Hydrogel Film on Si Wafers

It can be seen from the AFM image of the deposited hydrogel film (Figure 5.5 A, B) that the surface of the film was smooth and uniform and agreed well with the observation under the optical microscope. The thickness of the film was about 100 nm as measured by the AFM (Figure 5.6), suggesting that the films could be considered as being made of a monolayer of hydrogel particles.

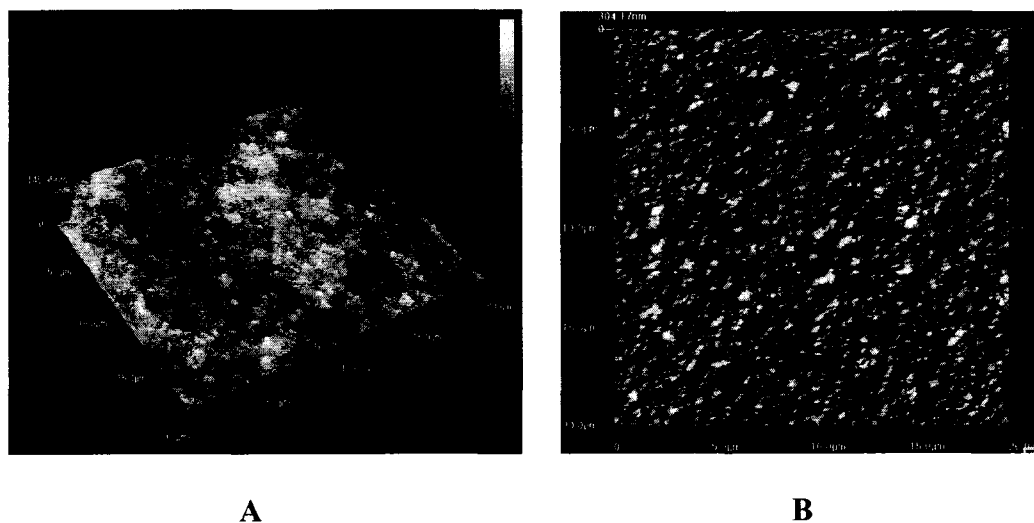


Figure 5.5 (A,B). AFM images of a film of 100-nm gel particles deposited on a Si plate through EPD at 2 V for 35 min. (A) 3-D image of the hydrogel film; (B) Tap mode image of the hydrogel film.

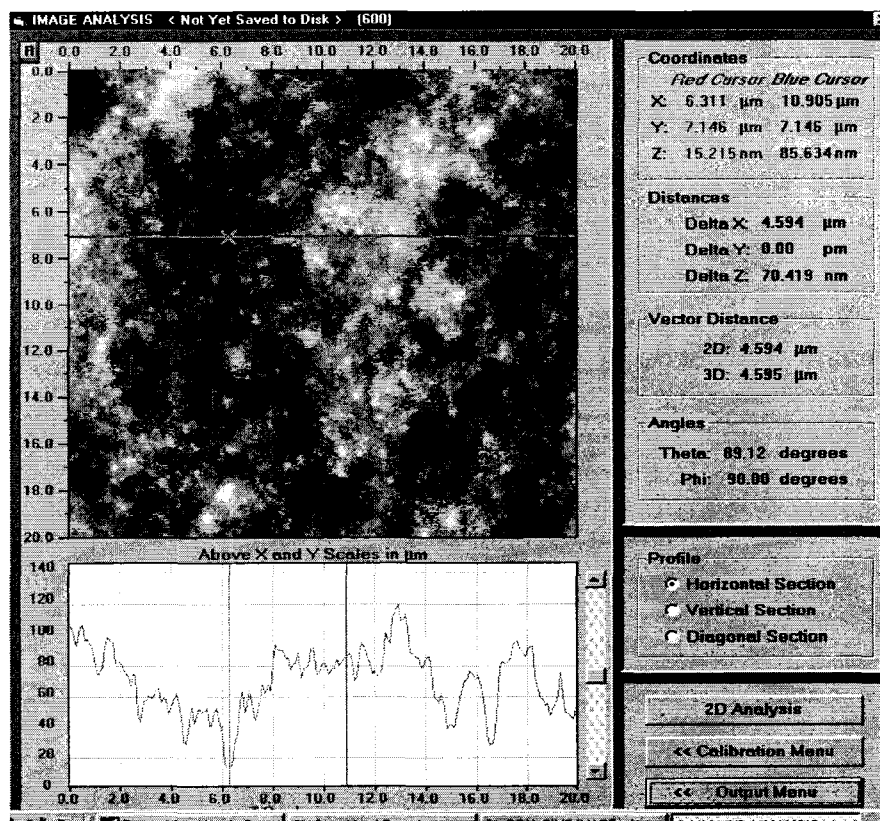


Figure 5.6 The roughness measurement (between lowest and highest points) of the hydrogel film of 100-nm gel particles deposited on a Si plate through EPD at 2 V for 35 min. The average thickness of the gel film was approximately 100 nm.

5.3.5 The Hydrogel Films on the Surface of Microcantilevers

The optical microscope image in Figure 5.7 (A-D) are the hydrogel film coated microcantilevers (B, D) and their corresponding hydrogel coated bodies (A, C). All the hydrogel films were prepared via EPD at 0.8 V for 20 min. It can be seen from the optical images that the hydrogel films on the microcantilevers are continuous, dense and cover almost all of the cantilever surface. This indicates that it is feasible to form a hydrogel film on the the microcantilever through EPD.

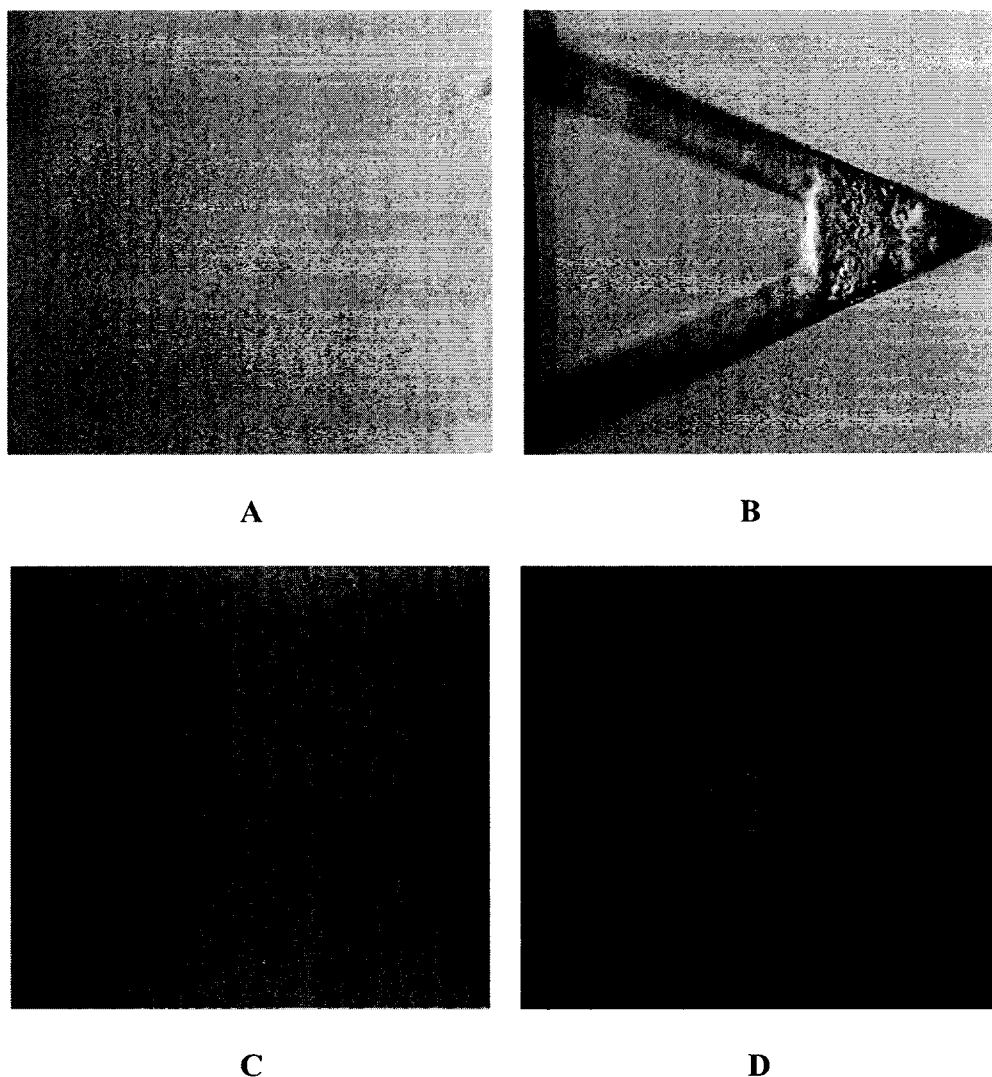


Figure 5.7(A-D) The optical images of the hydrogel film coated microcantilevers (B,D) and the hydrogel film coated bodies of the corresponding microcantilevers (A, C). The hydrogel films were produced by EPD of the suspension of hydrogel nanoparticles under 0.8 V for 20 min. The magnifications are 750 \times .

On the other hand, under the same EPD conditions, the hydrogel films on the bodies of the microcantilevers are smooth, uniform and dense. The quality is the same as that of hydrogel films prepared on the surface of the bulk silicon wafers via EPD and much better than that of the corresponding cantilevers. What is the reason that makes the body and the cantilever get a different hydrogel film even though they are deposited under the same EPD

conditions? We contribute this difference to the small size effect of the cantilever. The body of the microcantilever is about $1.5 \times 2.5 \text{ mm}^2$. It is a macrosized structure and its EPD behavior is the same as that of a bulk silicon wafer. However, the cantilever is a microsized structure. The surface electricstatic charge could not distribute evenly over the surface. For example, charge density on the edge is much greater than for other areas. This uneven surface charge arrangement can affect, or more specifically can reduce the distribution of the electric strength between the electrodes when an external potential is applied. So, the film on the edge of the cantilever could not grow at the same rate as the film does on the other areas of the cantilever. Thus, the film on the edge could not form very well (Figure 5.7 D) or be thinner (Figure 5.7 B) than the film in other areas. Another aspect is that the hydrogel surface coated on the cantilevers is not as smooth as that coated on the body. This may result from possible surface contamination of the cantilever even though it was carefully cleaned. This contamination, such as adsorption of organic molecules, will block the electric field to some extent and lead to an uneven drive force through the cantilever surface. Thus, the hydrogel film could not form evenly on the cantilever surface.

5.3.6 The Bending Measurement of the Hydrogel Coated Microcantilevers in Different pH Solutions

A microcantilever coated with a layer of hydrogel film through the EPD process was used for sensing validation. The experimental setup and the principle of the cantilever deflection measurement are the same as employed in the Chapter three [178]. The hydrogel film coated microcantilever was fixed in the fluid cell with the hydrogel film facing downward. The bending responses of the hydrogel coated cantilever with a change of

environmental pH were detected. Figure 5.8 shows the cantilever response to various pH in a series of 0.001 M phosphate buffer solutions.

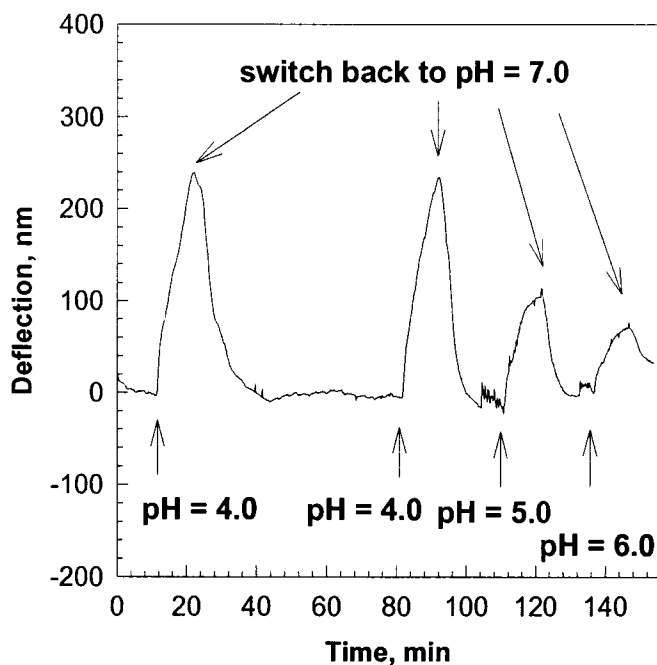


Figure 5.8 The Response of Hydrogel Coated Microcantilever to the Different pH Phosphate Buffer Solutions.

It can be seen that when the pH value of the medium was changed from 7.0 to 4.0, the hydrogel coated microcantilever underwent a significant bending, nearly 240 nm bending upward. After the pH was switched back from 4.0 to 7.0, the cantilever returned to its original position. This process was completely repeated about 1 hour later, which shows that the result is reproducible. When the pH was changed from 7.0 to 5.0 and 6.0, the microcantilever produced a net bending of about 120 nm and 80 nm respectively. In other words, the microcantilever underwent less bending at pH 5.0 and 6.0 compared with the bending at pH 4.0. The cantilever bending response to different pH values was coincident

with the observation on the cross-sectional radius change trend at different pH values by Yoshiyuki [158]. Yoshiyuki noticed that the cross-sectional radius of the poly(acrylamide-*co*-methacrylic acid) hydrogel particles tended to decrease at a high pH. It is obvious that the volume of the hydrogel film coated on the microcantilever is smallest at pH 7.0 and biggest at pH 4.0, and followed by those at pH 5.0 and 6.0. Thus, when the pH was changed from 7.0 to 4.0 the volume of the hydrogel film expanded or swelled and produced the greatest upward bending. When pH was switched from 7.0 to 5.0 and 6.0, the hydrogel swelled again, but in a relatively modest manner. This bending trend can also be further understood from the view of the molecular structure of the poly(acrylamide-*co*-methacrylic acid). Association/dissociation of poly-MAc segments in the hydrogel contributed to the free energy of hydrogel-solvent mixing. As soon as the pH was high enough to overcome the osmotic pressure, the dissociated poly-MAc segments simultaneously decreased the osmotic pressure and free energy of hydrogel-solvent mixing, thereby allowing a sharp, large volume transition [180]. In other words, when the hydrogel was at pH 7.0, the poly-MAc was dissociated and most of the H^+ moved out of the network of the hydrogel film. The osmotic pressure in the network decreased and the hydrogel shrunk. On the other hand, at pH 4.0, most of the H^+ moved from the medium into the network and the poly-MAc was associated with the osmotic pressure increasing inside and the hydrogel swelled.

The expected observation and theoretical explanation on the response of the hydrogel coated microcantilever to different values of pH showed that the hydrogel film produced using EPD was an easy and reliable approach for the modification of microcantilever sensors.

5.4 Conclusion

A continuous, uniform and dense thin hydrogel film can be prepared through EPD on bulk gold-coated silicon surfaces. Two distinct deposition patterns were observed during the EPD process at different applied voltages and were explained in terms of the effect of the electroosmotic flow. This research also demonstrated a convenient and reliable approach, based on the EPD process, to deposit a uniform and continuous hydrogel thin film on the microcantilever devices. The bending responses of the hydrogel coated microcantilever with a change in environmental pH were observed, demonstrating the feasibility of this hydrogel film for microsensor development. This hydrogel film formation approach may be used on many other microdevices for various applications.

CHAPTER SIX

FINAL CONCLUSIONS AND FUTURE WORK

6.1 Final Conclusions

In order to set a platform for the microcantilever based chemical and biological sensing, three approaches were investigated to modify the surface of the microcantilever with a multilayer and a hydrogel thin film based on polyelectrolyte alternate multilayer assembly, micro-, nano-, hydrogel particle deposition through Layer-by-Layer process and micro-, nano-, hydrogel particle electrophoretic deposition techniques.

Organic electro-enzymatic polyelectrolyte organophosphorus hydrolase (OPH) was successfully immobilized on the surface of the microcantilever in a multilayer consisting of PEI and PSS. The total thickness of the assembled film was estimated about 25 nm. The results showed that the multilayer coated microcantilever responded to paraoxon, diisopropyl fluorophosphates (DFP) and parathion at different bending amplitudes and bending rates and had a high sensitivity and selectivity to the organic phosphorus compound paraoxon in aqueous solutions with a detection range from 10^{-7} to 10^{-3} M. The deflection mechanism was investigated based on the thermodynamic and equilibrium study of the shrinking of the multilayer. The possible elements that could contribute to the deflection the multilayer modified microcantilevers were analyzed and discussed. The effect of the pH decreasing on the microcantilever bending in the solution was limited,

which was proven by the investigation. It suggested that the conformational change of the OPH might be the primary contributor of the microcantilever bending.

The micro-, nano- hydrogel particles, poly(AAm-*co*-MAc-*co*-MBAAm) consisting of monomers acrylamide (AAm), methacrylic acid (MAc) and methylenebisacrylamide (MBAAm), were successfully synthesized through precipitation polymerization in the alcohol medium with the aid of ultrasonic treatment. The micro-, nano- hydrogel particle deposition behavior on the silicon wafer and microcantilever through the LbL process was described and discussed based on the observation and characterization using optical microscope, SEM and AFM techniques. The electrostatic interactions between anionic hydrogel particles and polycationic PEI made the hydrogel particle deposition possible through the LbL process. The results showed that the particle deposition could be considered a pseudo-3D mechanism, where the first few particle depositions contribute to saturation of the substrate. Further depositions then proceed to build the film up in the *z*-direction. The small size ($\sim\mu\text{m}$) of the microcantilever and its surface contamination might be the main reasons preventing good quality hydrogel film formation on the gold surface through the LbL process.

Through the EPD, a continuous, uniform and dense thin hydrogel film was successfully prepared on bulk gold-coated silicon surfaces. Two distinct deposition patterns were observed during the EPD process at different applied voltages and were explained in terms of the effect of the electroosmotic flow. This research also demonstrated a convenient and reliable approach, based on the EPD process, to deposit a uniform and continuous hydrogel thin film on the microcantilever devices. The bending responses of the hydrogel coated microcantilever with a change in environmental pH

were observed, demonstrating the feasibility of this hydrogel film for microsensor development.

6.2 Future work

First, a further study could aim to investigate and confirm the deflection mechanism responsible for the bending of the microcantilever modified with the multilayer containing OPH. Although it was suggested that the conformation change was possibly the main contributor of the bending of multilayer modified microcantilevers and this suggestion was supported by the results of related research from another group, there is no direct evidences to support this conclusion. Thus, further research focusing on the morphology change of the OPH during its enzymatic activity is necessary.

Second, it will be much better if the process of the Layer-by-Layer process could be monitored and characterized through fluorescence labeling techniques and surface micro-FT-IR analysis. Layer-by-Layer process has been extensively performing over ten years in the world wide and its primary theory has been established based on the practice. On the other hand, the LbL process is usually performed in the molecular level or in nano-scale. The process is invisible and there is no phenomenon or director in the process to show the presenting of each molecular layer after each operation. In other wards, it is necessary to get proofs to show if the PSS or OPH molecular layer is present after each operation in the LbL process. Fluorescence labeling techniques and surface micro- FT-IR analysis might be helpful with respect to this concern. For example, if the OPH is labeled with fluorescence tag, it is visible under the confocal microscope if it assembles on the surface of the substrate. Surface micro- FT-IR is also helpful to get the chemistry

information on the molecules present on the surface since different molecule has its own characteristic IR spectrum. It is possible to identify the different molecules via surface FT-IR if they exist on the surface of substrates during the LbL process.

Thirdly, it is necessary to extensively carry on a thorough investigation on the surface physics and chemistry for commercial and experimental microcantilevers to learn the mechanisms or the reasons that the surface of microcantilevers presented different behavior from that of the bulk wafers when the LbL process or EPD technique were applied. Since the LbL assembly is actually a process performed on the surface of the subjects, the surface characteristics of the target subjects are crucial to this technique. The uniformity of chemical composition and physical characters plays a significant role for the microsized surface to interact with other materials in the molecular level. Thus, the study on the surface chemistry and surface physics of the microcantilever is necessary.

Fourth, a further study could focus on improvement to the quality of the hydrogel films prepared using the micro-, nano- hydrogel particle electrophoretic deposition. The hydrogel films with high quality should be uniform, smooth and continuous and the interactions between the particles are strong. A robust hydrogel film is important when it is involved in more complex procedures or harsh environments. The possible approaches include a) prepare micro-, nano- hydrogel particles with different compositions and b) improve the EPD process via adjusting experimental parameters (such as, electrode materials, pulse mode of the applied potential, etc.) and solvent systems.

Lastly, a feasible and effective approach should be found to characterize the thickness of the thin hydrogel films. The hydrogel film is a kind of soft materials. On one hand, it is difficult to prepare the sample without damaging the surface uniformity for the

measurement of the hydrogel thickness using AFM and SEM techniques. On the other hand, the traditional techniques for thin film thickness measurement could not be used to characterize the thickness of the hydrogel films. For example, the optical profilometer is not applicable to the measurement of the hydrogel films because the reflective index of the hydrogel film is not available. The stylus profilometer is not suitable either since the hydrogel is soft and the stylus can easily damage the film.

REFERENCES

- [1] Sepaniak, M., Datskos, P., Lavrik, N., Tipple, C., Microcantilever Transducers: A New Approach in Sensor Technology, *Analytical Chemistry*, 2002, 74, 568A-575A.
- [2] Thundat, T., Warmack, R. J., Chen, G. Y., Allison, D. P., Thermal and Ambient-induced Deflections of Scanning Force Microscope Cantilevers, *Applied Physics Letter*, 1994, 64, 2894-2903.
- [3] Wachter, E. A., Thundat, T., Micromechanical Sensors for Chemical and Physical Measurements, *Review of Scientific Instrument*, 1995, 66, 3662-3671.
- [4] Thundat, T., Wachter, E. A., Sharp, S. L., Warmack, R. J., Detection of Mercury Vapor Using Resonating Microcantilevers, *Applied Physics Letter*, 1995, 66, 1695-1697.
- [5] Thundat, T., Chen, G. Y., Warmack, R. J., Allison, D. P., Wachter, E. A., Vapor Detection Using Resonating Microcantilevers, *Analytical Chemistry*, 1995, 67, 519-521.
- [6] Barnes, J. R., Stephenson, R. J., Woodburn, C. N., O'Shea, S. J., Welland, M. E., Rayment, T.; Gimzewski, J. K., Gerber, C., A Femtojoule Calorimeter Using Micromechanical Sensors, *Review of Scientific Instrument*, 1994, 65, 3793-3798.
- [7] Preissig, F. J., Applicability of Classic Curvature-Stress Relation for Thin Films on Plate Substrates, *Applied Physics*, 1989, 66, 4262-4268.
- [8] Fritz, J., Baller, M. K., Lang, H. P., Rothuizen, H.; Vettiger, P., Meyer, E., Guntherodt, H.-J., Gerber, Ch., Gimzewski, J. K., Translating Biomolecular Recognition into Nanomechanics, *Science*, 2000, 288, 316-318.
- [9] Yang, Y., Ji, H.-F., Thundat, T., Detection of Nerve Agents Based on Cu^{2+} /Cysteine Modified Microcantilevers, *Journal of American Chemistry Society*, 2003, 125, 1124-1125.
- [10] Pinnaduwege, L. A., Gehl, A., Hedden, D. L., Muralidharan, G., Thundat, T., Lareau, R. T., Sulchek, T., Manning, L., Rogers, B., Jones, M., Adams, J. D., Explosives: A microsensor for Trinitrotoluene Vapor, *Nature*, 2003, 425, 474-477.

- [11] Battiston, F. M., Ramseyer, J.-P., Lang, H. P., Baller, M. K., Gerber, Ch., Gimzewski, J. K., Meyer, E., Guntherodt, H.-J., A Chemical Sensor Based on a Microfabricated Cantilever Array with Simultaneous Resonance-frequency and Bending Readout, *Sensors and Actuators B*, 2001, 77, 122-131.
- [12] Raiteri, R., Grattarola, M., Butt, H.-J., Skladal, P., Micromechanical Cantilever-based Biosensors, *Sensors and actuators B*, 2001, 79, 115-126.
- [13] Lang, H. P., Baller, M. K., Berger, R., Gerber, Ch., Gimzewski, J. K., Battiston, F. M., Fornaro, P., Ramseyer, J. P., Meyer, E., Guntherodt, H. J., An Artificial Nose Based on a Micromechanical Cantilever Array, *Analytica Chimica Acta*, 1999, 393, 59-65.
- [14] Fagan, B. C., Tipple, C. A., Xue, Z., Sepaniak, M. J., Datskos, P. G., Modification of Micro-Cantilever Sensors with Sol-Gels to Enhance Performance and Immobilize Chemically Selective Phases, *Talanta*, 2000, 53, 599-608.
- [15] Kobayashi, T., Tsauro, J., Ichiki, M., Maeda, R. Fabrication and Performance of a Flat Piezoelectric Cantilever Obtained Using a Sol-Gel Derived PZT Thick Film Deposited on a SOI Wafer, *Smart Materials and Structures*, 2006, 15, S137~S140.
- [16] Luginbuhl, Ph. Racine, G.-A., Lerch, Ph., Romanowicz, B., Brooks, K.G, De Rooij, N.F., Renaud, Ph., Setter, N., Piezoelectric Cantilever Beams Actuated by PZT Sol-Gel Thin Film, *Sensors and Actuators, A: Physical*, 1996, 54, 530-535.
- [17] Xie, J., Ling, S., Du, H., Fabrication and Characterization of Piezoelectric Cantilever for Micro Transducers, *Sensors and Actuators, A: Physical*, 2006, 126, 182-186.
- [18] Y. Zhang, H. -F. Ji, G. Brown, T. Thundat, Ultra sensitive Detection of CrO_4^{2-} Using a Hydrogel Swelling Microcantilever Sensor, *Analytical Chemistry*, 2003, 75, 4773-4777.
- [19] Liu, K., Ji, H.-F., Detection of Pb^{2+} Using a Hydrogel Swelling Microcantilever Sensor, *Analytical Chemistry*, 2004, 20, 9-11.
- [20] Mao, J., Kondu, S., Ji, H., McShane, M., Study of the pH-sensitivity of Chitosan/gelatin Hydrogel in Neutral pH Range by Microcantilever Methods, *Biotechnology and Bioengineering*, 2006, 95(3), 333-341.
- [21] Bashir, R., Hilt, J. Z., Elibol, O., Gupta, A., Peppas, N. A., Micromechanical Cantilever as an Ultrasensitive pH Microsensor, *Applied Physics Letter*, 2002, 81, 3091-3093 (2002).
- [22] Malinsky, M. D., Kelly, K. L., Schatz, G. C., Van Duyne, R. P., Chain Length Dependence and Sensing Capabilities of the Localized Surface Plasmon Resonance of Silver Nanoparticles Chemically Modified with Alkanethiol Self-assembled Monolayers, *Journal of American Chemistry Society*, 2001, 123, 1471-1482.

- [23] Gupta, P., Vermani, K., Garg, S., Hydrogels: from Controlled Release to pH-responsive Drug Delivery, *Drug Discovery Today*, 2002, 7, 569-579.
- [24] Moller, G., Harke, M., Motschmann, H., Prescher, D., Controlling Microdroplet Formation by Light, *Langmuir*, 1998, 14, 4955-4957.
- [25] Ozin, G. A., Yang, S. M., The Race for the Photonic Chip: Colloidal Crystal Assembly in Silicon Wafers, *Advanced Functional Materials*, 2001, 11, 95-104.
- [26] Chiarelli, P. A., Johal, M. S., Holmes, D. J., Casson, J. L., Robinson, J. M., Wang, H. L., Polyelectrolyte Spin-Assembly, *Langmuir*, 2002, 18, 168-173.
- [27] Blodgett, K. B., Monomolecular Films of Fatty Acids on Glass, *Journal of American Chemistry Society*, 1934, 56, 495.
- [28] Wong, E. M., Searson, P. C., Kinetics of Electrophoretic Deposition of Zinc Oxide Quantum Particle Thin Films, *Chemistry Materials*, 1999, 11, 1959 – 1961.
- [29] Ibn-Elhaj, M., Schadt, M., Optical Polymer Thin Films with Isotropic and Anisotropic Nano-corrugated Surface Topologies, *Nature*, 2001, 410, 796-799.
- [30] Decher, G., Toward Layered Polymeric Ultracomposites, *Science*, 1997, 277, 1232-1237.
- [31] Lvov, Y. M., Price, R. R., Selinger, J. V., Singh, A., Spector, M. S., Schnur, J. M., Imaging Nanoscale Patterns on Biologically Derived Microstructures, *Langmuir*, 2000, 16, 5932-5935.
- [32] Ai, H., Fang, M., Jones, S. A., Lvov, Y. M., Electrostatic Layer-by-Layer Nano-assembly on Biological Microtemplates: Platelets, *Biomacromolecules*, 2002, 3, 560-564.
- [33] Lvov, Y., Ariga, K., Onda, M., Ichinose, I., Kunitake, T., Alternate Assembly of Ordered Multilayers of SiO₂ and Other Nanoparticles and Polyions, *Langmuir*, 1997, 13, 6195-6203.
- [34] Sukhishvili, S. A., Granick, S., Layered, Erasable, Ultrathin Polymer Films, *Journal of American Chemistry Society*, 2000, 122, 9550-9551.
- [35] Brown, K. R., Lyon, L. A., Fox, A. P., Reiss, B. D., Natan, M. J., Hydroxylamine Seeding of Colloidal Au Nanoparticles. 3. Controlled Formation of Conductive Au Films, *Chemistry Materials*, 2000, 12, 314-323.
- [36] Porter, M. D.; Bright, T. B.; Allara, D. L.; Chidsey, C. E. D., Spontaneously Organized Molecular Assemblies 4:Structural Characterization of n-Alkyl Thiol

- Monolayers on Gold by Optical Ellipsometry, infrared Spectroscopy, and Electrochemistry, *Journal of American Chemistry Society*, 1987, 109, 3559-3568.
- [37] Nuzzo, R. G., Zegarski, B. R., Dubois, L. H., Fundamental Studies of the Chemisorption of Organosulfur Compounds on Au(111). Implications for Molecular Self-Assembly on Gold, *Journal of American Chemistry Society*, 1987, 109, 733-740.
- [38] Bain, C. D., Troughton, E. B., Tao, Y.-T., Evall, J., Whitesides, G. M., Nuzzo, R., Formation of Monolayer Films by Spontaneous Assembly of Organic Thiols from Solution onto Gold, *Journal of American Chemistry Society*, 1989, 111, 321-335.
- [39] Wasserman, S. R., Whitesides, G. M., Tidswell, I. M., Ocko, B. M., Pershan, P. S., Axe, J. D., The Structure of Self-Assembled Monolayers of Alkylsiloxanes on Silicon: A Comparison of Results from Ellipsometry and Low-Angle X-Ray Reflectivity, *Journal of American Chemistry Society*, 1989, 111, 5852-5861.
- [40] Peyratout, C. S., Dahne, L., Tailor-made Polyelectrolyte Microcapsules: from Multilayers to Smart Containers, *Angewandte Chemie International Edition*, 2004, 43, 3762-3783.
- [41] Groth, T., Lendlein, A., Layer-by-layer Deposition of Polyelectrolytes - a Versatile Tool for the in vivo Repair of Blood Vessels, *Angewandte Chemie International Edition*, 2004, 43, 926-928.
- [42] Liang, Z. J., Susha, A. S., Yu, A. M., Caruso, F., Nanotubes Prepared by Layer-by-Layer Coating of Porous Membranes, *Advanced Materials*, 2003, 15, 1849-1853.
- [43] Nolte, A. J., Rubner, M. F., Cohen, R. E., Creating Effective Refractive Index Gradients within Polyelectrolyte Multilayer Films: Molecularly Assembled Rugate Filters, *Langmuir*, 2004, 20, 3304-3310.
- [44] Lee, I., Ahn, J. S., Hendricks, T. R., Rubner, M. F., Hammond, P. T., Patterned and Controlled Polyelectrolyte Fractal Growth and Aggregations, *Langmuir*, 2004, 20, 2478-2483.
- [45] Liu, X. Y., Bruening, M. L., Size-Selective Transport of Uncharged Solutes through Multilayer Polyelectrolyte Membranes, *Chemistry Materials*, 2004, 16, 351-357.
- [46] Quinn, J. F., Caruso, F., Facile Tailoring of Film Morphology and Release Properties Using Layer-by-Layer Assembly of Thermoresponsive Materials, *Langmuir*, 2004, 20, 20-22.
- [47] Lvov, Y. M., Price, R. R., Selinger, J. V., Singh, A., Spector, M. S., Schnur, J. M., Imaging Nanoscale Patterns on Biologically Derived Microstructures, *Langmuir*, 2000, 16, 5932-5935.

- [48] Serizawa, T., Takeshita, H., Akashi, M., Electrostatic Adsorption of Polystyrene Nanospheres onto the Surface of an Ultrathin Polymer Film Prepared by Using an Alternate Adsorption Technique, *Langmuir*, 1998, 14, 4088-4094.
- [49] Schrof, W., Rozouvan, S., Van Keuren, E., Horn, D., Schmitt, J., Decher, G., Nonlinear Optical Properties of Polyelectrolyte Thin Film Containing Gold Nanoparticles Investigated by Wave Dispersive Femtosecond Degenerate 4 Wave mixing (dfwm), *Advanced Materials*, 1998, 10, 338-341.
- [50] Liu, Y. J., Wang, A. B., Claus, R. O., Layer-by-Layer Electrostatic Self-assembly of Nanoscale Fe₃O₄ Particles and Polyimide Precursor on Silicon and Silica Surfaces, *Applied Physics Letter*, 1997, 71, 2265-2267.
- [51] Hu, K., Brust, M., Bard, A. J., Characterization and Surface Charge Measurement of Self-Assembled CdS Nanoparticle Films, *Chemistry Materials*, 1998, 10, 1160-1165.
- [52] Yan, X., Ji, H.-F., Glucose Oxidase Multilayer Modified Microcantilever for Glucose Measurement, *Analytical Chemistry*, 2005, 77(19), 6197-6204.
- [53] Lvov, Y., Ariga, K., Ichinose, I., Kunitake, T., Assembly of Multicomponent Protein Films by Means of Electrostatic Layer-by-Layer Adsorption, *Journal of American Chemistry Society* 1995, 117, 6117-6123.
- [54] Sarkar, P., Nicholson, P. S., Electrophoretic Deposition (EPD): Mechanisms, Kinetics, and Applications to Ceramics, *Journal of American Ceramic Society*, 1996, 79, 1987-2002.
- [55] Bohmer, M., In Situ Observation of 2-Dimensional Clustering during Electrophoretic Deposition, *Langmuir*, 1996, 12, 5747-5750.
- [56] Teranishi, T., Hosoe, M., Tanaka, T., Miyake, M. Size Control of Monodispersed Pt Nanoparticles and Their 2D Organization by Electrophoretic Deposition, *Journal of Physical Chemistry B*, 1999, 103, 3818-3827.
- [57] Cao, G., Growth of Oxide Nanorod Arrays through Sol Electrophoretic Deposition, *Journal of Physical Chemistry B*, 2004, 108, 19921-19931.
- [58] Wladyslaw, J., Anna, G., Electrical Double Layer at Manganese Oxide/ 1:1 Electrolyte Solution Interface, *Physicochemical Problems of Mineral Processing*, 2001, 35, 31-41.
- [59] Chorom, M., Rengasamy, P., Dispersion and Zeta Potential of Pure Clays as Related to Net Particle Charge under Varying pH, Electrolyte Concentration and Cation Type, *European Journal of Soil Science*, 1995, 46, 657-665.

- [60] Zhitomirsky, I., Gal-Or, L. Formation of Hollow Fibers by Electrophoretic Deposition, *Materials Letter*, 1999, 38, 10-17.
- [61] Zhitomirsky, I, Electrophoretic Hydroxyapatite Coatings and Fibers, *Materials Letter*, 2000, 42, 262-271.
- [62] Zhitomirsky, I., Cathodic Electrophoretic Deposition of Diamond Particles, *Materials letter*, 1998, 37, 72-78.
- [63] Hunter, R. J. Zeta Potential in Colloid Science: Principles and Applications, Academic Press: London, 1981.
- [64] Zhitomirsky, I., Sumi, K., Muchi, T., A Highly Stable Nonaqueous Suspension for the Electrophoretic Deposition of Powdered Substances, *Journal of Electrochemistry Society*, 1983, 130, 1819-1825.
- [65] Zhitomirsky, I., Electrophoretic Deposition of Chemically Bonded Ceramics in the System CaO-SiO₂-P₂O₅, *Journal of Materials Science Letter*, 1998, 2101-2104.
- [66] Russ, B. E., Talbot, J.B., An Analysis of the Binder Formation in Electrophoretic Deposition, *Journal of Electrochemistry Society*, 1998, 145, 1253-1256.
- [67] Humphris, A., Miles, M., Hobbs, J., A Mechanical Microscope: High-speed Atomic Force Microscopy, *Applied Physics Letters*, 2005, 86, 034106-034109.
- [68] <http://stm2.nrl.navy.mil/how-afm/how-afm.html>
- [69] http://en.wikipedia.org/wiki/Atomic_force_microscope
- [70] <http://spm.phy.bris.ac.uk/techniques/AFM/>
- [71] http://en.wikipedia.org/wiki/Scanning_probe_microscopy
- [72] <http://www.chembio.uoguelph.ca/educmat/chm729/afm/general.htm>
- [73] <http://www.chembio.uoguelph.ca/educmat/chm729/afm/resolution.htm>
- [74] <http://www2.eng.cam.ac.uk/~bcb/history.htm>
- [75] http://en.wikipedia.org/wiki/Scanning_electron_microscope
- [76] <http://mse.iastate.edu/microscopy/choice.html>
- [77] <http://accept.asu.edu/PiN/rdg/elmicr/elmicr.shtml>

- [78] <http://www.photometrics.net/sem.html>
- [79] Tammelin, L.-E., The Alkaline Hydrolysis of Isopropoxy-methyl- Phosphoryl Fluoride (sarin), *Analytical Chemistry*, 1957, 11, 859–865.
- [80] Nassar, A.-E.F., Lucas, S.V., Smith, P.B.W., Hoffland, L.D., Determination of Nitrogen Containing Compounds, *ACS Symposium Series*, 2000, 740, 329–350.
- [81] Stuff, J.R., Creasy, W.R., Rodriguez, A.A., Durst, H.D., Gas Chromatography with Atomic Emission Detection as an Aid in the Identification of Chemical Warfare Related Material, *Journal of Microcolumn*, 1999, 11, 644–651.
- [82] Janata, J., Potentiometric Microsensors, *Chemistry Review* 1990, 90, 691–703.
- [83] Bachels, T., Schafer, R., Microfabricated Cantilever-based Detector for Molecular Beam Experiments, *Review of Scientific Instrument*, 1998, 69, 3794–3797.
- [84] Steiner, W.E., Clowers, B.H., Matz, L.M., Siems, W.F., Hill Jr, H.H., Rapid of Aqueous Chemical Warfare Agent Degradation Products: Ambient Pressure Ion Mobility Mass Spectrometry, *Analytical Chemistry*, 2002, 74, 4343–4352.
- [85] Erhard, M.H., Juengling, R., Schoeneberg, R., Szinicz, L., Loesch, U., A homogenic Immunological Detection System for Soman Using the in vitro Protection of Acetylcholinesterase by Monoclonal Antibodies, *Archives of Toxicology* 1993, 67, 220–223.
- [86] Epstein, J.R., Lee, M., Walt, D.R., High-Density Fiber-Optic Genosensor Microsphere Array Capable of Zeptomole Detection Limits, *Analytical Chemistry*, 2002, 74, 1836–1840.
- [87] Paddle, B.M., Biosensors for Chemical and Biological Agents of Defence Interest, *Biosensor Bioelectron*, 1996, 11, 1079–1113.
- [88] McGill, R., Nguyen, V.K., Chung, R., Shaffer, R.E., DiLella, D., Stepnowski, J.L., Mlsna, T.E., Venezky, D.L., Domingue, D., A Nose for Toxic Gases, *Advanced Scientific Technology*, 1999, 26, 369–374.
- [89] Chen, G.Y., Warmack, R.J., Thundat, T., Allison, D.P., Huang, A., Resonance Response of Scanning Force Microscopy Cantilevers, *Review of Scientific Instrument*, 1994, 65 (8), 2532–2537.
- [90] Gimzewski, J.K., Gerber, C., Meyer, E., Schlittler, R.R., Observation of a Chemical Reaction Using a Micromechanical Sensor, *Chemical Physics Letters*, 1994, 217 (5–6), 589–594.
- [91] Thundat, T., Warmack, R.J., Chen, G.Y., Allison, D.P., Thermal and Ambient-

- Induced Deflections of Scanning Force Microscope Cantilevers, *Applied Physics Letter*, 1994, 64 (21), 2894–2896.
- [92] Lang, H.P., Baller, M.K., Berger, R., Gerber, Ch., Gimzewski, J.K., Battiston, F.M., Fornaro, P., Ramseyer, J.P., Meyer, E., Guntherodt, H.J., An Artificial Nose Based on a Micromechanical Cantilever Array, *Analytica Chimica Acta* 1999, 393, 59–65.
- [93] Thundat, T., Chen, G.Y., Warmack, R.J., Allison, D.P., Wachter, E.A., Vapor Detection Using Resonating Microcantilevers, *Analytical Chemistry*, 1995, 67, 519–521.
- [94] Thundat, T., Wachter, E.A., Sharp, S.L., Warmack, R.J., Detection of Mercury Vapor Using Resonating Microcantilevers, *Applied Physics Letter*, 1995, 66, 1695–1697.
- [95] Fritz, J., Baller, M.K., Lang, H.P., Rothuizen, H., Vettiger, P., Meyer, E., Guntherodt, H.J., Gerber, C., Gimzewski, J.K., Translating Biomolecular Recognition into Nanomechanics, *Science*, 2000, 288 (5464), 316–318.
- [96] Ji, H.-F., Finot, E., Dabestani, R., Thundat, T., Brown, G.M., Britt, P.F., A Novel Self-Assembled Monolayer (SAM) Coated Microcantilever For Low Level Cs ion Detection, *Chemical Communications*, 2000, 6, 457–458.
- [97] Hansen, K.M., Ji, H.-F., Wu, G., Datar, R., Cote, R., Majumdar, A., Thundat, T., Cantilever-based Optical Deflection Assay for Discrimination of DNA Single-nucleotide Mismatches, *Analytical Chemistry* 2001, 73 (7), 1567–1571.
- [98] Zhang, J., Ji, H.-F., Antibody-immobilized Microcantilever for the Detection of Escherichia coli (E. coli), *Analytical Sciences*, 2004, 20 (4), 585–587.
- [99] Yang, Y., Ji, H.F., Thundat, T., Nerve Agents Detection Using a Cu²⁺/L-Cysteine Bilayer-Coated Microcantilever, *Journal of American Chemistry Society* 2003, 125 (5), 1124–1125.
- [100] Berger, R., Delamarche, E., Lang, H.P., Gerber, Ch., Gimzewski, J.K., Meyer, E., Guntherodt, H.-J., A Chemical Sensor Based on a Micromechanical Cantilever Array for the Identification of Gases and Vapors, *Applied Physics A*, 1998, 66, S55–S59.
- [101] Tang, Y., Fang, J., Xu, X., Ji, H.-F., Brown, G.M., Thundat, T., Detection of Femtomolar Concentration of HF Using a SiO₂ Microcantilever, *Analytical Chemistry*, 2004, 76 (9), 2478–2481.
- [102] Rosenberry, T.L., Acetylcholinesterase, *Advances in Enzymology & Related Areas of Molecular Biology*, 1975, 543, 103–218.
- [103] Lai, K., Dave, K.I., Wild, J.R., Bimetallic Binding Motifs in Organophosphorous

Hydrolase, *Journal of Biological Chemistry*, 1994, 269, 16579–16584.

- [104] Constantine, C.A., Mello, S.V., Dupont, A., Cao, X., Santos Jr, D., Strixino, F.T., Pereira, E.C., Cheng, T.-C., Defrank, J.J., Leblanc, R.M., Layer-by-Layer Self-Assembled Chitosan/Poly(thiophene-3-acetic acid) and Organophosphorus Hydrolase Multilayers, *Journal of American Chemistry Society*, 2003, 125 (7), 1805–1809.
- [105] Lee, Y., Stanish, I., Rastogi, V., Cheng, T.-C., Singh, A., Sustained Enzyme Activity of Organophosphorus Hydrolase in Polymer Encased Multilayer Assemblies, *Langmuir*, 2003, 19, 1330–1336.
- [106] Battiston, F.M., Ramseyer, J.-P., Lang, H.P., Baller, M.K., Gerber, Ch., Gimzewski, J.K., Meyer, E., Guntherodt, H.-J., A Chemical Sensor Based on a Microfabricated Cantilever Array with Simultaneous Resonance-frequency and Bending Readout, *Sensor Actuators B*, 2001, 77, 122–131.
- [107] Raiteri, R., Grattarola, M., Butt, H.-J., Skladal, P., Micromechanical Cantilever-based Biosensors, *Sensor Actuators B*, 2001, 79, 115–126.
- [108] Fagan, B.C., Tipple, C.A., Xue, Z., Sepaniak, M.J., Datskos, P.G., Modification of Micro-cantilever Sensors with Sol-gels to Enhance Performance and Immobilize Chemically Selective Phases, *Talanta*, 2000, 53, 599–608.
- [109] Bashir, R., Hilt, J.Z., Elibol, O., Gupta, A., Peppas, N.A., Micromechanical Cantilever as an Ultrasensitive pH Microsensor, *Applied Physics Letter*, 2002, 81, 3091–3093.
- [110] Zhang, Y., Ji, H.-F., Brown, G.M., Thundat, T., Detection of CrO_4^{2-} Using a Hydrogel Swelling Microcantilever Sensor, *Analytical Chemistry*, 2003, 75 (18), 4773–4777.
- [111] Liu, K., Ji, H.-F., Detection of Pb^{2+} Using a Hydrogel Swelling Microcantilever Sensor, *Analytical Sciences* 2004, 20 (1), 9–11.
- [112] Yan, X., Xu, K.X., Ji, H.-F., Glucose Oxidase Multilayer Modified Microcantilevers for Glucose Measurement, *Analytical Chemistry*, 2005, 77 (19), 6197–6204.
- [113] Lvov, Y., Decher, G., M^ohwald, H., Assembly, Structural Characterization and Thermal Behavior of Layer-by-Layer Deposited Ultrathin Films of Poly(vinylsulfate) and Poly(allylamine), *Langmuir*, 1993, 9, 481–486.
- [114] Lvov, Y., Ariga, K., Ichinose, I., Kunitake, T., Assembly of Multicomponent Protein Films by Means of Electrostatic Layer-by-Layer Adsorption, *Journal of American Chemistry Society* 1995, 117, 6117–6123.

- [115] Decher, G., Fuzzy Nanoassemblies: Toward Layered Polymeric Multicomposites, *Science*, 1997, 227, 1232–1237.
- [116] Yoo, D., Shiratori, S., Rubner, M., Controlling Bilayer Composition and Surface Wettability of Sequentially Adsorbed Multilayers of Wear Polyelectrolytes, *Macromolecules*, 1998, 31, 4309–4318.
- [117] Dubas, S., Schlenoff, J., Factors Controlling the Growth of Polyelectrolyte Multilayers, *Macromolecules*, 1999, 32, 8153–8160.
- [118] Ji, H. F., Thundat, T., Dabestani, R., Brown, G.M., Pritt, P.F., Bonnesen, P.V., Ultrasensitive Detection of CrO_4^{2-} Using Microcantilever Sensor, *Analytical Chemistry*, 2001, 73 (7), 1572–1576.
- [119] Yan, X., Ji, H.-F., Lvov, Yuri, Glucose Monitoring Using Microcantilever Modified by GOx Using Layer-by-Layer Technology, *Chemical Physics Letters*, 2004, 396, 34–37.
- [120] Mulchandani, A., Chen, W., Mulchandani, P., Wang, J., Rogers, K.R., Biosensors for Direct Determination of Organophosphate Pesticides, *Biosensors and Bioelectronics*, 2001, 16, 225–230.
- [121] Subramanian, A., Oden, P.I., Kennel, S.J., Jacobson, K.B., Warmack, R.J., Thundat, T., Doktycz, M.J., Microcantilever Based Calorimetric Biosensing, *Applied Physics Letter*, 2002, 81, 385–387.
- [122] diSioudi, B., Grimsley, J.K., Lai, K., Wild, J.R., Modification of Near Active Site Residues in Organophosphorus Hydrolase Reduces Metal Stoichiometry and Alters Substrate Specificity, *Biochemistry*, 1999, 38, 2866–2872.
- [123] Rani, R.P., Sudan, S.M., Takeyoshi, O., Takeo, O., Electrooxidation and Amperometric Detection of Ascorbic Acid at GC Electrode Modified by Electropolymerization of *N,N*-Dimethylaniline, *Electroanalysis*, 2004, 16, 289–297.
- [124] Walhout, P.K., Burden, D.L., 2004. 36th Great Lakes Regional Meeting of the American Chemical Society, 17.
- [125] Einstein, A., Über die von der molekularkinetischen Theorie der Wärme geforderte Bewegung von in ruhenden Flüssigkeiten suspendierten Teilchen, *Annals of Physics*, 1905, 17, 549–560.
- [126] Lei, C., Shin, Y., Liu, J., Ackerman, E.J., Entrapping Enzyme in a Functionalized Nanoporous Support, *Journal of American Chemistry Society* 2002, 124, 11242–11243.

- [127] Constantine, C.A., Gattas-Asfura, K.M., Mello, S.V., Crespo, G., Rastogi, V., Chen, T.-C., Defrank, J.J., Leblanc, R.M., Layer-by-Layer Films of Chitosan, Organophosphorus Hydrolase and Thioglycolic Acid-Capped CdSe Quantum Dots for the Detection of Paraoxon, *Journal of Physical Chemistry B*, 2003, 107 (50), 13762–13764.
- [128] Constantine, C.A., Gattas-Asfura, K.M., Mello, S.V., Crespo, G., Rastogi, V., Chen, T.-C., Defrank, J.J., Leblanc, R.M., Layer-by-Layer Biosensor Assembly Incorporating Functionalized Quantum Dots, *Langmuir*, 2003, 19 (23), 9863–9867.
- [129] Constantine, C.A., Mello, S.V., Dupont, A., Cao, X., Santos Jr., D., Oliverira Jr., O.N., Strixino, F.T., Pereira, E.C., Rastogi, V., Chen, T.-C., Defrank, J.J., Leblanc, R.M., Layer-by-Layer Self-Assembled Chitosan/Poly(thiophene-3-acetic acid) and Organophosphorus Hydrolase Multilayers, *Journal of American Chemistry Society*, 2003, 125 (21), 6595–6596.
- [130] Zheng, J., Constantine, C.A., Rastogi, V.K., Cheng, T.-C., DeFrank, J.J., Leblanc, R.M., Secondary Structure of Organophosphorus Hydrolase in Solution and in Langmuir-Blodgett Film Studied by Circular Dichroism Spectroscopy, *Journal of Physical Chemistry B*, 2004, 108 (44), 17238–17242.
- [131] Ji, X., Zheng, J., Xu, J., Rastogi, V.K., Cheng, T.-C., DeFrank, J.J., Leblanc, R.M., (CdSe)ZnS Quantum Dots and Organophosphorus Hydrolase Bioconjugate as Biosensors for Detection of Paraoxon *Journal of Physical Chemistry B*, 2005, 109 (9), 3793–3799.
- [132] Wu, G., Datar, R. H., Hansen, K. M., Thundat, T., Cote, R. J., Majumdar, A., Naomechanical Detection of Molecular Interactions, *Nature Biotechnology*, 2001, 19, 956-960.
- [133] Y. Zhang, H.-F. Ji, G. M. Brown and T. Thundat, Ultra sensitive Detection of CrO₄²⁻ Using a Hydrogel Swelling Microcantilever Sensor, *Analytical Chemistry*, 2003, 75(18), 4773-4777.
- [134] Decher, G., Toward Layered Polymeric Ultracomposites, *Science*, 1997, 277, 1232-1237.
- [135] Ai, H., Fang, M., Jones, S. A., Lvov, Y. M., Electrostatic Layer-by-Layer Nano-assembly on Biological Microtemplates: Platelets, *Biomacromolecules*, 2002, 3, 560-564.
- [136] Decher, G., Hong, J. D., Schmitt, J, Buildup of ultrathin multilayer films by a self-assembly process. III. Consecutively alternating adsorption of anionic and cationic polyelectrolytes on charged surfaces, *Thin Solid Films* 1992, 210, 831-835.

- [137] Brown, K. R., Lyon, L. A., Fox, A. P., Reiss, B. D., Natan, M. J., Hydroxylamine Seeding of Colloidal Au Nanoparticles. 3. Controlled Formation of Conductive Au Films, *Chemistry Materials*, 2000, 12, 314-323.
- [138] Liang, Z. J., Susha, A. S., Yu, A. M., Caruso, F., Nanotubes Prepared by Layer-by-Layer Coating of Porous Membranes, *Advanced Materials*, 2003, 15, 1849-1853.
- [139] Serizawa, T., Takeshita, H., Akashi, M., Electrostatic Adsorption of Polystyrene Nanospheres onto the Surface of an Ultrathin Polymer Film Prepared by Using an Alternate Adsorption Technique, *Langmuir*, 1998, 14, 4088-4094.
- [140] Schrof, W., Rozouvan, S., Van Keuren, E., Horn, D., Schmitt, J., Decher, G., Nonlinear Optical Properties of Polyelectrolyte Thin Film Containing Gold Nanoparticles Investigated by Wave Dispersive Femtosecond Degenerate 4 Wave mixing (dfwm), *Advanced Materials*, 1998, 10, 338-341.
- [141] Liu, Y. J., Wang, A. B., Claus, R. O., Layer-by-Layer Electrostatic Self-assembly of Nanoscale Fe_3O_4 Particles and Polyimide Precursor on Silicon and Silica Surfaces, *Applied Physics Letter*, 1997, 71, 2265-2267.
- [142] Hu, K., Brust, M., Bard, A. J., Characterization and Surface Charge Measurement of Self-Assembled CdS Nanoparticle Films, *Chemistry Materials*, 1998, 10, 1160-1165.
- [143] Kotov, N. A., Layer-by-layer Self-assembly: the Contribution of Hydrophobic Interactions, *Nanostructured. Materials*. 1999, 12, 789-796.
- [144] Dubas, S. T., Schlenoff, J. B., Factors Controlling the Growth of Polyelectrolyte Multilayers, *Macromolecules* 1999, 32, 8153-8160.
- [145] De, G. T., Sol-gel Synthesis of Metal Nanoclusters-silica Composite Films, *Journal of Sol-Gel science and technology* 1998, 11, 289-298.
- [146] Chevreau, A., Phillips, B., Higgins, B. G., Risbud, S. H., Processing and Optical Properties of Spin-coated Polystyrene Films Containing CdS Nanoparticles, *Journal of Materials Chemistry*, 1996, 6, 1643-1647.
- [147] Mattoussi, H., Radzilowski, L. H., Dabbousi, B. O., Fogg, D. E., Schrock, R. R., Thomas, E. L., Rubner, M. F., Bawendi, M. G., Composite Thin Films of CdSe Nanocrystals and a Surface Passivating/Electron Transporting Block Copolymer: Correlations between Film Microstructure by Transmission Electron Microscopy and Electroluminescence, *Journal of Applied Physics*, 1999, 86, 4390-4399.

- [148] Kawaguchi, H., Yamada, Y., Kataoka, S., Morita, Y., Hydrogel Microspheres II Precipitation Copolymerization of Acrylamide with Comonomers to Prepare Monodisperse Hydrogel Microspheres, *Polymer Journal*, 1991, 23, 955-962.
- [149] Kawaguchi, H., Fujimoto, K., Kawasaki, T., Urakami, Y., Preparation and Modification of Monodisperse Hydrogel Microspheres, *Polymer International*, 1993, 30, 225-231.
- [150] Serizawa, T., Takeshita, H., Akashi, M., Film Prepared by Using an Alternate Adsorption Technique, *Langmuir* 1998, 14, 4088-4094.
- [151] Jaffar, S., Nam, K. T., Khademhosseini, A., Xing, J., Langer, R., Belcher, A. M., Layer-by-layer Surface Modification and Patterned Electrostatic Deposition of Quantum Dots, *Nano Letters*, 2004, 4, 1421-1425, 2004,
- [152] Mamedov, A. A., Belov, A., Giersig, M., Mamedova, N. N., Kotov, N. A., Nanorainbows: Graded Semiconductors Films from Quantum Dots, *Journal of American Chemistry Society*, 2001, 123, 7738-7739.
- [153] Hobara, D., Yamamoto, M., Kakiuchi, T., Reconstruction of Au(111) Following the Reductive Desorption of Self-Assembled Monolayers of 2-Mercaptoethanesulfonic Acid Studied by in Situ Scanning Tunneling Microscopy, *Chemistry Letters*, 2001, 4, 374-380.
- [154] Wu, G., Datar, R. H., Hansen, K. M., Thundat, T., Cote, R. J., Majumdar, A., Naomechanical Detection of Molecular Interactions, *Nature Biotechnology*, 2001, 19, 956-960.
- [155] Yang, Y., Ji, H.-F., Thundat, T., Nerve Agents Detection Using a Cu^{2+} /L-cysteine Bilayer-Coated Microcantilever, *Journal of American Chemistry Society*, 2003, 125 (5), 1124-125.
- [156] Yan, X., Ji, H.-F., Glucose Oxidase Multilayer Modified Microcantilevers for Glucose Measurement, *Analytical Chemistry*, 2005, 77(19), 6197-204.
- [157] Gupta, A., Akin, D., Bashir, R., Single Virus Particle Mass Detection Using Microresonators with Nanoscale Thickness, *Applied Physics Letter* 2004, 84, 1976-1978.
- [158] Lang, H. P., Baller, M. K., Berger, R., Gerber, Ch., Gimzewski, J. K., F.M Battiston, P. Fornaro, J. P. Ramseyer, E. Meyer and H.J. Guntherodt, An Artificial Nose Based on a Micromechanical Cantilever Array, *Analytica Chimica Acta*, 1999, 393, 59-65.

- [159] H.-F. Ji, X. Yan and M. J. McShane, Experimental and Theoretical Aspects of Glucose Measurement Using a Microcantilever Modified by Enzyme-Containing Polyacrylamide, *Diabete Technology and Therapies*, 2005, 7, 986-995.
- [160] R. Bashir, J.Z. Hilt, O. Eliol, A. Gupta and N.A. Peppas, Micromechanical Cantilever as an Ultrasensitive pH Microsensor, *Applied Physics Letter*, 2002, 81, 3091-3093.
- [161] M. E. Harmon, M. Tang and C. W. Frank, A Microfluidic Actuator Based on Thermoresponsive Hydrogels, *Polymer*, 2003, 44, 4547-4556.
- [162] G. M. Eichenbaum, P. F. Kiser, S. A. Simon, and D. Needham, pH and Ion Triggered Volume Response of Anionic Hydrogel Microspheres, *Macromolecules*, 1998, 31, 5084-5090.
- [163] T. Tanaka, I. Nishiq, S. Sun and S. Ueno-Nishio, Collapse of Gels in an Electric Field, *Science*, 1982, 218, 467-469.
- [164] W.-G. Koh, A. Revzin and M. V. Pishko, Poly(ethylene glycol) Hydrogel Microstructures Encapsulating Living Cells, *Langmuir*, 2002, 18, 2459-2462.
- [165] Y. Zhang, H.-F. Ji, G. M. Brown and T. Thundat, Ultra sensitive Detection of CrO_4^{2-} Using a Hydrogel Swelling Microcantilever Sensor, *Analytical Chemistry*, 2003, 75(18), 4773-4777.
- [166] A. Guiseppi-Elie, S. I. Brahim and D. Narinesingh, A Chemically Synthesized Artificial Pancreas: Release of Insulin from Glucoseresponsive Hydrogels, *Advanced Materials*, 2002, 14, 743-746.
- [167] X. Zhang, Y. Yang, T. Chung and K. Ma, Preparation and Characterization of the Macroporous Poly(N-isopropylacrylamide) Hydrogel with Fast Response, *Langmuir*, 2001, 17(20), 6094.
- [168] T. Tanaka and D. Fillmore, Kinetics of Swelling of Gels, *Journal of Chemical Physics*, 1979, 70, 1214-1218.
- [169] G. Decher and J.B. Schlenoff, *Multilayer Thin Film: Sequential Assembly of Nanocomposite Materials*, Wiley-VCH, New York, 2003.
- [170] M. J. Serpe, C. D. Jones and L. A. Lyon, Layer-by-Layer Deposition of Thermoresponsive Microgel Thin Films, *Langmuir* 2003, 19, 8759-8764.
- [171] I. Zhitomirsky, Electrophoretic and Electrolytic Deposition of Ceramic Coatings on Carbon Fibers, *Journal of European Ceramic Society*, 1998, 18, 849-856.
- [172] R. C. Bailey, K. J. Stevenson and J. T. Hupp, Assembly of Micropatterned colloidal

Gold Thin Films via Microtransfer Molding and Electrophoretic Deposition, *Advanced Materials*, 2000, 12(24), 1930-1934.

- [173] Y. Solomentsev, M. Bohmer and J. L. Anderson, Particle Clustering and Pattern Formation during Electrophoretic Deposition: A Hydrodynamic Model, *Langmuir*, 1997, 13, 6058-6068.
- [174] Nakazawa, Y, Kamijo, Y., Fujimoto, K., Kawaguchi, H., Yuguchi, Y., Urakawa, H., Kajiwara, K, Preparation and Structural Characteristics of Stimuli-responsive Hydrogel Microsphere, *Angewandte Makromolekulare Chemie*, 1996, 240, 187-196.
- [175] Y. Tang, J. Fang, X. Yan, and H. -F. Ji, Fabrication and Characterization of SiO₂ Microcantilever for Microsensor Application, *Sensor and Actuators, B*, 2004, 97, 109-113.
- [176] X. Xu, T. Thundat, G. M. Brown, and H. F. Ji, Ultrasensitive Detection of Hg²⁺ Using Microcantilever Sensors, *Analytical Chemistry*, 2002, 74(15), 3611-3615.
- [177] Y. Solomentsev, S. A. Guelcher, M. Bevan and J. L. Anderson, Aggregation Dynamics for Two Particles during Electrophoretic Deposition under Steady Fields, *Langmuir*, 2000, 16, 9208-921
- [178] M. Böhmer, In Situ Observation of 2-Dimensional Clustering during Electrophoretic Deposition, *Langmuir*, 1996, 12, 57475750.
- [179] T. Teranishi, M. Hosoe, T. Tanaka and M. Miyake, Size Control of Monodispersed Pt Nanoparticles and Their 2D Organization by Electrophoretic Deposition, *Journal of Physical Chemistry B* 1999, 103(19), 3818-3827.
- [180] Ni, Henmei, Kawaguchi, Haruma, Endo, Takeshi, Preparation of pH-sensitive Hydrogel Microspheres of Poly(acrylamide-co-methacrylic acid) with Sharp pH-Volume Transition, *Colloid & Polymer Science*, 2007, 285, 819-826.